

2018

Lattice Qcd for Neutrinoless Double Beta Decay: Short Range Operator Contributions

Henry Jose Monge Camacho

College of William and Mary - Arts & Sciences, henrymonge@gmail.com

Follow this and additional works at: <https://scholarworks.wm.edu/etd>



Part of the [Physics Commons](#)

Recommended Citation

Monge Camacho, Henry Jose, "Lattice Qcd for Neutrinoless Double Beta Decay: Short Range Operator Contributions" (2018). *Dissertations, Theses, and Masters Projects*. Paper 1550153991.

<http://dx.doi.org/10.21220/s2-keqm-c011>

This Dissertation is brought to you for free and open access by the Theses, Dissertations, & Master Projects at W&M ScholarWorks. It has been accepted for inclusion in Dissertations, Theses, and Masters Projects by an authorized administrator of W&M ScholarWorks. For more information, please contact scholarworks@wm.edu.

Lattice QCD for Neutrinoless Double Beta Decay:
Short Range Operator Contributions

Henry J. Monge Camacho

San José, Costa Rica

Master of Science, College of William and Mary, 2016
Bachelor of Science, University of Costa Rica, 2008

A Dissertation presented to the Graduate Faculty
of The College of William and Mary in Candidacy for the Degree of
Doctor of Philosophy

Department of Physics

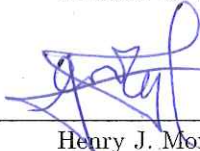
College of William and Mary
January 2019

©2018
Henry J. Monge Camacho
All rights reserved.

APPROVAL PAGE

This Dissertation is submitted in partial fulfillment of
the requirements for the degree of

Doctor of Philosophy



Henry J. Monge Camacho

Approved by the Committee August 2018




Committee Chair

Adjunct Assistant Professor André Walker-Loud, Physics
College of William & Mary



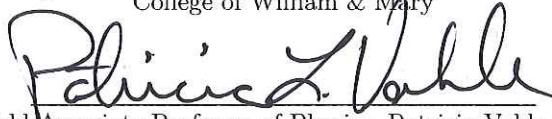
Co-committee Chair

Professor Konstantinos Orginos, Physics
College of William & Mary



Professor Joshua Erlich, Physics

College of William & Mary



Mansfield Associate Professor of Physics, Patricia Vahle, Physics
College of William & Mary



Dr. Emanuele Mereghetti, Physics

Los Alamos National Laboratory

ABSTRACT

The Standard Model (SM), the fundamental theory of particle physics, very successfully describes the world around us, and with a only a few tantalizing exceptions, all the experiments we have performed to understand the fundamental laws of nature. However, the SM accounts for only 4-5% of the matter and energy in the universe, with approximately 25% composed of dark matter (DM) and the remaining 70% composed of the more mysterious dark energy. Further, the SM content of the universe is composed of an excess of matter over anti-matter of about 1 part per billion. Despite being a small excess, it is orders of magnitude larger than can be explained by the SM alone. These observations strongly suggest there is new physics Beyond the Standard Model (BSM).

One of the most exciting prospects for searching for physics BSM is $0\nu\beta\beta$. Detecting $0\nu\beta\beta$ is one of the current top scientific priorities of The Nuclear Science Advisory Committee and a new initiative, a ton-scale $0\nu\beta\beta$ experiment, is described in their Long Range Plan for Nuclear Science [1]. There are many experiments designed world wide to search for evidence of physics BSM, however, the ton-scale search for $0\nu\beta\beta$ in large nuclei is the most prominent new nuclear physics (NP) experiment. $0\nu\beta\beta$, if allowed, is an extremely rare nuclear decay, which violates one of the fundamental symmetries of the Standard Model (SM). Therefore, if observed, $0\nu\beta\beta$ may provide a possible explanation for the observed abundance of matter over anti-matter in the universe as this lepton number violation could be converted to baryon number violation very early in the universe. $0\nu\beta\beta$ would happen in a process where two neutrons decay simultaneously into two protons and two electrons but without the emission of any neutrinos. If the neutrinos are their own antiparticles (Majorana-like), the most plausible case, a neutrino emitted from one of the beta-decaying neutrons can be absorbed by the other neutron. This interaction would happen at short distance scales. Thus, a series of calculations based on Quantum ChromoDynamics (QCD), the fundamental theory of nuclear strong interactions, will be required to interpret the results of $0\nu\beta\beta$ experiments, along with many other NP experiments. However, the only way to perform such calculations to the required accuracy is by using a numerical technique known as lattice QCD (LQCD).

TABLE OF CONTENTS

Acknowledgments	iv
Dedication	v
List of Tables	vi
List of Figures	vii
CHAPTER	
1 Introduction	2
1.1 Motivation	2
1.1.1 Baryon asymmetry	3
1.1.2 Neutrino masses	3
1.1.3 $0\nu\beta\beta$ Decay	4
1.2 Effective Field Theories	8
1.2.1 Effective Field Theory for Nuclear Physics	8
1.2.2 Effective Field Theory for $0\nu\beta\beta$	10
1.3 QCD basics	12
1.3.1 Quarks and Gluons	12
1.3.2 Path Integral Formulation of QCD	13
1.3.3 Fermion Action	14
1.3.4 Gluon Action	15
1.4 QCD on a Lattice	17
1.4.1 Gauge Invariant Fermion Action on the Lattice	18
1.4.2 Link variables and Gluon Action	19

1.4.3	Particles in the Lattice: Correlation Functions and Effective Mass	20
2	Non-perturbative Renormalization on the Lattice: Four-quark and Bilinear Operators	26
2.1	Background	28
2.2	Bilinear Operator Renormalization	31
2.2.1	Scheme Details	31
2.2.2	Results	34
2.3	Four-quark Operators Renormalization	39
2.3.1	Scheme Details	39
2.3.2	Four-quark Results	42
2.4	Raising The Renormalization Scale	44
2.5	$\overline{\text{MS}}$ Matching For Mixed Basis	47
3	Application: Nucleon Axial Charge	50
3.1	Feynman-Hellman Method	51
3.2	Lattice Calculation Details	54
3.3	Correlation functions analysis	56
3.3.1	Fitting procedure	56
3.4	Chiral, Continuum and infinite volume extrapolations	57
3.5	Final Result	63
4	Short Range Contributions to $0\nu\beta\beta$	64
4.1	$\pi^- \rightarrow \pi^+$ Contribution	67
4.1.1	Four-quark Operators	67
4.1.2	Numerical Method	67
4.1.3	Chiral, continuum and infinite volume extrapolations	71
4.1.4	Extrapolation and Results	76
4.1.5	Nuclear Potentials and $n\bar{n} \rightarrow ppe^-e^-$ Decay Amplitude	79

4.2 Four-quark Feynman-Hellman Method	81
5 Conclusions And Future Work	88
APPENDIX A	
Gamma Matrices	90
APPENDIX B	
Fierz Transformations	91
Bibliography	94
Vita	105

ACKNOWLEDGMENTS

In this journey, I have been blessed with the support of many people who I would like to thank. First, My wife Cristina and my children Henry and Emily have been always by my side. My parents, siblings and friends whose support has been invaluable in many occasions.

I am very grateful to my mentor Dr. André Walker-Loud who have always supported me beyond his duties. His knowledge, hard work and leadership have taught me a lot and helped me to move forward in my research, especially when research and work was not going as I expected.

I would like to thank to the people in the CalLat group whose work has provided me with data and code for my research. Their willingness to help and to share their knowledge will always be appreciated. I would like to thank as well to all the people involved in my different research projects, especially to those I closely worked with: Dr. Nicolas Garron, Dr. David Brantley, Dr. Amy Nicholson.

I thank Dr. rer. nat. Francisco Frutos Alfaro for encouraging me to pursue a graduate degree and supporting me since I was his student.

Finally, to those from who I learned to work hard: My parents, Dr. André Walker-Loud and Dr. rer. nat. Francisco Frutos Alfaro.

To those whose immensurable support and unconditional love have driven me to come this far: my wife Cristina, my children Henry and Emily, my parents Sara and Pablo, and my siblings Elizabeth, Pablo and Jairo. Thanks for always been there for me.

LIST OF TABLES

2.1	Parameter details of the ensembles employed in the renormalization.	32
2.2	g_V^b values determined in [2] and used here to determine g_V^r	34
2.3	Bilinear renormalization constants determined at the scale $\mu = 2\text{GeV}$ in the γ -scheme.	38
2.4	Bilinear renormalization constants determined at the scale $\mu = 2\text{GeV}$ in the \mathfrak{q} -scheme.	38
2.5	Renormalization matrix values determined at $\mu = 2\text{GeV}$ for four-quark operators	42
2.6	$\mu = 2\text{GeV} \rightarrow 3\text{GeV}$ step scaling function values for bilinear operators in the γ -scheme.	45
2.7	$\mu = 2\text{GeV} \rightarrow 3\text{GeV}$ step scaling function values for bilinear operators in the \mathfrak{q} -scheme.	45
2.8	$\mu : 2\text{GeV} \rightarrow 3\text{GeV}$ step scaling function values for four-quark operators in the γ -scheme.	46
2.9	Bilinear renormalization constants determined at the scale $\mu = 3\text{GeV}$ in the γ -scheme.	47
2.10	Bilinear renormalization constants determined at the scale $\mu = 3\text{GeV}$ in the \mathfrak{q} -scheme.	47
2.11	Renormalization matrix values determined at $\mu = 3\text{GeV}$ for four-quark operators.	48
4.1	LEC values determined from fits	78
4.2	Resulting matrix elements extrapolated to the physical point, renormalized in RI/SMOM and $\overline{\text{MS}}$, both at $\mu = 3\text{ GeV}$	79

LIST OF FIGURES

1.1	Observed electron energy spectrum for $2\nu\beta\beta$ and $0\nu\beta\beta$ decays.	5
1.2	Diagram for $0\nu\beta\beta$ arising from a heavy majorana neutrino exchange.	8
1.3	m_{eff} plots for Ω^- baryon (Top) and π^+ meson (bottom).	25
2.1	Kinematical configuration for the bilinear renormalization vertex in RI-MOM and RI-SMOM schemes.	32
2.2	Z_A/Z_V and Z_S/Z_P ratios for lattice spacings $a = 0.09, 0.12, 0.15$ fm and $m_\pi = 220$ MeV.	35
2.3	Quark wave function and quark mass amputated vertices $\frac{\Lambda_q}{\Lambda_V}$ and $\frac{\Lambda_m}{\Lambda_V}$ fits.	36
2.4	Scalar and Pseudoscalar bilinear currents amputated vertices $\frac{\Lambda_S}{\Lambda_V}$ and $\frac{\Lambda_P}{\Lambda_V}$ fits.	37
2.5	Scalar and Pseudoscalar bilinear currents amputated vertices $\frac{\Lambda_A}{\Lambda_V}$ and $\frac{\Lambda_T}{\Lambda_V}$ fits.	37
2.6	Kinematical configuration for the four-quark renormalization vertex in RI-MOM and RI-SMOM schemes.	40
2.7	Four-quark operators renormalization vertex matrix Λ fit samples.	43
2.8	Four-quark operator step scaling function Σ_{32} fit sample.	46
3.1	Feynman diagrams for computing the axial charge g_A in the standard and Feynman-Hellman methods.	55
3.2	g_A data fit example for ensemble with lattice spacing $a \approx 0.09$ fm and $m_\pi \approx 220$ MeV.	58
3.3	Extrapolating fits for contributions up to NNLO to g_A	59
3.4	Infinite volume extrapolation of g_A	60

3.5	Continuum extrapolation of g_A	62
4.1	Diagrams for processes contributing to $0\nu\beta\beta$ through short range interactions.	66
4.2	Three-point function diagram for four-quark operators contributing to $\pi^- \rightarrow \pi^+$	70
4.3	Fits to the ratios \mathcal{R}_i for the different operators.	76
4.4	Fits to the chiral extrapolation formulae for the different operators.	77
4.5	Diagram for the three-point function in the σ theory.	85

LATTICE QCD FOR NEUTRINOLESS DOUBLE BETA DECAY:
SHORT RANGE OPERATOR CONTRIBUTIONS

CHAPTER 1

Introduction

In this chapter, a review of neutrinoless double beta-decay ($0\nu\beta\beta$) including prospective short range contributions is presented along with the main theoretical tools used. This chapter will serve as well to introduce the notation to be used in the remaining text.

1.1 Motivation

The electromagnetic, strong and weak interactions of particles are currently well described by the SM, the fundamental theory of particle physics. While in excellent agreement with almost all the experiments that have been performed, there are few tantalizing exceptions. For example, the matter content of the early universe is slightly greater than the antimatter content which can not be explained alone with the SM and new physics BSM may hold the answer. Additionally, while SM neutrinos are massless, neutrino oscillation experiments have demonstrated they have non-zero mass, and to describe them, extending or modifying the SM to include massive neutrinos are some of the possibilities.

1.1.1 Baryon asymmetry

To the best of our knowledge, only 4-5% of the energy budget of the universe arises from the SM, approximately 25% composed of dark matter and the remaining $\approx 70\%$ composed of the more mysterious dark energy. In the early universe, the amount of matter exceeded that of anti-matter by about 1 part per billion, and due to this slight difference, matter and antimatter did not completely annihilate and matter was allowed to combine into the different existing elements.

Such baryonic matter asymmetry could be produced by baryonic number violating processes or by conversion of a lepton matter excess to baryon matter excess through sphaleron processes (where three leptons are converted into three baryons). In the second case for example, Leptogenesis, due to Lepton Number Violation (LNV) processes arising from CP violation from BSM physics, could give rise to the lepton matter excess. There are several LNV processes, such as $K^+ \rightarrow \mu^+ \mu^+ \pi^-$, $\mu^- + (Z, A) \rightarrow e^+ + (Z - 2, A)$ or $\bar{\nu}_e$ emission from the Sun and $0\nu\beta\beta$. $0\nu\beta\beta$ is one of the most sensitive tests for new LNV physics [3].

1.1.2 Neutrino masses

Until a few years ago, neutrinos appeared only as massless particles in the SM. However with the discovery of neutrino oscillations and its experimental confirmation [4, 5, 6, 7, 8, 9, 10, 11, 12, 13, 14, 15, 16, 17, 18, 19, 20, 21, 22, 23, 24, 25, 26, 27, 28] we now know they are massive. Even though oscillation experimental results demonstrated neutrinos have mass, no further information was obtained about the nature of their masses. Several mass models have been proposed, and two feasible options are Dirac and Majorana neutrino masses which are briefly discussed in [29]. In the case of Majorana neutrinos, these are not forbidden by unbroken SM gauge symmetries, and thus are considered a plau-

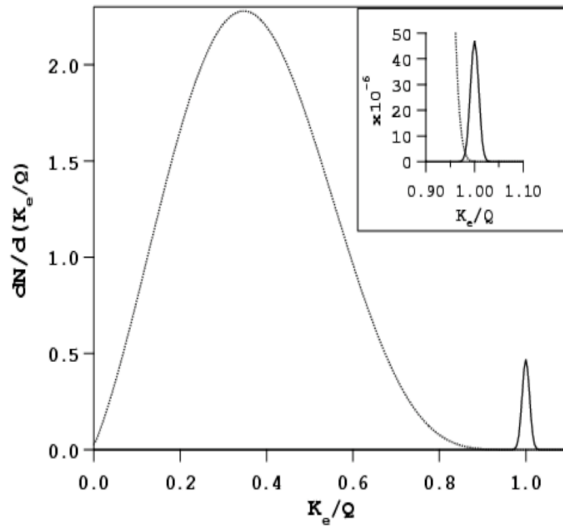
sible possibility. Most importantly, understanding the generating mechanisms and type of neutrino masses can significantly impact our view of the universe. As a consequence, world wide efforts in search of observational evidence are underway to look for information on the neutrino masses. At the present time, current experimental limits on $0\nu\beta\beta$ half-lives are given in [30, 31, 32, 33, 34, 35, 36, 37, 38, 39], and for example are set to $T_{1/2}^{0\nu} > 2.1 \cdot 10^{25}$ yr for ^{76}Ge [36] and $T_{1/2}^{0\nu} > 1.07 \cdot 10^{26}$ yr for ^{136}Xe [34]. Among them, several experiments to search for $0\nu\beta\beta$ decay, such as LEGEND [40], CUORE [41], GERDA [42], AMoRE [43], KamLAND-Zen [44], nEXO [45] and NEXT [46] represent major efforts to better understand the nature of the neutrino masses.

1.1.3 $0\nu\beta\beta$ Decay

Double β decays are second order weak processes, where a nucleus emits two electrons and thus changes its charge in two units:

$$(A, Z) \rightarrow (A, Z + 2) + 2e^- \quad (1.1)$$

When two neutrinos are emitted in the process, the decay is known as $2\nu\beta\beta$ whereas the decay without neutrinos is called $0\nu\beta\beta$. To date, only $2\nu\beta\beta$ has been observed and its typical half-life is $\approx 10^{19-20}$ years for the nuclei where Q values (the energies released in the reaction) are above 2 MeV [3]. On the other hand $0\nu\beta\beta$ still remains unobserved with limits to its half-life set to several orders of magnitude higher than those of $2\nu\beta\beta$. For both decays, most of the energy is carried by the leptons, however an important difference between these decays is the shape of the distribution of the emitted electron's kinetic energy spectrum, which in the case of $2\nu\beta\beta$ is continuous and peaked below $Q/2$. On the other hand, in $0\nu\beta\beta$ decays the energy released must be distributed only among two electrons, as a consequence the distribution is highly peaked at Q . Therefore, the peak



(a)

FIG. 1.1: Observed electron energy spectrum for $2\nu\beta\beta$ and $0\nu\beta\beta$ decays. The left peak corresponds to $2\nu\beta\beta$ and the right peak to $0\nu\beta\beta$. Figure obtained from [3]

separation allows one to experimentally distinguish between $2\nu\beta\beta$ and $0\nu\beta\beta$ as long as the instrument's energy resolution is enough to separate both peaks. These peaks are shown in figure 1.1.

In practice, to observe a signal of such rare decays, large detectors are required to observe signals, especially in the case of a neutrino mass inverted hierarchy for which the half-life is expected to be higher. For example, one complication arising is the fact that background contamination is high at energies below 3 MeV. Nevertheless, some key features of these decays can help to overcome the difficulties. For example, the long life time of $\beta\beta$ isotopes makes it possible to collect enough $\beta\beta$ isotopes to perform ton-scale (10^{28}) experiments and there are even-even nuclei where the double beta decays are allowed but single β decay is not. These and other experimental features are detailed in [47].

From these experiments searching $0\nu\beta\beta$, what can be determined are the corresponding decay rates. Nevertheless, in the case a positive signal is observed theoretical input is

required to interpret the results as the mechanisms responsible for $0\nu\beta\beta$ are still unknown. For example, observed decay rates may not be compatible with a particular model and thus lead to constraints on the possible mechanisms. Additionally, with sufficient theoretical control, it should be in principle possible to separate contributions from different LNV sources through different isotope measurements, the angular or energy distributions of the outgoing electrons, or looking at correlations with collider observables [48].

Then, in order to extract information from the observed decay rates, the half-life for the different mechanisms must be considered. For example, for long range processes mediated by a neutrino exchange, the half-life is given by:

$$\frac{1}{T_{1/2}^\nu} = G^\nu(Q, Z)|M^\nu|^2 \langle m_{\beta\beta} \rangle^2 \quad (1.2)$$

Where the neutrino masses are included in the $m_{\beta\beta}$ effective neutrino masses. The quantity $G^\nu(Q, Z)$ is the phase space factor which has been previously calculated for both decays in [49, 50, 51]. $|M^\nu|^2$ is the Nuclear Matrix Element (NME) which can not be determined alone from experiment, therefore it must be determined theoretically and, due to the nuclear many-body nature of the process, only approximate estimates have been obtained [52]. For $0\nu\beta\beta$ mediated by a Majorana neutrino, the diagram showing the quark level interactions mediated by W^- bosons is shown in figure 1.2.

On the other hand, for the short range mechanisms addressed here, no neutrinos are exchanged, and thus a half-life is given by:

$$\frac{1}{T_{1/2}^\nu} = G^\nu(Q, Z)|M^\nu|^2 |\epsilon_\nu|^2 \quad (1.3)$$

In this case, instead of being proportional to the neutrino masses, the half-life involves the coupling constant ϵ_ν which parametrizes the underlying particle physics dynamics [53].

Moreover, it is also possible that long and short processes contributions are similar. For example, this would be the case for models where long range contributions originate from LNV at scales between $1 - 10$ TeV [48]. In such a case, the $0\nu\beta\beta$ half life is given by the sum of both types of contributions:

$$\frac{1}{T_{1/2}^\nu} = G^\nu(Q, Z)|M^\nu|^2\langle m_{\beta\beta} \rangle^2 + G^\nu(Q, Z)|M^\nu|^2|\epsilon_\nu|^2, \quad (1.4)$$

then the long and short range contributions can not be isolated with a single measurement, however improvements on the theory side might allow to separate contributions from different LNV sources through different isotope measurements, the angular or energy distributions of the outgoing electrons, or looking at correlations with collider observables.

It is to the determination of $|M^\nu|^2$ (for the short range interactions) where Lattice QCD can contribute. In fact, as the short range contributions arise from the non-perturbative regime of QCD, LQCD is the only tool available to perform such task, and calculations in this work corresponds to the first numerical determination of short range interaction contributions to $0\nu\beta\beta$.

Another important aspect are the nuclear transitions, which can help identify the processes contributing the most. In particular for $0\nu\beta\beta$, the most significant contributions come from $0^+ \rightarrow 0^+$ while $0^+ \rightarrow 2^+$ contributions are greatly suppressed [54]. For this reason, the experimental efforts are focused on the $0^+ \rightarrow 0^+$ transitions and only those will be considered here.

Finally, two major reasons driving the searches for $0\nu\beta\beta$ are the demonstration of LNV and the existence of a neutrino Majorana mass [56]. Both would significantly impact physics as it could help us to understand the neutrino mass generating mechanisms, and to possibly explain the universe matter-antimatter asymmetry as LNV leads to Leptogenesis [57, 58].

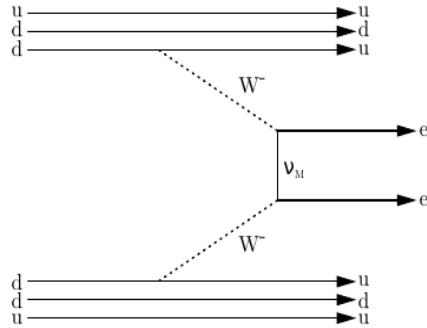


FIG. 1.2: Diagram for $0\nu\beta\beta$ arising from a heavy majorana neutrino exchange. Figure taken from [55]

1.2 Effective Field Theories

1.2.1 Effective Field Theory for Nuclear Physics

One of the major challenges in nuclear physics is to understand different phenomena and nuclei directly from the fundamental theory of the strong interactions QCD. However, there is no analytical solution for QCD, and Perturbation Theory can only be used at high energies where the coupling decreases. On the other hand, at the low energies relevant for nuclear physics the coupling increases and a non-perturbative solution as LQCD is required. However, in some cases we will need to incorporate QCD effects arising at high energies to describe low energy phenomena, this is just what Effective Field Theory (EFT) can do. EFT was first developed by Weinberg [59] and later proposed for its application to nuclear physics [60].

In an EFT, a description in terms of the most relevant degrees of freedom is done while the effects of the remaining degrees of freedom, appearing in the underlying theory, are parameterised into low-energy constants usually known as Wilson coefficients which encapsulate the high energy physics details.

However, to distinguish between the appropriate degrees of freedom to keep and the

non-relevant, high and low energy scales must be clearly separated, such that the energy regimes to be described by the different sets of degrees of freedom can be identified [61]. In such a case, the first step is to write down a Lagrangian with all the operators consistent with the symmetries of the underlying theory, and a power counting scheme must be found to organize the contributions from these operators by their relative size. For example, a small parameter suppressing the different operators must be found such that contributions can be organized by their orders in this parameter, and thus a systematic way to improve calculations exists.

In nuclear physics, a proper and precise description of experiments in the low-energy regime does not usually require a complete consideration of short range interactions, indicating that the use of EFTs may be feasible. Moreover, clear separation of scales appear, for example, the nucleon binding energies are of the order of a few MeV while at next scale lies the pion with mass of $m_\pi = 140\text{MeV}$ resulted in the development of what is known as pionless EFT [62] for the study of two-nucleon systems where external momenta is much lower than the pion mass. This has been very successful for low-energy and the first few nuclei. To understand larger nuclei or larger energies, an EFT with explicit pions is needed [63]. This is becoming a very useful tool for understanding of nuclear properties from the strong interactions, where the increasing number of nucleons further limits our ability to predict these properties from QCD [64].

For nuclear processes where strong interactions are relevant, EFTs may provide a framework to separately solve the underlying interactions, i.e. QCD, to then incorporate their effects into the theory describing the nucleon interactions. This would not only simplify the task but also remove nuclear model dependent assumptions from the QCD solution. For example, using LQCD, matrix elements can be calculated non-perturbatively and using EFT, the results can be matched into a particular phenomenological nuclear model.

Hence EFTs provide nuclear physics with an useful tool to understand nuclear properties from strong interactions, where the increasing number of nucleons further limits our ability to predict these properties from QCD [64]. In addition, the possibility to systematically improve the calculations represents an additional advantage over other approaches.

1.2.2 Effective Field Theory for $0\nu\beta\beta$

In $0\nu\beta\beta$ decay lepton number conservation is violated by 2 units and thus it is not allowed in SM. Nevertheless, as Lepton number conservation is an accidental symmetry in the SM, it may be violated at energies higher than those of SM. Thus, if SM is considered a low-energy effective theory, LNV effects originating at a high energy scale Λ can be described using an EFT approach.

Due to the different energy scales involved in $0\nu\beta\beta$, it is possible to find a sequence of EFTs to describe LNV effects arising at high energy scales leading to $0\nu\beta\beta$ at the low-energy scales relevant to nuclear physics. In these EFTs, high order operators and low energy constants are used to incorporate the high energy physics into the low-energy theory. This process is described in detail in [48] and it will be reviewed next.

The first step is to extend the SM Lagrangian with the relevant high order operators and then this must be matched into an EFT at energies below the electroweak symmetry breaking scale. For $\Delta L = 2$ processes these operators must be of odd dimensions [65] and for this discussion $\text{dim}=5,7,9$ are considered. Renormalization of these operators requires that they are suppressed by powers of Λ^{-1} , Λ^{-3} , Λ^{-5} and therefore their contributions will depend on the models as it will be seen next for the dim-5 operator case.

Dim-5 operator contributions are naively expected to be the most significant. There is only one dim-5 operator that can be written down in terms of SM fields: the Weinberg operator, which violates Lepton number in 2 units. At the GUT-scale $\Lambda \approx 10^{15}$ GeV, heavy

right-handed neutrinos can be integrated out and lead to this operator contributing to the Majorana neutrino mass [66] after electroweak symmetry breaking. This corresponds to what is known as the type-I see-saw mechanism, and in this case the contributions would be suppressed by powers of $\nu/\Lambda \approx 10^{-13}$ where $\nu = 246$ GeV is the electroweak scale.

For lower LNV scales, this dim-5 operator may be suppressed as well. For example, loop factors or small yukawa couplings \mathbf{y} could lead to suppression factors $\mathbf{y}^2/\Lambda \approx 10^{-6}$. In the case of operators of higher dimensions, the suppression factor may be instead proportional \mathbf{y} , \mathbf{y}^0 , in such cases short range operator contributions may contribute as much as long range ones.

Dimension-7 operators have been previously found in [67]. These operators contribute to $0\nu\beta\beta$ by inducing dimension-5 (a neutrino Majorana mass), dimension-six, -seven, and -nine operators after electroweak symmetry breaking [68] and lead to long and short range contributions. On the other hand, for dim-9 operators there are only eleven operators which contain four quarks and two electrons, these are found in [69], however, other types of dim-9 operators could lead unsuppressed contributions.

The operators described above must then first be matched onto a low-energy EFT (below the electroweak symmetry breaking scale) where dim=3,6,7,9 operators are induced and lead to different long and short range contributions. For example, dim-3 and -7 lead to long range interactions mediated by a neutrino exchange, whereas dim-9 operators lead to short range contributions which are not mediated by neutrinos and thus not proportional to neutrino masses. The latter are the focus of this work.

Afterwards, to compute the contributions from the short range interactions, the corresponding operators must be evolved to the QCD scale, where LQCD and then χ PT, the low-energy theory of QCD, can be used to compute matrix elements arising from these operators.

Then, in order to perform the matching of χ PT to a theory at the nucleon level, parity

and chiral symmetries are used to identify the relevant local quark-lepton operators, these have been previously found in [3], and the long and short range interactions they induce will be further discussed in chapter 4. Once these local quark-lepton operators are identified, the only way to compute their contributions to $0\nu\beta\beta$ decay is to use LQCD due to the non-perturbative nature of these contributions. Then, these results can be employed in the two nucleon interactions relevant to $0\nu\beta\beta$. The two nucleon interactions can then be used to compute the nuclear matrix elements and the $0\nu\beta\beta$ decay rate can be estimated.

1.3 QCD basics

QCD is the theory of the strong interactions between quarks and gluons. These interactions obey the principles of a relativistic Quantum Field Theory, with an additional non-abelian gauge invariance, color $\mathbf{SU}(3)$, which is an exact symmetry. The strength of QCD interactions at distances $\gtrsim 1$ fm leads to color confinement [70]: colored quarks and gluons are bound inside color neutral hadrons and never observed as asymptotic states. Conversely, the strength of the interaction decreases at shorter distance scales, a property known as asymptotic freedom [71, 72, 73, 74].

1.3.1 Quarks and Gluons

The strongly interacting particles are the quarks and gluons. The quarks are massive particles, with spin $1/2$ and two additional intrinsic properties: color and flavor. Hence they can be mathematically represented by Dirac spinors which also carry color and flavor indices. The six flavors are up, down, strange, charm, bottom, top, and the three colors usually identified by red, green, blue or by the indices 1,2,3. Here, lower greek and latin letters will denote Lorentz and color indices respectively. Flavor indices will be displayed with an f upper index, and finally x represents the space-time position. With this

convention, a quark field will be represented as:

$$\psi^f(x)_{\alpha,c} \quad \alpha = 1, 2, 3, 4 \quad c = 1, 2, 3 \quad f = 1, 2, 3, 4, 5, 6 \quad (1.5)$$

The gluons are spin 1 vector gauge fields which carry a lorentz index corresponding to its direction and two color indices, hence they are represented as:

$$A(x)_{\mu,cd} \quad \mu = 1, 2, 3, 4 \quad c, d = 1, 2, 3 \quad (1.6)$$

Moreover, the color structure of the gluon fields is represented by traceless Hermitian matrices (Gell-Mann matrices for example), which is a consequence of the SU(3) gauge invariance of QCD.

1.3.2 Path Integral Formulation of QCD

The path integral formulation of QCD is a framework which uses the action principle and path integrals to describe QCD. The action contains all the details of the interaction, and contributions from all those interactions to a certain amplitude are computed through the path integral. Because a numerical solution will be used, we work on a Euclidean space and this choice will be discussed in when the LQCD foundations introduced. In Euclidean space instead of the usual Minkowski space, this formalism presents similarities to Statistical Mechanics. In this formulation, the expectation value of an observable \mathcal{O} is given by:

$$\langle \mathcal{O} \rangle = \frac{1}{Z} \int \mathcal{D}A_\mu \mathcal{D}\psi \mathcal{D}\bar{\psi} \mathcal{O} e^{-S} \quad (1.7)$$

where $\mathcal{D}A_\mu$ represents the measure corresponding to all the possible gauge fields A_μ . In the case of interest, QCD, the action is given by $S_{\text{QCD}} = S_G + S_F$, with the gluon action

S_G and the fermion S_F , which can be separated and will be described next.

Finally, the partition function Z is given by:

$$Z = \int \mathcal{D}A_\mu \mathcal{D}\psi \mathcal{D}\bar{\psi} e^{-S} \quad (1.8)$$

Using this path integral formulation, the method of sources can be used to compute matrix elements. The basic idea is to add an interaction term $S_{\text{int}} = \lambda \tilde{S}_{\text{int}}$ to the action, such that a matrix element can be obtained by applications of ∂_λ to the path integral; then by setting $\lambda = 0$ the matrix element is related to the non-interacting theory.

1.3.3 Fermion Action

The fermion action in QCD is required to be Lorentz and gauge invariant under $SU(3)$ (local rotations of color indices). Gauge invariance is achieved through a covariant derivative which contains a term coupling the quarks and gluons. Showing explicitly how the different fields are coupled, spin and color indices are kept to write the fermion action (in Euclidean space) as follows:

$$S_F^0[\psi, \bar{\psi}] = \sum_{f=1}^{N_f} \int d^4x \bar{\psi}^f(x)_{\alpha,c} \left((\gamma^\mu)_{\alpha\beta} (\delta_{cd} \partial_\mu + ig A(x)_{\mu,cd}) + m \delta_{cd} \delta_{\alpha\beta} \right) \psi^f(x)_{\beta,d} \quad (1.9)$$

Here, γ^μ correspond to the Euclidean version of the γ matrices in Minkowski space. These and the conventions used for the Dirac matrices, are available in appendix A.

From 1.9 it is easy to see that quark and gluons couple, at a given space-time point, only in color space, hence their coupling is independent of the quark flavour. The gauge invariance requirement for this action can be fulfilled in a similar fashion to the QED action, that is by definition of proper covariant derivatives and gauge fields.

To verify gauge invariance, let $\Omega(\mathbf{x})$ be an independent complex 3×3 unitary matrix, i.e. a matrix in the $SU(3)$ group. Thus, a local rotation in color space of the quark fields corresponds to:

$$\psi(\mathbf{x}) \rightarrow \psi'(\mathbf{x}) = \Omega(\mathbf{x})\psi(\mathbf{x}) \quad \bar{\psi}(\mathbf{x}) \rightarrow \bar{\psi}'(\mathbf{x}) = \bar{\psi}(\mathbf{x})\Omega(\mathbf{x})^\dagger \quad (1.10)$$

Applying this transformation to the fermion action 1.9, shows that mass term is invariant and that the covariant derivative D_μ must transform as follows:

$$\partial_\mu + i\mathbf{A}(\mathbf{x})_\mu \rightarrow \Omega(\mathbf{x})^\dagger(\partial_\mu + i\mathbf{A}'(\mathbf{x})_\mu)\Omega(\mathbf{x}) \quad (1.11)$$

$$\rightarrow \partial_\mu + \Omega(\mathbf{x})^\dagger(\partial_\mu\Omega(\mathbf{x})) + i\Omega(\mathbf{x})^\dagger\mathbf{A}'_\mu(\mathbf{x})\Omega(\mathbf{x}) \quad (1.12)$$

The fermion action is then gauge invariant if the gluon fields are hermitian and traceless matrices transforming as:

$$\mathbf{A}(\mathbf{x})_\mu \rightarrow \mathbf{A}'(\mathbf{x})_\mu = \Omega(\mathbf{x})^\dagger\mathbf{A}_\mu(\mathbf{x})\Omega(\mathbf{x}) + i(\partial_\mu\Omega(\mathbf{x}))\Omega(\mathbf{x})^\dagger \quad (1.13)$$

1.3.4 Gluon Action

The gluon field in QCD appears as consequence of the gauge invariance requirement for the free fermions. For example, if \mathbf{A}_μ is set to zero in the fermion action, 1.12 shows that a rotation in color space would introduce an additional term through the derivative's transformation.

Nevertheless, when introducing gauge fields which transform as in 1.13, the action for these fields must also be invariant under the transformation 1.10. In a similar manner to

QED, a proposed gluon action is:

$$S_G^0[A] = \frac{1}{4} \int d^4x F_{\mu\nu}^a(x) F^{\mu\nu,a}(x) \quad (1.14)$$

where the $F_{\mu\nu}^a = \partial_\mu A_\nu^a - \partial_\nu A_\mu^a + i[A_\mu, A_\nu]$ and the sum over the index \mathbf{a} is required to obtain a gauge invariant S_G . The replacement for A_μ^a here is based on the fact that A_μ is a hermitian traceless matrix, belongs to the Lie Algebra $SU(3)$, and thus can be written as:

$$A_\mu = \sum_{a=1}^8 A_\mu^a T_a \quad (1.15)$$

For T_i corresponding to a basis of hermitian 3×3 matrices. Then, after simplifying the commutator, the gluon field strength tensor can be written as:

$$F_{\mu\nu}^a = \partial_\mu A_\nu^a - \partial_\nu A_\mu^a + g f^{abc} A_\mu^b A_\nu^c \quad (1.16)$$

where f^{abc} are structure constants of the Lie Algebra. It is also easy to see from 1.16 that the a difference between QCD with QED arises from the last term which includes the self interaction of the gluons.

Moreover, the strong coupling g between the gluons and quarks behaves differently than its QED analog as the first one becomes smaller at higher energies. This property is known as asymptotic freedom [71, 72, 73, 74] and is what enables a perturbative treatment of the strong interactions at high energies.

1.4 QCD on a Lattice

In order to develop a useful numerical version of QCD, the standard framework to use is the Euclidean Path Integral formalism, which will be used from here on. The connection of which to the respective Minkowski space-time version is found by analytical continuation, or Wick rotating the time direction. Using this formalism, the numerical task at hand is then calculation of a path integral with a very large number of degrees of freedom, and thus solving the integral for each degree of freedom becomes prohibitive.

However, one important feature of the Euclidean path integral is the fact that the action S in the term $\text{Det}[\not{D} + \mathbf{m}] \mathcal{D}A_\mu e^{-S}$ in 1.7, for zero chemical potential, is real and bounded from below, whereas this is not necessarily the case on Minkowski space-time. This guarantees that the exponential e^{-S} is a decaying instead of a largely oscillating quantity. Therefore, $\text{Det}[\not{D} + \mathbf{m}] \mathcal{D}A_\mu e^{-S}$ can be reinterpreted as a probability and the calculation of observables becomes analogous to Statistical Mechanics calculations. Moreover, this enables the use Monte Carlo techniques which are very efficient for problems with a large number of degrees of freedom. Hence, solving the path of integral in QCD can be performed with Monte Carlo techniques, and further simplified by the separation of the fermionic and gluonic components.

The first goal is then to find a discrete expression for 1.7. For that purpose, consider a finite volume space-time V , and represent it on a lattice Λ :

$$\Lambda = \{\mathbf{n} = (\mathbf{n}_1, \mathbf{n}_2, \mathbf{n}_3, \mathbf{n}_4) | \mathbf{n}_1, \mathbf{n}_2, \mathbf{n}_3 = 0, 1, \dots, N - 1; \mathbf{n}_4 = 0, \dots, N_T - 1\} \quad (1.17)$$

The space-time points in this lattice are separated by a distance “ \mathbf{a} ”, which is called the lattice spacing. Thus a point \mathbf{n} in the lattice represents a physical space-time point with value $x = \mathbf{a}\mathbf{n}$. Then, a space vector will be represented as $\mathbf{n} = (\mathbf{n}_1, \mathbf{n}_2, \mathbf{n}_3)$ and

a space-time vector is represented by $\mathbf{n} = (n_1, n_2, n_3, n_4)$, where n_4 is the time. With this convention, a quark field $\psi(\mathbf{x})$ will be defined at each lattice site “ \mathbf{n} ” as $\psi(\mathbf{n})$. The boundary condition commonly used in the lattice is periodic for gauge fields and anti-periodic in time for all other fields.

1.4.1 Gauge Invariant Fermion Action on the Lattice

To discretize the fermion action, we will first look at the free fermion action (where $A_\mu = 0$). This is achieved by replacing the integration by a sum and then, discretizing the partial derivatives acting on the quarks. A simple discretization of $\partial_\mu \psi(\mathbf{x})$ is

$$\partial_\mu \psi(\mathbf{x}) \rightarrow \frac{1}{2a} (\psi(\mathbf{n} + \hat{\mu}) - \psi(\mathbf{n} - \hat{\mu})) \quad (1.18)$$

Upon replacement onto 1.9, the naively discretized fermion action is [75]:

$$S_F^0[\psi, \bar{\psi}] = a^4 \sum_{\mathbf{n} \in \Lambda} \bar{\psi}(\mathbf{n}) \left(\sum_{\mu=1}^4 \gamma_\mu \frac{\psi(\mathbf{n} + \hat{\mu}) - \psi(\mathbf{n} - \hat{\mu})}{2a} + m\psi(\mathbf{n}) \right) \quad (1.19)$$

The problem with the above action is that it is not gauge invariant and A_μ can not be used to make it gauge invariant because different space-time points are connected in the derivative. However, this can be solved by introducing a gauge link $U_\mu(\mathbf{n})$ with a directional index μ and transforming under a color rotation in the lattice as:

$$U_\mu(\mathbf{n}) \rightarrow U'_\mu(\mathbf{n}) = \Omega(\mathbf{n}) U_\mu(\mathbf{n}) \Omega(\mathbf{n} + \hat{\mu})^\dagger \quad (1.20)$$

where $\Omega(\mathbf{n})$ is a $SU(3)$ matrix (equivalent to $\Omega(\mathbf{x})$ in 1.10 in the continuum). Then, the term $\bar{\psi}(\mathbf{n})\psi(\mathbf{n}+\hat{\mu})$ can be replaced in the action by the gauge invariant term $\bar{\psi}(\mathbf{n})U_\mu(\mathbf{n})\psi(\mathbf{n}+$

$\hat{\mu}$) and thus a gauge invariant action for fermions in a external gauge \mathbf{U} can be defined as [76]:

$$S_F^0[\psi, \bar{\psi}] = a^4 \sum_{\mathbf{n} \in \Lambda} \bar{\psi}(\mathbf{n}) \left(\sum_{\mu=1}^4 \gamma_\mu \frac{\mathbf{U}_\mu(\mathbf{n})\psi(\mathbf{n} + \hat{\mu}) - \mathbf{U}_{-\mu}(\mathbf{n})\psi(\mathbf{n} - \hat{\mu})}{2a} + m\psi(\mathbf{n}) \right) \quad (1.21)$$

1.4.2 Link variables and Gluon Action

The gauge fields \mathbf{U}_μ introduced above are known as link variables, as they connect to different lattices sites, transform in the same way the continuum gauge transporter does and it thus possible to relate them to lattice gauge fields \mathbf{A}_μ which satisfy:

$$\mathbf{U}_\mu(\mathbf{n}) = e^{ia\mathbf{A}_\mu(\mathbf{n})} \quad (1.22)$$

with such connection between \mathbf{U}_μ and \mathbf{A}_μ , an expression for the gluon action on the Lattice can be proposed [75]:

$$S_G[\mathbf{U}] = 2 \sum_{\mathbf{n} \in \Lambda} \sum_{\mu < \nu} \text{Re tr}[1 - \mathbf{U}_{\mu\nu}(\mathbf{n})] \quad (1.23)$$

where $\mathbf{U}_{\mu\nu}(\mathbf{n})$ is know as the plaquette and is given by:

$$\mathbf{U}_{\mu\nu}(\mathbf{n}) = \mathbf{U}_\mu(\mathbf{n})\mathbf{U}_\nu(\mathbf{n} + \hat{\mu})\mathbf{U}_{-\mu}(\mathbf{n} + \hat{\mu} + \hat{\nu})\mathbf{U}_{-\nu}(\mathbf{n} + \hat{\nu}) \quad (1.24)$$

The sum of all the plaquettes in the lattice is a gauge invariant and so leads to a gauge invariant gluon action S_G .

1.4.3 Particles in the Lattice: Correlation Functions and Effective Mass

In order to provide the reader with an idea of how LQCD calculations work, I will describe the construction of a correlation function that is used to determine the pion mass.

In the lattice, before computing any quantity, it is necessary to construct a proper representations of the particle states. In QFT, states can be created by successive application of creation and annihilation operators to the vacuum. This method is also used in LQCD, where interpolating operators are used to create or annihilate desired particles states. These interpolating fields are functionals of the lattice fields, and must have quantum numbers matching the state of interest. This will be illustrated by studying the π^+ and the proton correlation functions and their effective masses m_{eff} and further details can be found in [76].

In practice, to obtain a field interpolator one would combine quark and gluons fields, together with different gamma matrices to get the desired particle states. For example for the π^+ meson, the interpolator only needs to involve two quarks: u and d. The possible combinations between u and d quarks can be further combined into an iso-triplet containing π^+, π^0, π^- , with corresponding isospin components $I_z = 1, 0, -1$ and electric charges $e, 0, -e$. Furthermore they have spin $J = 0$ and negative parity. Therefore, the following interpolators can be used for the iso-triplet:

$$O_{\pi^+} = \bar{d}(\mathbf{n})\gamma_5 u(\mathbf{n}) \quad (1.25)$$

$$O_{\pi^-} = \bar{u}(\mathbf{n})\gamma_5 d(\mathbf{n}) \quad (1.26)$$

$$O_{\pi^0} = \frac{1}{\sqrt{2}}(\bar{u}(\mathbf{n})\gamma_5 u(\mathbf{n}) - \bar{d}(\mathbf{n})\gamma_5 d(\mathbf{n})) \quad (1.27)$$

To verify that these operators are parity negative, a parity transformation is applied on

1.27. As an example, consider O_{π^+} . Under parity the quark fields transform as:

$$\psi(\mathbf{n}, \mathbf{n}_4) \rightarrow \psi'(\mathbf{n}, \mathbf{n}_4) = \gamma_4 \psi(-\mathbf{n}, \mathbf{n}_4) \quad (1.28)$$

$$\bar{\psi}(\mathbf{n}, \mathbf{n}_4) \rightarrow \bar{\psi}'(\mathbf{n}, \mathbf{n}_4) = \bar{\psi}(-\mathbf{n}, \mathbf{n}_4) \gamma_4 \quad (1.29)$$

Thus,

$$O_{\pi^+}(\mathbf{n}, \mathbf{n}_4) \rightarrow \bar{\mathbf{d}}(-\mathbf{n}, \mathbf{n}_4) \gamma_4 \gamma_5 \gamma_4 \mathbf{u}(-\mathbf{n}, \mathbf{n}_4) \quad (1.30)$$

$$= -\bar{\mathbf{d}}(-\mathbf{n}, \mathbf{n}_4) \gamma_5 \mathbf{u}(-\mathbf{n}, \mathbf{n}_4) = -O_{\pi^+}(-\mathbf{n}, \mathbf{n}_4) \quad (1.31)$$

To construct the correlator, we also need the corresponding O^\dagger operator. This is done easily by conjugation of the interpolator O :

$$O_{\pi^+} = \bar{\mathbf{d}} \gamma_5 \mathbf{u} \rightarrow (\bar{\mathbf{u}} \gamma_5 \mathbf{d})^\dagger = -\mathbf{d}^\dagger \gamma_5^\dagger \bar{\mathbf{u}}^\dagger = -\bar{\mathbf{d}} \gamma_4 \gamma_5 \gamma_4 \mathbf{u} = O_{\pi^-} \quad (1.32)$$

The correlation function for π^+ created at the point \mathbf{m} and annihilated at \mathbf{n} is then simply,

$$\langle O_{\pi^+}(\mathbf{n}) O_{\pi^+}^\dagger(\mathbf{m}) \rangle = \langle \bar{\mathbf{d}}(\mathbf{n}) \gamma_5 \mathbf{u}(\mathbf{m}) \bar{\mathbf{u}}(\mathbf{m}) \gamma_5 \mathbf{d}(\mathbf{n}) \rangle \quad (1.33)$$

Then, after performing the appropriate Wick contractions, the correlation function becomes:

$$\langle O_{\pi^+}(\mathbf{n}) O_{\pi^+}^\dagger(\mathbf{m}) \rangle = -\text{tr}(\gamma_5 D_{\mathbf{u}}^{-1}(\mathbf{n}|\mathbf{m}) \gamma_5 D_{\mathbf{d}}^{-1}(\mathbf{m}|\mathbf{n})) \quad (1.34)$$

where the quark propagator $D^{-1}(\mathbf{n}|\mathbf{m})$ from source position \mathbf{m} to sink position \mathbf{n} is defined

as:

$$\langle \psi(\mathbf{n})_{\alpha\alpha} \bar{\psi}(\mathbf{m})_{\beta\beta} \rangle = D^{-1}(\mathbf{n}, \mathbf{m})_{\alpha\alpha, \beta\beta} \quad (1.35)$$

and corresponds to the inverse of the Dirac operator. Hence, once quark propagators are computed on the lattice, computing the π^+ correlation function just requires contracting propagators with γ_5 . Moreover, in a LQCD calculation, this correlation function can be further analyzed to extract the π^+ mass.

The standard method to extract the mass and other observables is to insert the identity operator between the operators projected at zero momentum. For the identity operator, greek letters will be used as a reminder that the vacuum Ω is to be included in the sum, thus from here on is defined as:

$$1 = \sum_{\alpha} |\alpha\rangle \langle \alpha| = |\Omega\rangle \langle \Omega| + \sum_{\mathbf{k}} |\mathbf{k}\rangle \langle \mathbf{k}| \quad (1.36)$$

and sums over latin letters will correspond to sums over ground and excited states. Hence, the correlation function can be written in analogy to Statistical Mechanics as:

$$\begin{aligned} C(\mathbf{n}_t) &\equiv \left\langle O_{\pi^+}(\mathbf{n}_t) O_{\pi^+}^\dagger(0) \right\rangle = \sum_{\beta} \sum_{\mathbf{x}} \langle \beta | \mathcal{O}(\mathbf{x}, \mathbf{n}_t) \mathcal{O}^\dagger(\mathbf{0}, 0) | \beta \rangle e^{-E_{\beta} N_T} \quad (1.37) \\ &= \sum_{\beta} \sum_{\mathbf{x}} \langle \beta | e^{n_t \hat{H}} \mathcal{O}(\mathbf{0}, 0) e^{-n_t \hat{H}} \mathcal{O}^\dagger(\mathbf{0}, 0) | \beta \rangle e^{-E_{\beta} N_T} \\ &= \sum_{\mathbf{k}} \langle \Omega | O_{\pi^+} | \mathbf{k} \rangle \langle \mathbf{k} | O_{\pi^+}^\dagger | \Omega \rangle e^{-E_{\mathbf{k}} n_t} + \langle \mathbf{k} | O_{\pi^+} | \Omega \rangle \langle \Omega | O_{\pi^+}^\dagger | \mathbf{k} \rangle e^{-E_{\mathbf{k}} (N_T - n_t)} \\ &= \sum_{\mathbf{k}} A_{\mathbf{k}} (e^{-E_{\mathbf{k}} n_t} + e^{-E_{\mathbf{k}} (N_T - n_t)}) \end{aligned}$$

with the sum over \mathbf{x} in the last equation's first line a projection to zero momentum is accomplished and N_T is the lattice time extent. Moreover, the sum over the discrete set

of states \mathbf{k} appears because the operator interpolators can couple to any particle state and thus create or annihilate towers of states with the same quantum numbers. Lastly, as quark boundary conditions are anti-periodic in time, meson correlation functions turn out to be periodic in the lattice. Therefore, in general mesons correlation functions time dependence is given by 1.37.

On the other hand the proton and neutron, which correspond to the $I_z = 1/2, -1/2$ components of the nucleon iso-doublet, are composed of uud and ddu quarks and have respective electric charges $+e, 0$. Then, for the proton the following interpolator can be employed:

$$\mathcal{O}_p(\mathbf{n}) = \epsilon_{abc} \mathbf{u}(\mathbf{n})_a (\mathbf{u}(\mathbf{n})_b^\dagger \mathbf{C} \gamma_5 \mathbf{d}(\mathbf{n})_c) \quad (1.38)$$

The parity of the proton and the neutron is $\mathcal{P} = +1$, and the same is required for their respective interpolators. Hence, it is necessary to look at the parity transformation of the above interpolator, which is:

$$\mathcal{O}_p(\mathbf{n}, \mathbf{n}_4) \rightarrow \epsilon_{abc} \mathbf{u}(-\mathbf{n}, \mathbf{n}_4)_a (\mathbf{u}(-\mathbf{n}, \mathbf{n}_4)_b^\dagger \gamma_4^\dagger \mathbf{C} \gamma_5 \gamma_4 \mathbf{d}(-\mathbf{n}, \mathbf{n}_4)_c) = \gamma_4 \mathcal{O}_p(-\mathbf{n}, \mathbf{n}_4) \quad (1.39)$$

Therefore, as \mathcal{O}_p does not have the appropriate parity, a parity projection is required to obtain:

$$\mathcal{O}_p(\mathbf{n}) = \mathcal{P}_+ \epsilon_{abc} \mathbf{u}(\mathbf{n})_a (\mathbf{u}(\mathbf{n})_b^\dagger \mathbf{C} \gamma_5 \mathbf{d}(\mathbf{n})_c) \quad (1.40)$$

and the corresponding creating operator can be obtained in the same way as in the case

of the pion and leads to:

$$\overline{\mathcal{O}}_p(\mathbf{n}) = \epsilon_{abc} (\bar{\mathbf{u}}(\mathbf{n})_a C \gamma_5 \bar{\mathbf{d}}(\mathbf{n})_b^\dagger) \bar{\mathbf{u}}(\mathbf{n})_c \mathcal{P}_+ \quad (1.41)$$

Using the above interpolators, the two-point correlation function for the proton can be constructed, however performing the Wick contractions is a little more involved as there are three quarks instead of two.

The derivation of time dependence for the proton correlation function is analogous to that of pion, with the exception that for baryons the term $e^{-E_k(N_\tau - n_t)}$ is dropped as for baryons $e^{-E_k N_\tau} \ll e^{-E_k n_t}$, and the result is:

$$C^P(\mathbf{n}_t) = \sum_k A_k e^{-n_t E_k} \quad (1.42)$$

Finally, for both cases, the excited states are suppressed (with respect to E_0) as time increases and the ground state saturates $C(\mathbf{n}_t)$. Thus to extract E_0 from the $C(\mathbf{n}_t)$, an effective mass \mathbf{m}_{eff} is defined in general for baryons and mesons as follows:

$$\mathbf{m}_{\text{eff}}^{\text{baryons}}(\mathbf{n}_t, \tau) = \frac{1}{\tau} \ln \left(\frac{C(\mathbf{n}_t)}{C(\mathbf{n}_t + \tau)} \right) \quad (1.43)$$

$$\mathbf{m}_{\text{eff}}^{\text{mesons}}(\mathbf{n}_t, \tau) = \frac{1}{\tau} \cosh^{-1} \left(\frac{C(\mathbf{n}_t + \tau) + C(\mathbf{n}_t - \tau)}{2C(\mathbf{n}_t)} \right) \quad (1.44)$$

After a sufficiently large time, a plateau should be observed in a \mathbf{m}_{eff} plot against time. The value at this plateau corresponds to E_0 and can be determined with a fit as shown in 1.3.

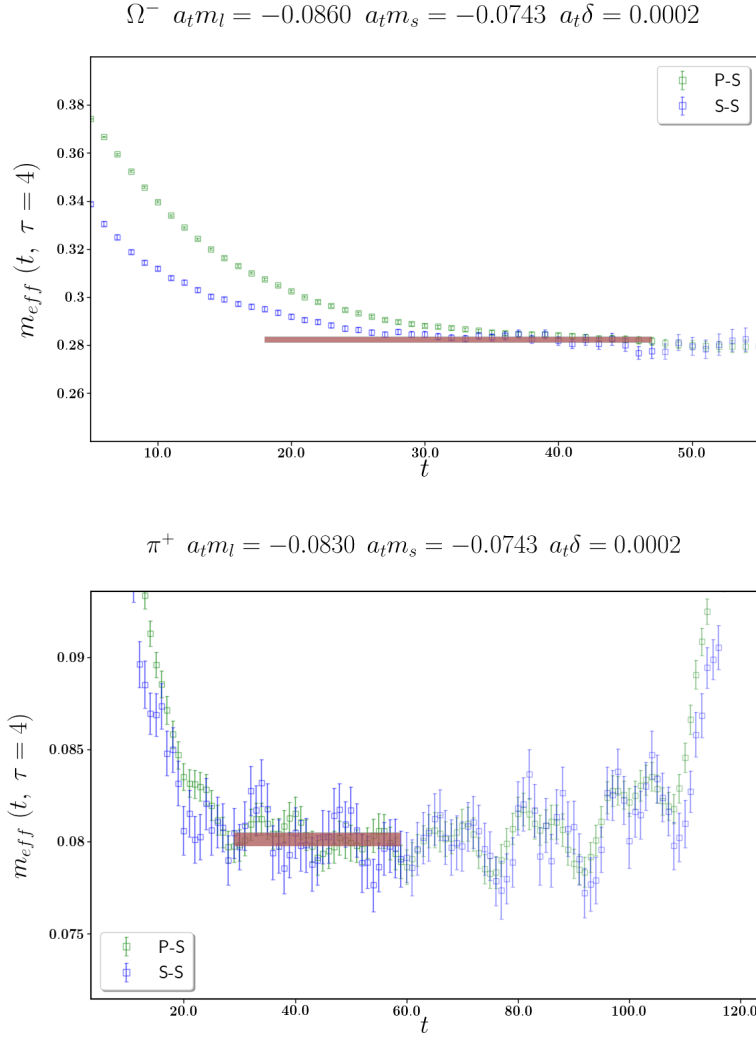


FIG. 1.3: m_{eff} plots for Ω^- baryon (Top) and π^+ meson (bottom). The pink band corresponds to the E_0 value determined from a fit to 1.43 and 1.44 respectively. The proton was fit using a 2-exponential function which included the first excited state, but only E_0 is shown. These are my previous work in [77].

CHAPTER 2

Non-perturbative Renormalization on the Lattice: Four-quark and Bilinear Operators

In Quantum Field Theories, the Lagrangian \mathcal{L} encodes the information about the phenomena and interactions between particles and fields. Therefore, one would expect that the different parameters appearing in \mathcal{L} could be identified with physical parameters describing the physics involved. However, this is not necessarily the case, and usually lagrangians are at first written in terms of ‘bare’ parameters which may be different from physical ones in important ways.

Furthermore, in QFT theories, calculations of certain quantities lead to diverging results at first, observable quantities must be finite, therefore singularities must be removed to render a theory with well defined observables. This is achieved by means of regularization, a process to treat the singularities and obtain finite quantities ~~contributions~~. For example in perturbative QFT calculations, this is usually done by calculating divergent

integrals in $d > 4$ dimensions to then analytically continue to $d = 4$, which is called dimensional regularization. Other methods use a cut-off for the theory such that integrals and physical quantities are both well defined. In LQCD, a cut-off is set by the lattice scale so the theory is automatically regularized. Nevertheless, the trade off in LQCD is that well-defined quantities now become dependent on the regularization scale. As a consequence, to obtain regularization independent physical results, i.e. observables, proper limits must be taken on the regulator.

Next, the replacing of bare parameters by their corresponding physical counterparts is performed in a process called renormalization. In LQCD and QFTs in general, this is a necessary step to obtain physically meaningful quantities from observables computed in the theory. Moreover, there is not a unique renormalization procedure and instead there are several methods and schemes available to perform perturbative and non-perturbative renormalization which will be discussed in the next section.

This chapter will focus on the renormalization of operators relevant to $0\nu\beta\beta$ and quark bilinear operators. In the case of $0\nu\beta\beta$, determination of its half-life requires the calculation of NME, which involves four-quark operators for short range contributions computed here. The renormalization of four quark operators appearing here has not been done before, and it is necessary to produce LQCD results that can later be incorporated into $0\nu\beta\beta$ decay rate calculations.

On the other hand, quark bilinear operators, specifically the axial current, enters in the determination of the nucleon axial charge g_A , an input in the determination of the neutron decay life-time. As the latter is an observable, and thus must not depend on any scale, g_A must be renormalized if physical results are desired.

2.1 Background

Non-perturbative renormalization on the Lattice is commonly performed using either the Schrödinger Functional Method [78] or the Regularisation Independent Moment Subtraction Method (RI/MOM)[79]. The first method is most convenient for studies with dedicated small volumes while RI-MOM methods are commonly used when large volume ensembles are reused [80]. For this work, the RI/MOM method will be adopted which was first proposed in [79] and has been applied successfully in calculations such as meson decay constants [81], form factors [82] and mixing amplitudes [83].

RI/MOM has the advantage that, because it is regularisation independent, it is well suited to be used as an intermediate renormalization scheme. Therefore, conversion of renormalized operators to a different scheme such as the Modified Minimal Subtraction scheme ($\overline{\text{MS}}$) is facilitated. Furthermore, as the operators considered in this work are involved in the $0\nu\beta\beta$ matrix elements, this matching to $\overline{\text{MS}}$ is desired to provide results to contribute to phenomenology and thus it will be performed here. In this way, the renormalized operators can later be combined with Wilson coefficients computed in the same scheme for a given EFT.

There are two different schemes that have been developed for the RI/MOM method. The original scheme is usually referred to as RI/MOM and uses an exceptional kinematical configuration where the momentum \mathbf{q}^2 inserted at the operator is 0, and thus much smaller than the typical large scale. The second method is known as RI/SMOM [84] (where the S stands for symmetric) and instead uses a non-exceptional configuration where $\mathbf{q}^2 \neq 0$. Here the RI/SMOM scheme will be used. The starting point to describe this method is the definition of the renormalization constants. For example in the continuum, the quark mass wave function and quark mass renormalization constants, Z_q and Z_m respectively,

are fixed by the following conditions:

$$\psi_r = Z_q^{1/2} \psi_b \quad (2.1)$$

$$m_r = Z_m m_b \quad (2.2)$$

In a similar way, for lattice operators that renormalize multiplicatively, at a given renormalization scale μ , their relation is expressed by the following equation:

$$\hat{\mathcal{O}}_r(\mu) = \lim_{a^2 \rightarrow 0} Z(\mu, a) \hat{\mathcal{O}}_b^{\text{Latt}}(a) \quad (2.3)$$

where the subindices r and b , are used to label renormalized and bare operators respectively and the limit is taken with a^2 due to discretization errors starting at $\mathcal{O}(a^2)$ for the action employed here.

Therefore, what is first required is a relation from which the constants $Z(\mu, a)$ fixed by 2.3 can be determined. In the RI-MOM and RI-SMOM methods, such relation is obtained by imposing renormalization conditions on the quark and gluon Green functions computed from external off-shell states with large virtualities, and for a fixed gauge (Landau gauge in this case) [79]. The condition to impose is that a renormalized amputated vertex function, at a given momentum scale, is equal to its tree level value. Furthermore, to guarantee that non-perturbative effects (required for matching results to $\overline{\text{MS}}$ using perturbation theory) and lattice artifacts are simultaneously small, the external states momenta μ must be chosen to satisfy:

$$\Lambda_{\text{QCD}} \ll \mu \ll \frac{1}{a} \quad (2.4)$$

which is also known as the Rome-Southampton window. Next, the kinematical configura-

tion must be considered. In its original formulation, the RI/MOM scheme imposed kinematical conditions such that the momentum transfer q^2 through the vertex was zero, i.e. $p_{\text{in}}^2 = p_{\text{out}}^2$. Nevertheless, this configuration leads to problems such as the presence of pion pole contamination from Spontaneous Symmetry Breaking in the infrared energy regime which manifests as a $1/\mu^2$ divergence at low momenta. In the RI/SMOM scheme [84], a non-exceptional and symmetric momentum configuration was proposed, such that all the incoming p_{in} , all outgoing p_{out} and transfer momenta are of the same magnitude, i.e. $p_{\text{in}}^2 = p_{\text{out}}^2 = (p_1 - p_2)^2 = q^2$. In this case, the pion pole contamination is reduced for $q^2 \gg m_\pi^2$ and, only slightly different renormalization conditions from those used in RI/MOM are required to ensure that Ward-Takahashi Identities are satisfied by the resulting renormalized quantities. Finally, as only one momentum magnitude enters in the RI/SMOM scheme, the renormalization scale is easily identified as $\mu = p_{\text{in}}^2 = p_{\text{out}}^2 = q^2$.

Now, before proceeding to the bilinear and four-quark operator specific details, the quark Green functions to be employed for both are first considered. These can be computed from single point sources, however momentum sources developed in [85] have shown to improve statistical errors to around 0.1%. Thus the latter will be used here, such that uncertainties should be dominated by systematic effects, for example $\mathcal{O}(4)$ breaking lattice artifacts [86].

To generate the volume sources, incoming and outgoing momentum source propagators are obtained by solving for the propagator from a momentum source:

$$\sum_{\mathbf{x}} D(\mathbf{y}, \mathbf{x}) G'_{\mathbf{x}}(\mathbf{p}) = e^{i\mathbf{p}\cdot\mathbf{y}} \quad (2.5)$$

Then, for position \mathbf{x} with respect to the vertex, an incoming quark with momentum \mathbf{p} and an outgoing quark with momentum $-\mathbf{p}$, $G_{\mathbf{x}}(\mathbf{p})$ and $\bar{G}_{\mathbf{x}}(\mathbf{p})$ respectively, are defined

as follows:

$$G_x(\mathbf{p}) = G'_x(\mathbf{p})e^{-i\mathbf{p}\cdot\mathbf{x}} = \sum_{\mathbf{y}} D^{-1}(\mathbf{x}, \mathbf{y})e^{-i\mathbf{p}\cdot(\mathbf{x}-\mathbf{y})} \quad (2.6)$$

$$\bar{G}_x(\mathbf{p}) = \gamma^5 G'_x(\mathbf{p})\gamma^5 \quad (2.7)$$

Where the γ^5 hermiticity of lattice propagators was used to defined the outgoing propagator.

Furthermore, to perform the necessary vertex amputation, the momentum space propagator, average over all momentum sources in the volume will be required, and it is given by:

$$G(\mathbf{p}) = \frac{1}{V} \sum_x G_x(\mathbf{p}) \quad (2.8)$$

2.2 Bilinear Operator Renormalization

In order to renormalize the nucleon axial charge \mathbf{g}_A , or to normalize the four-quark operators renormalization matrix, quark bilinear renormalization constants are required. All the bilinear current renormalization constants are determined here and will be employed first in the renormalization of the four-quark operators and later in precise calculation of \mathbf{g}_A presented in chapter 3.

Finally, the details of the ensembles used for the calculations in this chapter are summarized in table 2.1.

2.2.1 Scheme Details

In general, the quark bilinear operators are defined as:

$$\mathcal{O}^\Gamma = \bar{q}\Gamma q \quad (2.9)$$

abbr.	N_{cfg}	volume	$\sim \mathbf{a}$ [fm]	$\sim m_{\pi_5}$ [MeV]
a09m310	10	$32^3 \times 96$	0.09	310
a09m220	10	$48^3 \times 96$	0.09	220
a12m350	10	$24^3 \times 64$	0.12	350
a12m310	10	$24^3 \times 64$	0.12	310
a12m220	10	$32^3 \times 64$	0.12	220
a12m130	10	$48^3 \times 64$	0.12	130
a15m350	10	$16^3 \times 48$	0.15	350
a15m310	10	$16^3 \times 48$	0.15	310
a15m220	10	$24^3 \times 48$	0.15	220
a15m130	10	$32^3 \times 48$	0.15	130

TABLE 2.1: Parameter details of the ensembles employed in the renormalization.

where $\Gamma = \{\mathbf{1}, \gamma_5, \gamma_\mu, \gamma_5 \gamma_\mu, \sigma_{\mu\nu}\}$ are the scalar, pseudoscalar, vector, axial vector, and tensor Dirac structures respectively. With the general form of the operator at hand, the unamputated vertex function is first defined by:

$$V_\Gamma^{\text{qq}}(\mathbf{p}_2, \mathbf{p}_1) = \sum_x \bar{G}(x, \mathbf{p}_2) \Gamma G(x, \mathbf{p}_1). \quad (2.10)$$

and the vertex kinematical configuration is showed in figure 2.1. V_Γ^{qq} must be then amputated using momentum space Green functions 2.8 which leads to the following amputated vertex:

$$\Pi_\Gamma(\mathbf{p}_2, \mathbf{p}_1) = G^{-1}(\mathbf{p}_2) V_\Gamma^{\text{qq}}(\mathbf{p}_2, \mathbf{p}_1) \gamma^5 [G^{-1}(\mathbf{p}_1)]^\dagger \gamma^5 \quad (2.11)$$

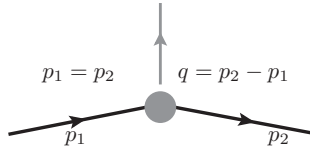


FIG. 2.1: Kinematical configuration for the bilinear renormalization vertex in RI-MOM and RI-SMOM schemes. The momentum transfer is $q^2 = 0$ for RI-MOM scheme while $q^2 = p_1^2 = p_2^2$ for RI-SMOM.

Afterwards by projecting the amputated vertex, the operator bare amplitudes are obtained Λ_Γ :

$$\Lambda_\Gamma(\mathbf{p}_2, \mathbf{p}_1) = P_\Gamma \Pi_\Gamma(\mathbf{p}_2, \mathbf{p}_1) \quad (2.12)$$

The projectors P_Γ are not unique, and thus each choice defines a new scheme. For this work, two schemes will be used which are denoted gamma (γ) and q-slash (\not{q}). For bilinear operators, P^γ projectors have an identical Dirac and color structure to the operator Γ , while $P^\not{q}$ are obtained by replacing $\gamma_\mu \rightarrow \not{q}\gamma_\mu/q^2$ in Γ 's dirac structure.

Finally, the renormalization conditions to be satisfied are that the bare amplitudes, arising from the projected amputated vertex, are equal to its tree level value. This leads to the following equation for the lattice renormalization constants:

$$\frac{Z_\Gamma(\mu, \mathbf{a})}{Z_q(\mu, \mathbf{a})} \Lambda_\Gamma(\mu, \mathbf{a}) = \Lambda_\Gamma^{\text{tree}} \quad (2.13)$$

where the \mathbf{a} dependence is included as these quantities are to be computed at finite lattice spacings. With this condition, the dependence on the external momenta is exchanged for a μ dependence. This is justified by the fact that there is only one momentum magnitude entering the process, and thus defines the renormalization scale μ . Moreover, as the amputation process has to be performed with the renormalized quark Green functions, the corresponding constants Z_q must be included. Finally, 2.13 is to be satisfied in the chiral limit, i.e. $m_q \rightarrow 0$, however $\Lambda_\Gamma(\mu, \mathbf{a})$'s computed in the lattice may have a non-zero quark mass dependence. Hence, $\Lambda_\Gamma(\mu, \mathbf{a}, m_q)$'s obtained in the computation must be extrapolated to zero quark mass.

In practice, such a extrapolation requires a combined fit in μ and m_q . The reason is that fourier modes for different ensembles, corresponding to different quark masses, in general do not match exactly. These fits are performed here with the ansatz:

$$\Lambda_\Gamma(\mu, a, m_q) = \left(1 + \sum_{n=-1,1,2} b_n (am_q)^n\right) \left(\sum_m c_m (a\mu)^m\right) + \sum_k d_k (a\mu)^k \quad (2.14)$$

The term in the first parenthesis on the left hand side of 2.14 gives the quark mass dependence with $m_q = m_l + m_{res}$ and is observed to be very mild such that data is described well enough with a $n = 1$ term and in the worst cases with $n = -1, 1, 2$. The remaining momentum dependence in the ansatz is due to the running of the operator, non-perturbative effects and lattice errors [87].

ensemble	g_V^b
a09m400	1.023(01)
a09m350	1.024(02)
a09m310	1.024(01)
a09m220	1.022(02)
a12m400	1.016(01)
a12m350	1.016(01)
a12m310	1.021(02)
a12m220	1.015(02)
a12m130	1.020(08)
a15m400	0.998(01)
a15m350	0.997(01)
a15m310	1.001(02)
a15m220	1.000(04)
a15m130	0.994(35)

TABLE 2.2: g_V^b values determined in [2] and used here to determine g_V^r .

2.2.2 Results

The first renormalization constant to consider is that of nucleon vector charge. Conservation of the vector charge requires $g_V^r = 1$. However, due to lattice discretization errors

and chiral symmetry breaking in the lattice, g_V^b is not exactly one and the corresponding renormalization constant Z_V must be determined from $Z_V = 1/g_V^b$, and in the chiral limit, should lead to a scale independent value for Z_V . Therefore, using bare nucleon vector data, an extrapolation to the chiral limit can be performed to obtain Z_V . The data used here for such determination is summarized in table 2.2, and in this case a very mild quark mass dependence was observed as well as negligible residual scale dependence. Furthermore, from the Ward identities, at small quark mass it is expected that $Z_A \approx Z_V$, hence this relation provides a means to check for chiral symmetry breaking contamination.

For MDWF fermions (used in this work), chiral symmetry is preserved to a good degree and this is observed in the ratio Z_A/Z_V which is found to be very close to one as figure 2.2 shows. Therefore, as Z_V/Z_A is determined very precisely to be one, their renor-

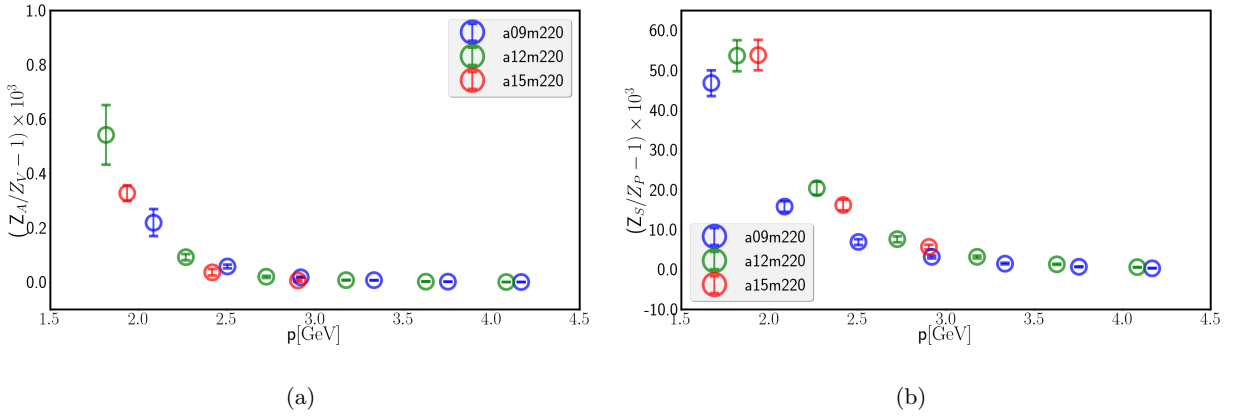


FIG. 2.2: Z_A/Z_V and Z_S/Z_P ratios for lattice spacings $a = 0.09, 0.12, 0.15$ fm and $m_\pi = 220$ MeV. a) Z_A/Z_V and b) Z_S/Z_P plots shows that both ratios are very close to one and almost scale independent, as it should be when chiral symmetry is preserved. This is expected because chiral symmetry is almost preserved by action employed.

malization conditions set by 2.13 can be combined to compute the quark wave function renormalization constant Z_q as follows:

$$Z_q = Z_V \frac{\Lambda_V + \Lambda_A}{2} \quad (2.15)$$

In a similar way, the quark mass renormalization Z_m constant can be obtained. In this case, from chiral symmetry properties for the scalar and pseudo scalar operators, $Z_P \approx Z_S$ which is again satisfied by the data as the ratio Z_S/Z_P is very close to one as shown in figure 2.2. This, together with the relations $Z_m Z_P = 1$ and $Z_m Z_S = 1$ [88], lead to the following relation:

$$Z_m = \frac{\Lambda_P + \Lambda_S}{Z_V(\Lambda_V + \Lambda_A)} \quad (2.16)$$

where Z_q was substituted from 2.15. Finally, with the determined values for Z_V , the Z_q dependence of the remaining operators Z_P, Z_S, Z_T can be removed. Then, following the fitting procedure previously described, the renormalization constants for the bilinears are obtained. Sample plots for these fits are shown in figures 2.3, 2.4 and 2.5; and the values obtained are summarized in tables 2.3 and 2.4.

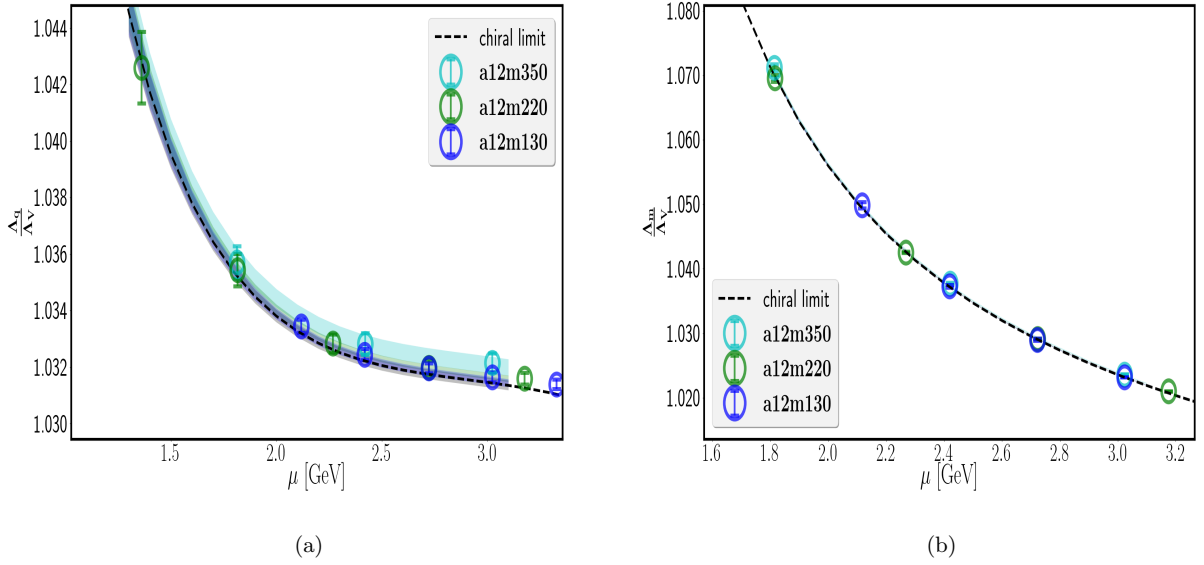


FIG. 2.3: Quark wave function and quark mass amputated vertices $\frac{\hat{\Lambda}_V^q}{\Lambda_V^q}$ and $\frac{\hat{\Lambda}_V^m}{\Lambda_V^m}$ fits. a) $\frac{\hat{\Lambda}_V^q}{\Lambda_V^q}$ and b) $\frac{\hat{\Lambda}_V^m}{\Lambda_V^m}$ fits for ensemble with $a = 0.12$ fm, $m_\pi = 130, 220, 350$ MeV. The result in the chiral limit and the error bands are indicated respectively by the dashed line and color bands.

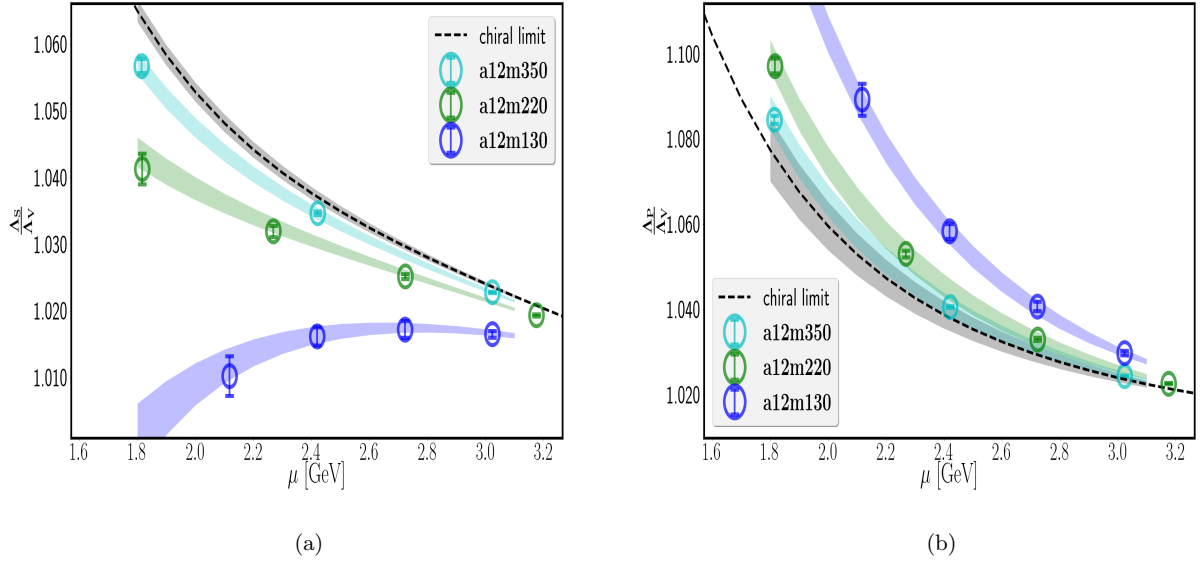


FIG. 2.4: Scalar and Pseudoscalar bilinear currents amputated vertices $\frac{\Lambda_s}{\Lambda_V}$ and $\frac{\Lambda_P}{\Lambda_V}$ fits. a) $\frac{\Lambda_s}{\Lambda_V}$ and b) $\frac{\Lambda_P}{\Lambda_V}$ fits for ensemble with $a = 0.12$ fm, $m_\pi = 130, 220, 350$ MeV. The result in the chiral limit and the error bands are indicated respectively by the dashed line and color bands.

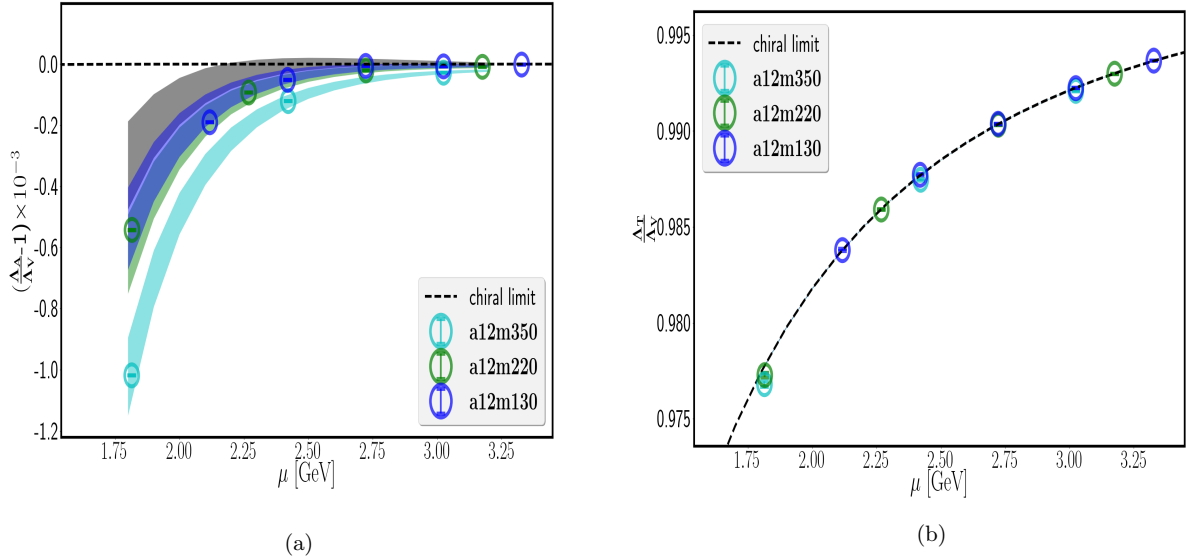


FIG. 2.5: Scalar and Pseudoscalar bilinear currents amputated vertices $\frac{\Lambda_A}{\Lambda_V}$ and $\frac{\Lambda_T}{\Lambda_V}$ fits. a) $\frac{\Lambda_A}{\Lambda_V}$ and b) $\frac{\Lambda_T}{\Lambda_V}$ fits for ensemble with $a = 0.12$ fm, $m_\pi = 130, 220, 350$ MeV. The result in the chiral limit and the error bands are indicated respectively by the dashed line and color bands.

γ - scheme $\mu = 2\text{GeV}$					
ensemble	Z_q	Z_m	Z_S	Z_P	Z_T
a09	1.0073(21)	1.1062(23)	0.9557(20)	0.9396(20)	1.0505(22)
a12	1.0161(23)	1.0743(24)	0.9664(23)	0.9602(38)	1.0363(23)
a15	1.0384(33)	1.0439(33)	0.9630(31)	0.9473(47)	1.0146(31)

TABLE 2.3: Bilinear renormalization constants determined at the scale $\mu = 2\text{GeV}$ in the γ -scheme.

\not{q} - scheme $\mu = 2\text{GeV}$					
ensemble	Z_q	Z_m	Z_S	Z_P	Z_T
a09	1.0818(22)	1.0303(21)	1.0189(25)	1.0082(21)	1.1273(23)
a12	1.0814(24)	1.0092(23)	1.0348(39)	1.0216(41)	1.1029(25)
a15	1.1006(35)	0.9841(31)	1.0192(35)	1.0176(39)	1.0759(33)

TABLE 2.4: Bilinear renormalization constants determined at the scale $\mu = 2\text{GeV}$ in the \not{q} -scheme.

In general, the results for the renormalization constants show small statistical errors in spite of the small number of configurations used. The reason for this is the used of momentum sources, which here was previously pointed out to yield small statistical errors.

Additionally, in the case of Z_V and Z_A , these quantities are observed to be scale independent as the scale is increased and their values are very close to one. This is consistent with the fact that chiral symmetry is preserved to a good degree for the action employed. For the infrared region of QCD, large vacuum chiral symmetry breaking can introduce further errors and thus these quantities are observed to start deviating from one. The above properties of Z_V are convenient for determination of the remaining renormalization constants, this is in the sense that Z_q dependences can be removed by taking ratios with Z_V which will not introduce a scale dependence.

For the two finest lattice spacings, no significant discretization errors are observed

around the $\mu = 3$ GeV which is the desired scale, however for the coarsest lattice $\mathbf{a} = 0.15$ fm these effects start to show up before the $\mu = 3$ GeV scale, however, this will be addressed later in this chapter by employing the renormalization constants running.

2.3 Four-quark Operators Renormalization

In the short range interactions contributing to $0\nu\beta\beta$, four-quark operators arise from LO contributions coming from pion exchange processes, i.e $\pi^- \rightarrow \pi^+$. In this section, the renormalization of these operators is presented while other details are left to chapter 4 where their calculation is presented.

2.3.1 Scheme Details

The set of operators to consider is composed of five parity even operators: three color unmixed operators and two color-mixed. The color mixed operators arise from renormalization from the electroweak scale to the QCD scale. The mixing under renormalization is specified by the chiral properties of these operators and it is discussed in [69, 89, 90]. Moreover, Using Fierz Transformations, the operator basis can be related ¹ to a color diagonal basis. Thus, for practical reasons the following color diagonal basis [89] is employed:

$$Q_1 = [\bar{\Psi}_a^1 \gamma_\mu (1 - \gamma_5) \Psi_a^2] (\bar{\Psi}_b^1 \gamma^\mu (1 - \gamma_5) \Psi_b^2) \quad (2.17a)$$

$$Q_2 = [\bar{\Psi}_a^1 \gamma_\mu (1 - \gamma_5) \Psi_a^2] (\bar{\Psi}_b^1 \gamma^\mu (1 + \gamma_5) \Psi_b^2) \quad (2.17b)$$

$$Q_3 = [\bar{\Psi}_a^1 (1 - \gamma_5) \Psi_a^2] (\bar{\Psi}_b^1 (1 + \gamma_5) \Psi_b^2) \quad (2.17c)$$

$$Q_4 = [\bar{\Psi}_a^1 (1 - \gamma_5) \Psi_a^2] (\bar{\Psi}_b^1 (1 - \gamma_5) \Psi_b^2) \quad (2.17d)$$

$$Q_5 = \frac{1}{4} [\bar{\Psi}_a^1 \sigma_{\mu\nu} (1 - \gamma_5) \Psi_a^2] (\bar{\Psi}_b^1 \sigma^{\mu\nu} (1 - \gamma_5) \Psi_b^2) \quad (2.17e)$$

¹We summarize the transformations [91] in appendix B.

where color indices for the contractions are shown explicitly for clarity. For these set of four-quark operators, the kinematic configuration at the vertex is shown in figure 2.6.

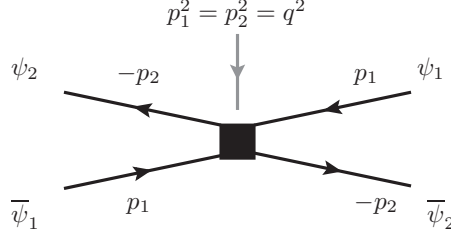


FIG. 2.6: Kinematical configuration for the four-quark renormalization vertex in RI-MOM and RI-SMOM schemes. The momentum transfer is $q^2 = 0$ for RI-MOM scheme while $q^2 = p_1^2 = p_2^2$ for RI-SMOM.

Now, the definition of the amputated Green Functions proceeds in a similar fashion as for the bilinear case. Hence, for each basis element Q_i , an unamputated Green Function is constructed with the following form:

$$V_{\Gamma_1 \Gamma_2}^{4q}(\mathbf{p}_2, \mathbf{p}_1) = 2 \sum_x \left\langle [\bar{G}(x, \mathbf{p}_1) \Gamma^1 G(x, \mathbf{p}_2)]^{ij, \alpha\beta} [G(\bar{x}, \mathbf{p}_1) \Gamma^2 G(x, \mathbf{p}_2)]^{kl, \gamma\delta} \right\rangle \quad (2.18)$$

$-\beta \leftrightarrow \delta \quad j \leftrightarrow l$

where $\Gamma^i = \gamma_\mu(1 - \gamma_5), \gamma_\mu(1 + \gamma_5), (1 - \gamma_5), (1 + \gamma_5), \sigma_{\mu\nu}(1 - \gamma_5)$. Amputating $V_{\Gamma_1 \Gamma_2}^{4q}(\mathbf{p}_2, \mathbf{p}_1)$ leads to:

$$\Pi_{\Gamma}^{4q}(\mathbf{p}_2, \mathbf{p}_1) = G^{-1}(\mathbf{p}_2) G^{-1}(\mathbf{p}_1) V_{\Gamma_1 \Gamma_2}^{4q}(\mathbf{p}_2, \mathbf{p}_1) \gamma_5 [G^{-1}(\mathbf{p}_1)]^\dagger \gamma_5 \gamma_5 [G^{-1}(\mathbf{p}_2)]^\dagger \gamma_5 \quad (2.19)$$

after projection of the amputated Greens functions $\Pi_{\Gamma}^{4q}(\mathbf{p}_2, \mathbf{p}_1)$, the bare vertex amplitudes are obtained:

$$\Lambda'_{ij} = P_j \Pi_i \quad (2.20)$$

The projector schemes used for these amplitudes corresponds to the γ -scheme. In the γ -scheme the projector P_i^γ is define exactly as the Dirac and color structure of the operator Q_i . It is also possible to use the \not{q} -scheme, with projectors $P_i^{\not{q}}$ found by replacing in P_i^γ the following quantities:

$$\begin{aligned}\gamma^\mu &\rightarrow \frac{\not{q}}{\sqrt{q^2}} \\ \sigma^{\mu\nu} P_L &\rightarrow \frac{p^\mu \sigma^{\mu\nu} p^\nu P_L}{\sqrt{p_1^2 p_2^2 - (p_1 \cdot p_2)^2}}\end{aligned}$$

where $P_L = \frac{1-\gamma^5}{2}$. However, results in the \not{q} -scheme have not been obtained for this work.

Finally, the amputated projected vertices are required to satisfy the following renormalization conditions which will fix the renormalization constant matrix:

$$\frac{Z_{ik}}{Z_q^2} \Lambda_{kj}^{\prime b} = \Lambda_{ij}^{\text{tree}} / \Lambda_q^{\text{tree}} \quad (2.21)$$

For practical reasons, Λ^{tree} can be moved to left hand side and absorbed in $\Lambda^b = \Lambda^{\prime b} \cdot (\Lambda^{\text{tree}})^{-1}$ as:

$$\frac{Z_{ik}}{Z_q^2} = (\Lambda^b)_{ik}^{-1} / (\Lambda^b)_q^{-1} \quad (2.22)$$

This last equation defines a matrix Z which renormalizes the five elements of the basis. The form and entry values of Z are determined by the allowed mixing between the different operators according to their chiral symmetry properties. The operators that are allowed to mixed are Q_2, Q_3 and Q_4, Q_5 , therefore the Z -matrix should be block diagonal Z -matrix. Nevertheless, chiral symmetry is not perfectly preserved and entries corresponding to forbidden mixing are suppressed but non-zero and must be taken into consideration.

2.3.2 Four-quark Results

For the determination of the Z -matrix that renormalizes the four-quark set of operators, each entry μ and a dependence is fitted in the same manner as for the bilinears, i.e. by employing the fit ansatz 2.14. In order to remove the Z_q dependence, 2.22 is divided by Z_V . Sample fits for some Λ/Λ_V^2 entries corresponding to chirally allowed mixing of operators are showed in figure 2.7. Λ components expected to be zero from chiral symmetry were observed to be several orders of magnitude smaller, and the error due to setting those to zero is within the statistical errors.

In figure 2.7, sample fits are presented. The numerical Z/Z_V results at 2GeV and for the three lattice spacings used in this work are displayed in table 2.5.

		γ - scheme		$\mu = 2\text{GeV}$	
ensemble	Z_{11}	Z_{2-3}		Z_{4-5}	
a09	0.92514(94)	$\begin{pmatrix} 0.9986(10) & 0.16018(52) \\ 0.013738(45) & 0.8529(12) \end{pmatrix}$	$\begin{pmatrix} 0.8727(13) & -0.011218(44) \\ -0.14809(56) & 1.0090(15) \end{pmatrix}$		
a12	0.92463(90)	$\begin{pmatrix} 0.9925(11) & 0.13533(90) \\ 0.015730(59) & 0.89205(78) \end{pmatrix}$	$\begin{pmatrix} 0.90530(79) & -0.01327(24) \\ -0.12196(29) & 0.9881(12) \end{pmatrix}$		
a15	0.9214(37)	$\begin{pmatrix} 0.9892(40) & 0.13262(92) \\ 0.01876(17) & 0.9136(33) \end{pmatrix}$	$\begin{pmatrix} 0.9264(32) & -0.01643(33) \\ -0.11501(92) & 0.9762(41) \end{pmatrix}$		

TABLE 2.5: Renormalization matrix values determined at $\mu = 2\text{GeV}$ for four-quark operators

As in the case of the bilinear operators, the use of momentum sources leads to small statistical errors. In general, as the momentum scale μ raises chiral symmetry effects should become smaller (especially because the action used here has good chiral symmetry) while at low energies they can become more significant due to chirally symmetry breaking effects.

The above features are observed in general, for example as the momentum μ increases the renormalization constants approach the value 1 corresponding to their tree level value,

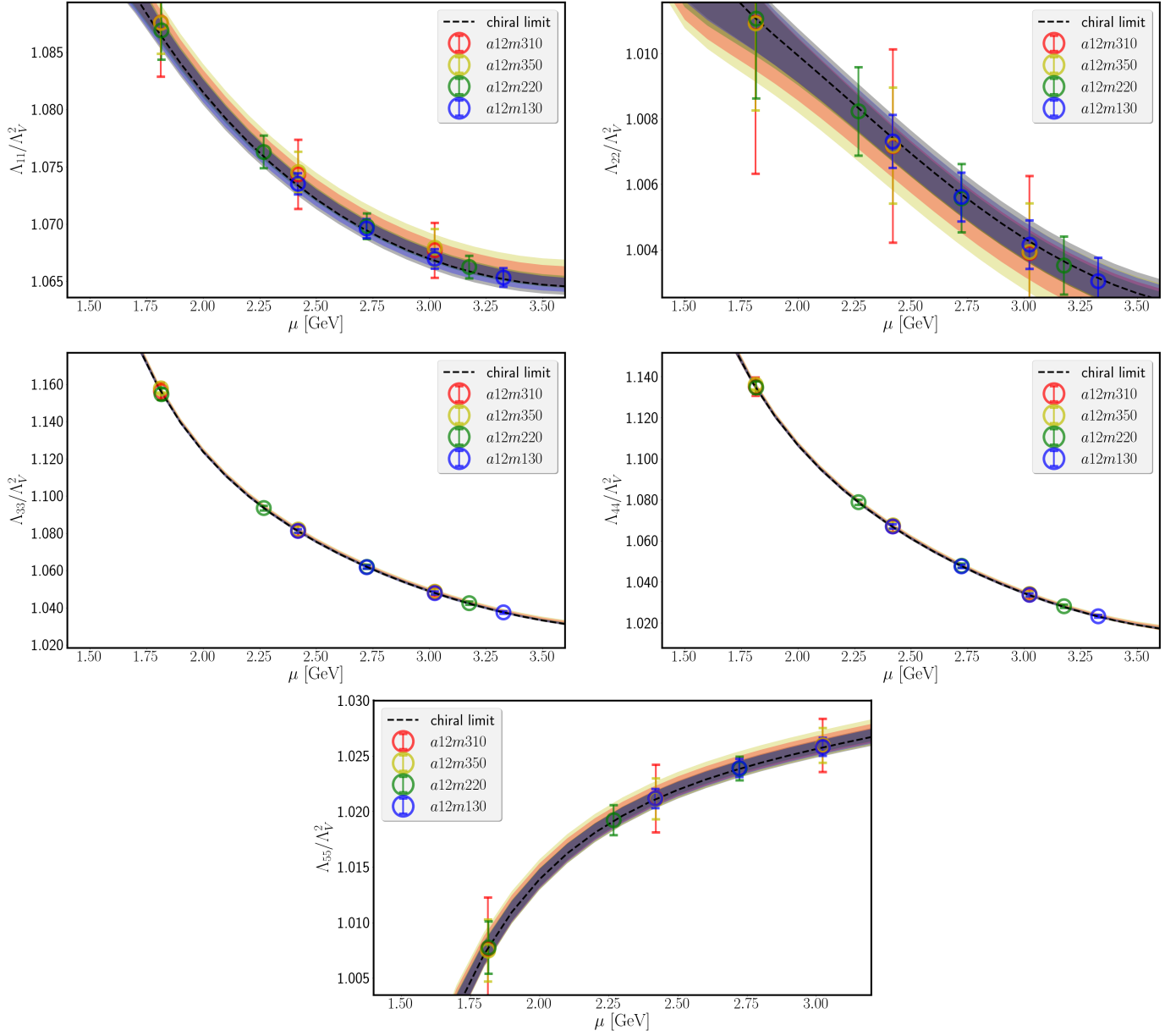


FIG. 2.7: Four-quark operators renormalization vertex matrix Λ fit samples. The plots show the renormalized vertices (normalized by its tree level value) which are related to the renormalization matrix by $Z = \Lambda^{-1}$. Only entries allowed to be non-zero by chiral symmetry conservation are shown. The result in the chiral limit and the error bands are indicated respectively by the dashed line and color bands.

this is shown in the plots in 2.7 corresponding to the diagonal components of the renormalization matrix. On the other hand, Z off-diagonal entries become closer to zero as the momentum scale is raised.

Z off-diagonal entries which mix the different operators are suppressed with respect to the diagonal terms as these are subleading effects, and the off-diagonal entries for mixings not allowed by chiral symmetry should be even more suppressed. These are consistent with the results found, and in the case of entries for chirally forbidden mixings, their effects were found to be within statistical errors compared to when they are set to 0 explicitly.

2.4 Raising The Renormalization Scale

In the description of the RI/MOM method, a condition for the validity was given by the Rome-Southampton window. This condition is required to ensure that non-perturbative and discretization errors are well under control. In certain cases, specially for large lattice spacing ensembles, the high-momentum end of this window is reduced. This poses a problem to further match the renormalized operators to the $\overline{\text{MS}}$ -scheme because some of the constants cannot be obtained at the desired scale $\mu = 3\text{GeV}$. To overcome this, the running of the operator can be employed such that the renormalization scale can be raised.

The technique that will be adopted here is known as step scaling and has been previously used together with the RI-SMOM scheme [86]. The process consists in finding the step scaling function which describes the running of the operators in the continuum limit. This step scaling function is defined by the ratio of two renormalization constants at different momenta:

$$\Sigma(\mu_1, \mu_2, \mathbf{a}) = Z(\mu_1, \mathbf{a})Z^{-1}(\mu_2, \mathbf{a}) \quad (2.23)$$

where Z is a matrix for four-quark operators and a number for bilinears. Furthermore, this quantity is well defined in the continuum limit, and can usually be determined by a linear fit in a^2 , however in some cases adding a a^4 term may be necessary. The step scaling function relation to its continuum limit is given by:

$$\Sigma(\mu_1, \mu_2, a) = \Sigma(\mu_1, \mu_2) + f(\mu)(b_2 a^2 + b_4 a^4). \quad (2.24)$$

Here, to determine $\Sigma(\mu_1, \mu_2)$, three different types of fits were employed. In the first method, at each momenta, a fit is performed to find the a dependence. A second fit uses the combined a and μ dependence to fit the data simultaneously at all μ .

A third procedure determines the discretization errors by fitting quantities of the form

γ - scheme		$\mu : 2\text{GeV} \rightarrow 3\text{GeV}$		
Σ_q	Σ_m	Σ_S	Σ_P	Σ_T
0.98905(47)	0.92890(66)	0.9695(15)	0.9171(67)	1.0241(11)

TABLE 2.6: $\mu = 2\text{GeV} \rightarrow 3\text{GeV}$ step scaling function values for bilinear operators in the γ -scheme.

\not{q} - scheme		$\mu : 2\text{GeV} \rightarrow 3\text{GeV}$		
Σ_q	Σ_m	Σ_S	Σ_P	Σ_T
0.95437(35)	0.96263(96)	0.9968(95)	0.9557(69)	0.94365(26)

TABLE 2.7: $\mu = 2\text{GeV} \rightarrow 3\text{GeV}$ step scaling function values for bilinear operators in the \not{q} -scheme.

$\Sigma(\mu_1, \mu_2, a_1) - \Sigma(\mu_1, \mu_2, a_2)$ and then solving for the continuum limit $\Sigma(\mu_1, \mu_2)$ in 2.24. We find consistent results with all three methods. A sample fit for the step scaling function is shown in figure 2.8.

The values obtained for the step scaling function for bilinears and four-quark operators

γ - scheme			$\mu = 2\text{GeV} \rightarrow 3\text{GeV}$	
Σ_{11}	Σ_{2-3}		Σ_{4-5}	
0.9783(22)	$\begin{pmatrix} 1.0042(32) & 0.1157(29) \\ 0.00334(24) & 0.8602(22) \end{pmatrix}$	$\begin{pmatrix} 0.8883(23) & -0.00123(67) \\ -0.09959(90) & 1.0448(38) \end{pmatrix}$		

TABLE 2.8: $\mu : 2\text{GeV} \rightarrow 3\text{GeV}$ step scaling function values for four-quark operators in the γ -scheme.

are summarized in tables 2.6, 2.7 and 2.8. Also, the renormalization constants at the scale $\mu = 3\text{GeV}$ results are displayed in tables 2.9, 2.10, 2.11.

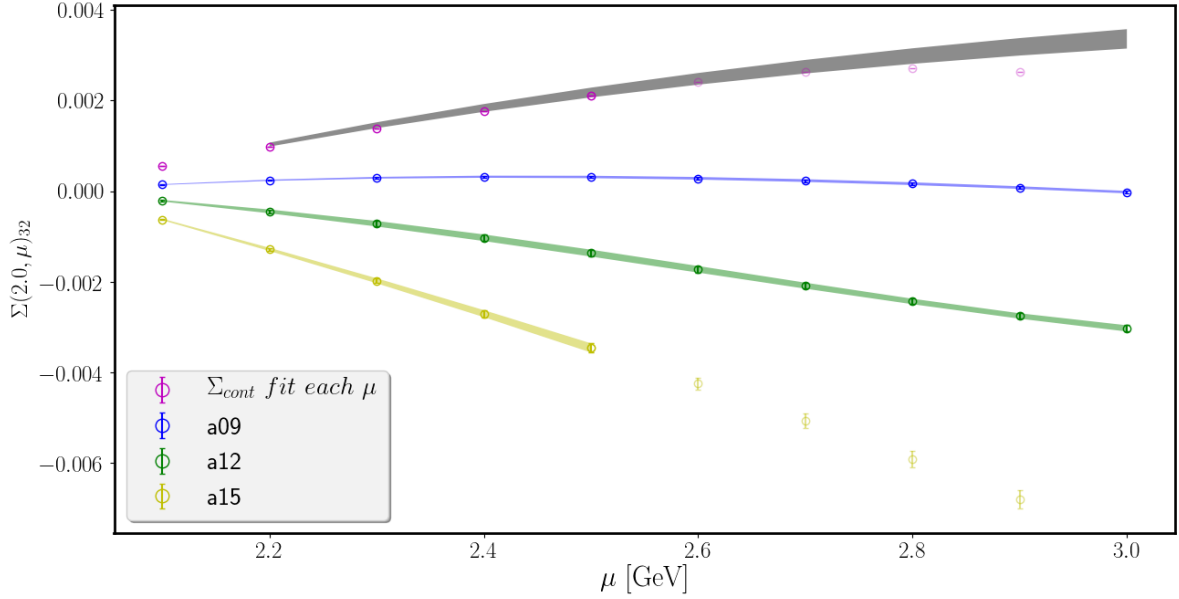


FIG. 2.8: Four-quark operator step scaling function Σ_{32} fit sample. The gray band corresponds to the fit to discretization errors in 2.24 simultaneously at all μ to determine the continuum step scaling function by subtraction. The magenta points corresponds to the fit to 2.24 separately at each μ .

γ - scheme $\mu = 3\text{GeV}$					
ensemble	Z_q	Z_m	Z_S	Z_P	Z_T
a09	0.9965(21)	1.00576(88)	0.9682(23)	1.027(12)	1.00172(13)
a12	1.0052(23)	0.98270(84)	0.9850(23)	1.056(12)	0.99413(12)
a15	1.0272(33)	0.97150(90)	0.9986(24)	1.060(12)	0.99029(13)

TABLE 2.9: Bilinear renormalization constants determined at the scale $\mu = 3\text{GeV}$ in the γ -scheme.

\mathfrak{q} - scheme $\mu = 3\text{GeV}$					
ensemble	Z_q	Z_m	Z_S	Z_P	Z_T
a09	1.05634(59)	0.9714(11)	1.0473(81)	1.0046(89)	1.03794(28)
a12	1.04952(54)	0.9573(11)	1.0701(84)	1.0240(94)	1.02160(28)
a15	1.04993(72)	0.9497(12)	1.0723(80)	1.0379(89)	1.01390(36)

TABLE 2.10: Bilinear renormalization constants determined at the scale $\mu = 3\text{GeV}$ in the \mathfrak{q} -scheme.

2.5 $\overline{\text{MS}}$ Matching For Mixed Basis

Before the short range contributions computed in this work can be input into nuclear matrix element calculations, it is necessary to express them in a scheme where the matching to the original nuclear theory can be done. This requires that the operators and the Wilson coefficients are computed in the same renormalization scheme. A common used scheme is $\overline{\text{MS}}$ at $\mu = 3\text{GeV}$.

The conversion from $\text{RI} - \text{SMOM}$ to $\overline{\text{MS}}$ is performed by means of continuum perturbation theory. First, the renormalization constants for the schemes must be related. For example, for an operator that renormalizes multiplicatively, the renormalized operators differ only by a factor due to the different values of the renormalization constants, that is $\mathcal{O}_i^r = C^{ij}\mathcal{O}_j^r = C^{ij}Z\mathcal{O}^b$, where i denotes the renormalization scheme. Then, using perturbation theory, an expression for the renormalization constants, up to a given constant can

		γ - scheme		$\mu = 3\text{GeV}$	
ensemble	Z_{11}	Z_{2-3}		Z_{4-5}	
a09	0.9453(25)	$\begin{pmatrix} 0.9927(35) & 0.0503(27) \\ 0.01224(26) & 0.9856(26) \end{pmatrix}$	$\begin{pmatrix} 0.9796(12) & -0.01130(70) \\ -0.0492(11) & 0.9637(40) \end{pmatrix}$		
a12	0.9445(25)	$\begin{pmatrix} 0.9862(34) & 0.0205(29) \\ 0.01456(26) & 1.0309(24) \end{pmatrix}$	$\begin{pmatrix} 1.0162(35) & -0.01363(74) \\ -0.02076(99) & 0.9434(38) \end{pmatrix}$		
a15	0.9412(44)	$\begin{pmatrix} 0.9824(51) & 0.0150(30) \\ 0.01807(32) & 1.0558(44) \end{pmatrix}$	$\begin{pmatrix} 1.0399(43) & -0.01719(77) \\ -0.0119(13) & 0.9317(53) \end{pmatrix}$		

TABLE 2.11: Renormalization matrix values determined at $\mu = 3\text{GeV}$ for four-quark operators.

be found and replaced in the above expression. In this way, it is possible to solve for the constants C^{ij} necessary for the conversion from one renormalization scheme to another.

For the four quark operators used in this work, the necessary factors have been previously obtained in [83], and are thus employed here. It is also important to note that as the operators are renormalized with a matrix Z , the required constants to match to $\overline{\text{MS}}$ are arranged in a matrix as well.

Finally, in order to use these results to renormalize the operators calculated in chapter 4, the basis must be switched to the corresponding color mixed basis. The procedure is shown in the appendix B where Fierz Transformations are used to find:

$$\mathcal{O}_{1+}^{++} = (1/4) * Q_2 \quad (2.25)$$

$$\mathcal{O}_{2+}^{++} = (1/4) * 2 * Q_4 \quad (2.26)$$

$$\mathcal{O}_{3+}^{++} = (1/4) * 2 * Q_1 \quad (2.27)$$

$$\mathcal{O}'_{1+}{}^{++} = -(1/4) * 2 * Q_3 \quad (2.28)$$

$$\mathcal{O}'_{2+}{}^{++} = -(1/4) * (Q_4 - Q_5) \quad (2.29)$$

Then, the mixed basis renormalized operators in $\overline{\text{MS}}$ are given by $\mathcal{O}^{\overline{\text{MS}}} = \mathbf{R}\mathcal{O}^{\text{RI-SMOM}}$,

where $\mathcal{O}^{\text{RI-SMOM}} = (\mathcal{O}_1^{++}, \mathcal{O}'_1^{++}, \mathcal{O}_2^{++}, \mathcal{O}'_2^{++}, \mathcal{O}_3^{++})$ and \mathbf{R} is a matrix containing the conversion factors. For completeness the matrix \mathbf{R} , obtained from A.Nicholson, E. Berkowitz, H. Monge-Camacho, D. Brantley, N. Garron, C.C. Chang, E. Rinaldi, M.A. Clark, B. Joó, T. Kurth, B. Tiburzi, P. Vranas, A. Walker-Loud [92] is given below:

$$\mathbf{R} = \begin{pmatrix} 1.0009 & -0.0026 & 0 & 0 & 0 \\ -0.0326 & 1.0909 & 0 & 0 & 0 \\ 0 & 0 & 1.0308 & 0.0201 & 0 \\ 0 & 0 & 0.0135 & 1.1060 & 0 \\ 0 & 0 & 0 & 0 & 1.0043 \end{pmatrix} \quad (2.30)$$

Summary

In this chapter renormalization constants for bilinear and four-quark operators were computed using Mobius Domain Wall Fermions at the scale $\mu = 2$ GeV. In the case of the bilinear operators, these quantities have been computed before but not for all the ensembles used for the calculations presented in this work. On the other hand, renormalization constants for four quark operators have been performed for kaon mixing, however for $\pi^- \rightarrow \pi^+$ matrix elements these are computed here for the first time.

In addition, the corresponding running of these constants was determined as well, and thus enabled the used of three lattice spacing to determine the constants at the renormalization scale $\mu = 3$ GeV. Prior to this work, only two lattice spacings have been used, and thus the results presented here should have an improved control over the continuum extrapolation as compared to others.

CHAPTER 3

Application: Nucleon Axial Charge

The nucleon coupling to the weak axial charge plays an important role in many fundamental nuclear processes, such as nuclear beta decay and pion exchange. The strength of this coupling is determined by a quantity known as the axial charge, and corresponds to the nucleon axial form factor at the limit of zero momentum transfer and it is usually represented by g_A . Thus, the axial charge not only plays a major role in characterizing the nucleon, but its determination from QCD is fundamental to better understand and test nuclear physics processes from the SM.

However, as energies relevant to nuclear physics processes lie in the strong interactions low-energy regime, determination of the axial charge poses further complications as perturbation theory breaks down and a non-perturbative solution is required. Solving QCD non-perturbatively is possible numerically with LQCD, and in fact, previous determinations of the nucleon axial charge from LQCD have been performed in [93, 94, 95, 96, 97, 98, 99, 100]. Nevertheless, achieving precisions at the experimental level has been a major issue, and according to the LQCD community, overcoming this problem requires a good control of the excited state contamination and high statistical precision [101]. In this chapter, a

method which provides a good control of the excited state contamination and high statistical precision is used to determine, at a precision not achieved before, the nucleon axial charge, which enters in the neutron to proton decay rate.

The calculation starting point is the matrix element of the isovector axial current $A_\mu^a = \bar{q}\gamma_\mu\gamma_5\frac{\tau^a}{2}q$, which is described by the axial vector and pseudo axial form factors as given in the following equation:

$$\langle N(\mathbf{p}', s') | A_\mu^a | P, S \rangle = \bar{U}(P', S') \left[\gamma_\mu G_A(Q^2) + \frac{(P' - P)_\mu}{2M_N} G_P(Q^2) \right] \gamma^5 \tau^a U(P, S) \quad (3.1)$$

At zero momentum transfer $Q^2 = -(P' - P)^2 = 0$, the above matrix element is related to the nucleon axial charge, and can thus be used to determine the latter with a LQCD calculation.

3.1 Feynman-Hellman Method

The Feynman-Hellman theorem provides a relation between the variations, with respect to a given parameter, of both the energy spectrum and the matrix element of the Hamiltonian. This relation, is given by:

$$\partial_\lambda E_\lambda^n = \langle \mathbf{n} | H_\lambda | \mathbf{n} \rangle \quad (3.2)$$

Where the Hamiltonian is given by $H = H_0 + H_\lambda$.

In LQCD, computation of the energy spectrum is standard and relies on two-point correlation function calculations. Thus, energy spectrum variations, appearing in left hand side of 3.2, can be analysed using the same techniques. In the case of the nucleon axial charge for example, the matrix element of interest is given by 3.1. The energy spectrum

can be obtained from the following correlation function:

$$C_\lambda(t) = \langle \lambda | \mathcal{O}(t) \mathcal{O}^\dagger(0) | \lambda \rangle = \frac{1}{\mathcal{Z}} \int \mathcal{D}\Phi e^{-S-S_\lambda} \mathcal{O}(t) \mathcal{O}^\dagger(0) \quad (3.3)$$

Here the operators \mathcal{O}^\dagger and \mathcal{O} are creation and annihilation interpolating operators. λ indicates that the quantity is computed in the presence of a source term H_λ , and the corresponding vacuum state is denoted by $|\lambda\rangle$. In the limit $\lambda \rightarrow 0$, and for a source proportional to λ , the source-less vacuum state $|\Omega\rangle$ is recovered and 3.3 becomes:

$$C_\lambda(t) \Big|_{\lambda=0} = \langle \Omega | \mathcal{O}(t) \mathcal{O}^\dagger(0) | \Omega \rangle = C(t) \quad (3.4)$$

We can use the method of sources, to relate $\partial_\lambda C(t)$ to a correlation function with an insertion between \mathcal{O} and \mathcal{O}^\dagger :

$$\partial_\lambda C_\lambda(t) \Big|_{\lambda=0} = \frac{-1}{\mathcal{Z}} \int \mathcal{D}\Phi e^{-S} \mathcal{T} \{ \mathcal{O}(t) (\partial_\lambda S_\lambda) \Big|_{\lambda=0} \mathcal{O}^\dagger(0) \} = \langle \Omega | \mathcal{O}(t) (\partial_\lambda S_\lambda) \Big|_{\lambda=0} \mathcal{O}^\dagger(0) | \Omega \rangle \quad (3.5)$$

As λ dependent expressions are to be evaluated at $\lambda = 0$, from here on, the evaluation indication will be removed, for example:

$$\frac{C_\lambda(t)}{\partial_\lambda} \Big|_{\lambda=0} \equiv \partial_\lambda C_\lambda(t) \quad C_\lambda(t) \Big|_{\lambda=0} \equiv C(t)$$

Using the two-point function in 3.3, an effective mass can be constructed in the same way it was done in the first chapter, which in the case of baryons is given by 1.43. The variations in the effective mass with respect to λ for baryons, as derived in [102], are given

by:

$$\left. \frac{\partial \mathbf{m}_{\text{eff}}}{\partial \lambda} \right|_{\lambda=0} = \frac{1}{\tau} \left\{ \frac{\partial_\lambda C(t)}{C(t)} - \frac{\partial_\lambda C(t+\tau)}{C(t+\tau)} \right\} \Big|_{\lambda=0} \quad (3.6)$$

and for mesons the derivation is straightforward as well and leads to:

$$\left. \frac{\partial \mathbf{m}_{\text{eff}}}{\partial \lambda} \right|_{\lambda=0} = \frac{-\partial_\lambda C(t+\tau) + \partial_\lambda C(t-\tau) - 2\cosh(\mathbf{m}_{\text{eff}}\tau)\partial_\lambda C(t)}{2\tau C(t)\sinh(\mathbf{m}_{\text{eff}}\tau)} \quad (3.7)$$

The last two equations show that only C_λ and $\partial_\lambda C_\lambda$ are necessary to determine the effective mass variations. Therefore, in order to extract the matrix element from its relation with $\partial_\lambda \mathbf{m}_{\text{eff}}$, an expression for $\partial_\lambda C_\lambda$ which includes the matrix element is necessary. This can be obtained by taking the partial derivative of the expression 3.3 and corresponds to:

$$\left. \frac{\partial C_\lambda(t)}{\partial \lambda} \right|_{\lambda=0} = -C(t) \int dt' \langle \Omega | J(t') | \Omega \rangle + \int dt' \langle \Omega | T \mathcal{O}(t) J(t') \mathcal{O}^\dagger(0) | \Omega \rangle \quad (3.8)$$

For currents without vacuum quantum numbers the first term in last equations right-hand side does not contribute. However, in the case of baryons, even if that is not the case, this term would cancel in the difference appearing in 3.6. For that reason, only the second term will be considered here, which in the lattice corresponds to:

$$N(t) = \sum_{t'=0}^{T-1} \langle \Omega | T \mathcal{O}(t) J(t') \mathcal{O}^\dagger(0) | \Omega \rangle \quad (3.9)$$

Then, using the spectral decomposition on the second term, the $\partial_\lambda C_\lambda$ explicit time depen-

dence can be found for baryons and mesons, in the first case the result is [102]:

$$N(t) = \sum_n \left[(t-1)z_n g_{nn} z_n^\dagger + d_n \right] e^{-E_n t} + \sum_{n,m \neq n} \frac{e^{-E_n t + \Delta_{nm}/2}}{e^{\Delta_{mn}/2} - e^{\Delta_{nm}/2}} (z_n g_{nm} z_m^\dagger + z_m g_{mn} z_n^\dagger) \quad (3.10)$$

where:

$$\Delta_{mn} = E_m - E_n, \quad g_{nm}^J \equiv \frac{J_{nm}}{\sqrt{4E_n E_m}} \quad (3.11)$$

and

$$d_n^J \equiv Z_n Z_{j:n}^\dagger + Z_{j:n} Z_n^\dagger + Z_n Z_n^\dagger \langle \Omega | J | \Omega \rangle + \frac{Z_n Z_{nj}^\dagger J_j^\dagger + J_j Z_{nj} Z_n^\dagger}{2E_j (e^{E_j} - 1)} \quad (3.12)$$

and the overlap factors are given by:

$$\begin{aligned} Z_{j:n}^\dagger &= \langle n | \mathcal{J} \mathcal{O}^\dagger | \Omega \rangle & Z_{j:n} &= \langle \Omega | \mathcal{O} \mathcal{J} | n \rangle \\ Z_n^\dagger &= \langle n | \mathcal{O}^\dagger(0, \mathbf{0}) | \Omega \rangle & Z_n^p &= \sum_{\mathbf{x}} e^{i\mathbf{p} \cdot \mathbf{x}} \langle \Omega | \mathcal{O}(0, \mathbf{x}) | n \rangle \end{aligned}$$

and in the case of mesons a similar expression can be determined.

3.2 Lattice Calculation Details

A subset of the publicly available Highly Improved Staggered Quark (HISQ) with dynamical light, strange and charm quarks ($N_f = 2+1+1$) previously generated by the MILC Collaboration [103] was used for the calculations. They were generated with near-physical values of the strange and charm quark masses, three values of the pion mass, $m_\pi \approx 130, 220, 310$ MeV and at three lattice spacings $a \approx 0.15, 0.12, 0.09$ fm. Ad-

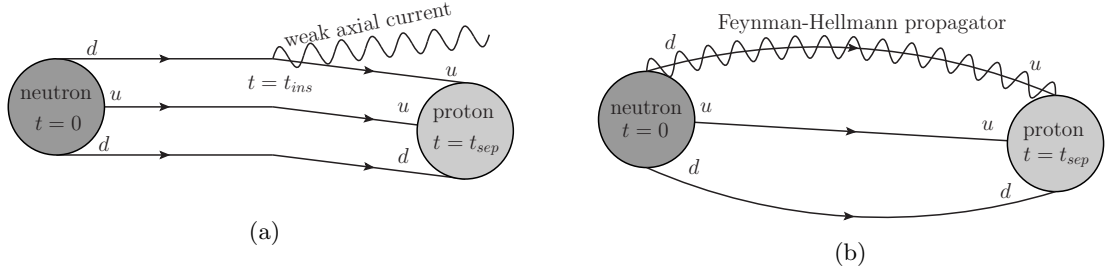


FIG. 3.1: Feynman diagrams for computing the axial charge g_A in the standard and Feynman-Hellman methods. In the neutron β – decay into a proton a neutron d quark converts into a proton u quark via the weak axial current. Only valence quark diagrams are shown while the diagrams corresponding to gluons coupled to quarks and gluons to gluons, and the dynamical quark/anti-quark pairs are excluded. In the standard method a) the axial current is inserted at t_{ins} . For the Feynman-Hellmann method b) the weak axial current is inserted and sum over all possible insertion times (t_{ins}).

ditional HISQ ensembles were generated at $m_\pi \approx 350, 400$ MeV with the above lattice spacings. The purpose of using this ensembles is to provide enough data to control the continuum limit, infinite volume and physical pion mass extrapolation. Additional important factors to consider in this calculation are the discretization errors and chiral symmetry breaking. For the HISQ action errors start at $O(\alpha_s^2, a^2, a^4)$, and improved link-smearing can further reduce these errors due to suppression of taste-changing interactions. The tadpole-improved, one-loop Symanzik gauge action is used for gluons, with discretization errors starting at $O(\alpha_s^2, a^2, a^4)$. Valence quarks use MDWF action, which together with gradient-flow smearing of HISQ ensemble, highly suppresses the residual chiral symmetry breaking of the MDWF action, and discretization errors from this action begin at $O(a^2)$ [104]. The smearing used is gradient flow smearing with a flow time fixed to $t_{gf} = 1.0$ in lattice units on all gauge configurations and computed with the Wilson-flow diffusion equation. Effects due to this smearing are studied following [105] and checked in this work using three different flow times, $t_{gf} = 1.0, 0.6, 0.2$, which showed little effects due to smearing and smaller stochastic uncertainties at increasingly larger values of t_{gf} were

observed.

3.3 Correlation functions analysis

Correlations functions are created in the lattice by using interpolating fields to create or annihilate particles. When acting on the vacuum, these interpolators do not create/annihilate isolated states, but instead tower of states. Thus, an exact wavefunction for the ground state nucleon cannot be obtained. As a consequence, in order to extract information from lattice calculations, the ground and excited states must be disentangled to obtain only the contributions of interest. This requires a careful analysis of the correlation functions, and has become one of the major challenges for past calculations of g_A .

One advantage of the method used in this work, is that the correlation function can be accessed at both earlier and later time separations between the initial and final states. This facilitates a more complete study of excited state contributions to better separate the ground and excited states contributions. Moreover, at earlier times, the exponentially growing noise for nucleon observables is less severe, hence access to earlier times leads to reduced statistical errors.

3.3.1 Fitting procedure

To extract information from the correlation functions, a simultaneous fit to the nucleon two-point correlation function and the vector and axial-vector FH ratios 3.6 was done. Additionally, for each of these, two different types of sink smearing for the quark fields are used as well. The purpose of this strategy is to enhance the amount of correlated data when determining a large subset of shared parameters. Unknown parameters are estimated following the work on [102] and the parameter space in t is explored by first using a two-state Bayesian constrained fit which is followed by a two-state unconstrained fit using the

non-linear least-squares method to minimize the χ^2 functional.

From the bayesian fit, a posterior distribution is found and its central value is employed as an input guess value for the second fit. The purpose of this preconditioning of the unconstrained fit is to explore the large parameter space while minimizing the number of iterations required for convergence. Moreover, the input from the bayesian posterior distribution also helps in avoiding unphysical local minima in the χ^2 manifold.

To discriminate from acceptable and poor fits, the p-value and effects of excited states contamination are considered. Only fits with a p-value greater than 0.05 are used and fits where excited state contamination is stable with respect to time separation variations. The fits stability analysis for this method is possible due to the Feynman-Hellmann method implemented in this work which grants access to all possible initial and final state separation times. Information from correlation functions data at earlier times, where excited state contamination is greater, allows for a better understanding and control of excited states contributions, a significant challenge for this type of calculation. A sample fit to g_A with this procedure is shown in figure 3.2.

Finally, determination of the matrix element statistical uncertainty is performed using a 5000 bootstrap sample. Also, as data at smaller time separations can be used in this calculation, where the signal-to-noise ratio is smaller, an exponentially more precise determination of the nucleon couplings is possible.

3.4 Chiral, Continuum and infinite volume extrapolations

Turning lattice results into physical meaningful quantities usually requires continuum limit, chiral, infinite volume extrapolations and renormalization (which was performed on

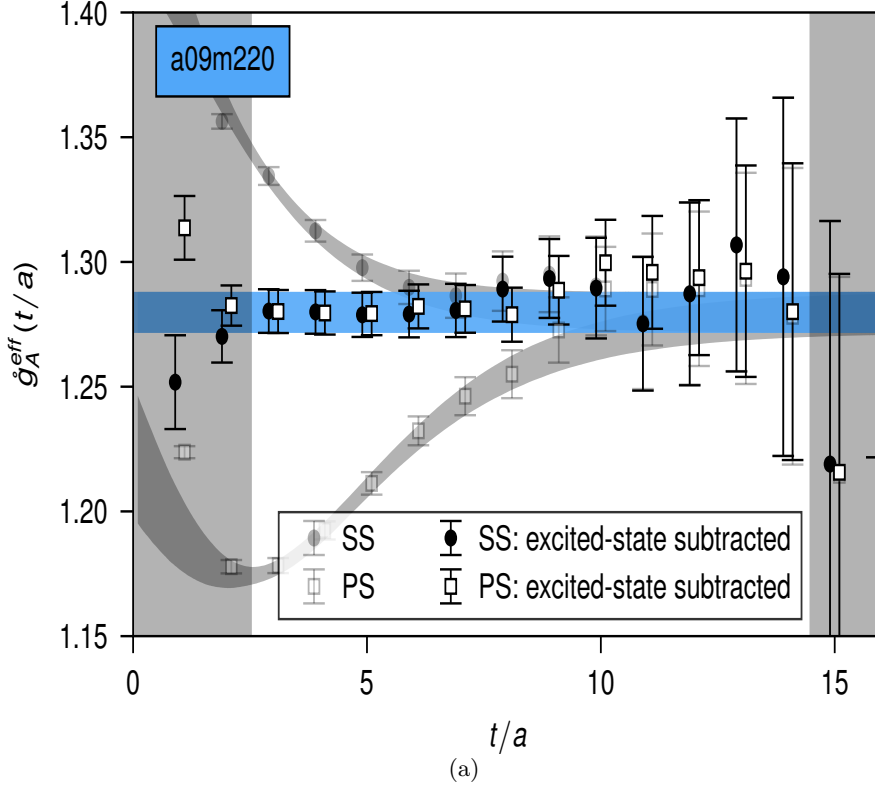


FIG. 3.2: g_A data fit example for ensemble with lattice spacing $a \approx 0.09\text{fm}$ and $m_\pi \approx 220\text{MeV}$. The raw numerical data (points) and its fits (bands) are displayed in gray as well as vertical bands indicating excluded regions from the fits. The solid black and white data corresponds to original data with contributions from excited states (determined in the fit) subtracted. The full fit result to the ground state value of g_A is shown with solid blue band. The two data sets corresponds to different sink-source types: smeared-smeared (SS) and point-smearing.

the previous chapter). Additionally, when quantities of interest are dimensional, conversion to physical units is necessary as well. In this calculation however, g_A is a dimensionless quantity, and conversion to physical units can be avoided by employing dimensionless ratios at the time of extrapolating to the physical point. Hence, no scale setting is required and only three quantities are necessary to parameterise the physical point extrapolations, these are:

$$\epsilon_a^2 = \frac{1}{4\pi} \frac{a^2}{w_0^2}, \quad m_\pi L, \quad \epsilon_\pi = \frac{m_\pi}{4\pi F_\pi}, \quad (3.13)$$

These quantities parameterise the continuum limit, infinite volume and physical pion mass respectively. The gradient flow scale w_0 can be determined as in [106] and $F_\pi \approx 92$ MeV is the pion decay constant. An appropriate framework for the above extrapolations is EFT which provides a rigorous prescription and more control over systematic uncertainties.

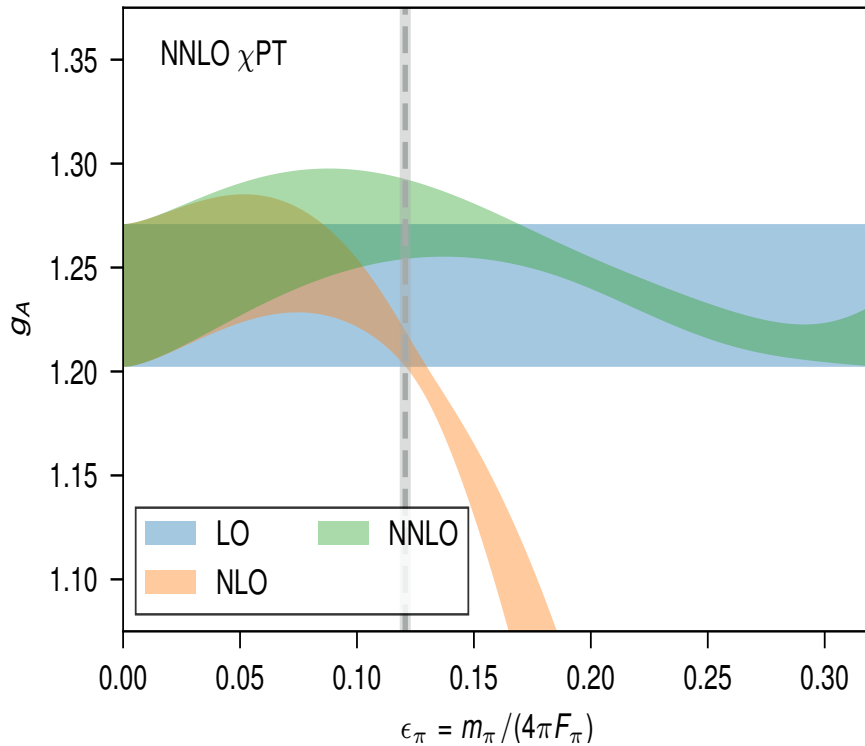


FIG. 3.3: Extrapolating fits for contributions up to NNLO to g_A . The gray vertical band indicates the physical point.

First, for the chiral extrapolation, two-flavor Heavy Baryon χ PT(HB χ PT) [107] is necessary for a controlled extrapolation of the pion mass dependence. The expression for the g_A pion mass dependence is known through $\mathcal{O}(m_\pi^3)$ [107, 108, 109] or next-to-next-to-

leading order (NNLO) in the chiral expansion, and is given in terms of ϵ_π by:

$$g_A = g_0 + c_2 \epsilon_\pi^2 - \epsilon_\pi^2 (g_0 + 2g_0^3) \ln(\epsilon_\pi^2) + g_0 c_3 \epsilon_\pi^3, \quad (3.14)$$

For the last expression the χ PT renormalization scale was set to $\mu = 4\pi F_\pi$ and g_0 , c_2 and c_3 are low-energy constants (LECs) to be determined in the analysis. A fit presenting the contributions to g_A , up to NNLO in the χ PT expansion, is shown in figure 3.3.

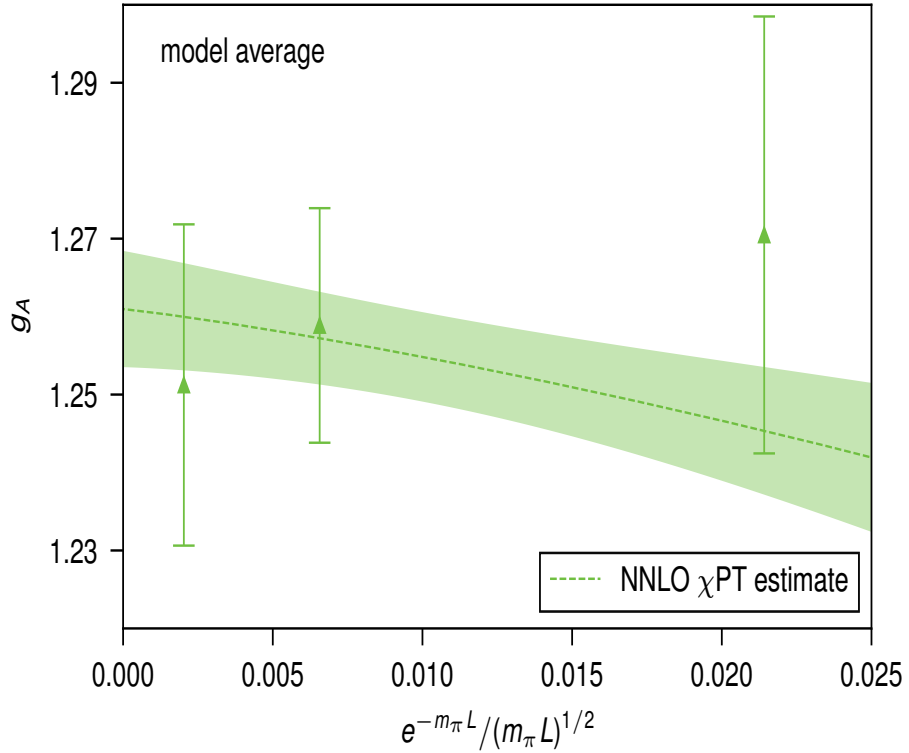


FIG. 3.4: Infinite volume extrapolation of g_A . The data points correspond to $m_\pi L = 5.36, 4.30, 3.25$ for ensembles with lattice spacing $a \approx 0.12\text{fm}$ and $m_\pi \approx 220\text{MeV}$. The green band and dashed curve (central value) correspond to the NLO finite-volume dependence predicted from the model averaged extrapolation (to all data points in the analysis)

Second, for the infinite volume extrapolation, an infrared modification of the pion propagators [110] can be performed in order to include these corrections into the EFT. These corrections are expected to fall off at least as fast as $e^{-m_\pi L}$ in the large volume limit.

For g_A , the leading volume corrections are found in [111] to be:

$$\delta_L \equiv g_A(L) - g_A(\infty) = \frac{8}{3} \epsilon_\pi^2 [g_0^3 F_1(m_\pi L) + g_0 F_3(m_\pi L)]$$

where

$$F_1(x) = \sum_{\mathbf{n} \neq 0} \left[K_0(x|\mathbf{n}|) - \frac{K_1(x|\mathbf{n}|)}{x|\mathbf{n}|} \right] \quad F_3(x) = -\frac{3}{2} \sum_{\mathbf{n} \neq 0} \frac{K_1(x|\mathbf{n}|)}{x|\mathbf{n}|}. \quad (3.15)$$

g_0 is the leading order(LO) contribution to g_A in the chiral expansion and $K_\nu(z)$ are modified Bessel functions of the second kind. In the limit of large $m_\pi L$ (infinite volume) these corrections become:

$$\delta_L = 8g_0^3 \epsilon_\pi^2 \sqrt{2\pi} \frac{e^{-m_\pi L}}{\sqrt{m_\pi L}} + O\left(e^{-\sqrt{2}m_\pi L}, \frac{1}{(m_\pi L)^{3/2}}\right). \quad (3.16)$$

The finite volume effects for g_A are presented in figure 3.4 where a finite volume extrapolation fit is performed.

Finally, for the continuum limit, a Taylor expansion in the discretisation scale is used with a $\epsilon_a^2 \epsilon_\pi^2$ included. An alternative for MDWF on HISQ action is to use mixed-action EFT (MAEFT) to describe discretisation effects, however the data used in these work does not constrain the parameters introduced by MAEFT [2]. Then, possible discretisation effects are given to NNLO in the Symanzik expansion [112, 113] by:

$$\delta_a = \mathbf{a}_2 \epsilon^2 + \mathbf{b}_4 \epsilon_a^2 \epsilon_\pi^2 + \mathbf{a}_4 \epsilon_a^4, \quad (3.17)$$

the first and second term correspond respectively to NLO and NNLO corrections, with the second arising from a power counting in $\epsilon_\pi^2 \approx \epsilon_a^2$. The unknown coefficients $\mathbf{a}_2, \mathbf{b}_4$ and \mathbf{a}_4 are constants obtained from the data extrapolation analysis. Additionally, corrections

arising from residual chiral symmetry breaking due to the use of local axial and vector currents and from generic one-loop radiative gluon corrections at finite lattice spacing are given by the first and second term of the following equation:

$$\delta'_a = \mathbf{a}_1 \sqrt{4\pi} \epsilon_a + s_2 \alpha_s \epsilon_a^2, \quad (3.18)$$

where $\mathbf{a}_1 = O(m_{\text{res}})$ and $s_2 = O(1)$.

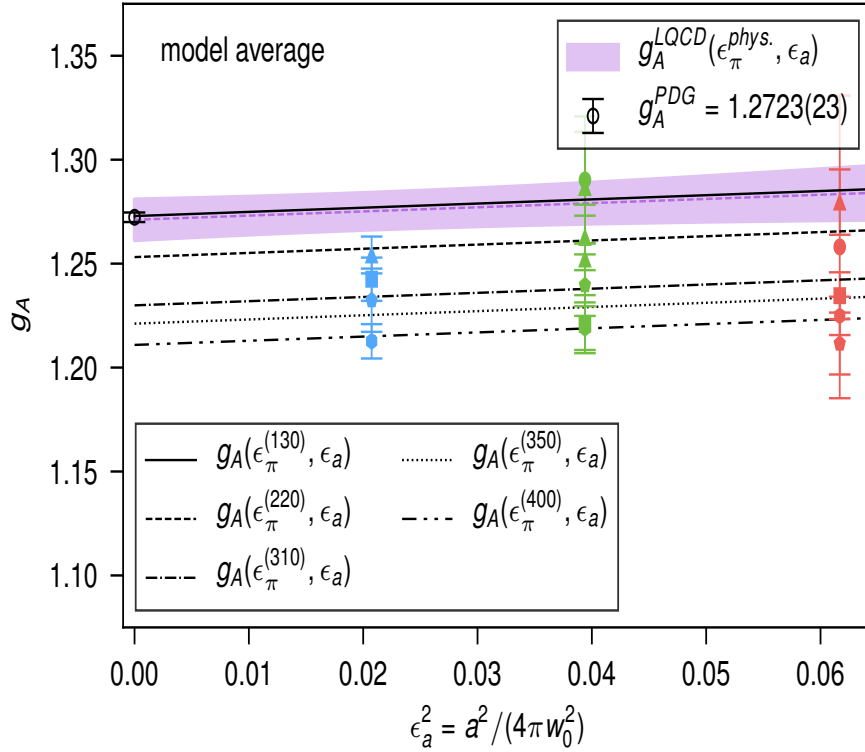


FIG. 3.5: Continuum extrapolation of g_A . The nucleon axial coupling lattice spacing is parameterised by using ϵ_a^2 . The magenta band and dashed magenta curve (central value) indicate the physical point limit. Central value curves are plotted for $m_\pi \approx 220\text{MeV}$ (dashed), $m_\pi \approx 310\text{MeV}$ (dot-dashed), $m_\pi \approx 350\text{MeV}$ (dotted), and $m_\pi \approx 400\text{MeV}$ (dot-dot-dashed).

3.5 Final Result

The final value determined for the nucleon axial charge g_A at the physical point in this work is obtained from a model average. The uncertainty is computed by adding in quadrature the statistical(s), chiral(χ), continuum(a), infinite volume(v), isospin breaking(I) and model(M) contributions and the result with the uncertainties breakdown is:

$$g_A = 1.2711(103)^s(39)^{\chi}(15)^a(19)^v(04)^I(55)^M. \quad (3.19)$$

The good control over finite temporal effects, and the relatively low computational cost of the method employed were key factors to achieve these precise result and further improvements can be obtained by increasing the statistics.

This result is consistent with the experimental value, determined from neutron β decay $g_A^{\text{PDG}} = 1.2723(23)$ [114]. From LQCD, this is the first calculation to achieve errors at the percent level and the second to account for all the systematics. Moreover, with uncertainties similar to those of experiments, such calculations may help us understand the upward trend from experimental determinations [114]. On the phenomenological side, collider and low-energy experiments results have been used together with EFT to look for bounds on right-handed BSM currents [115]. One way to constrain these currents is by using results from cold neutron decay experiments, for which the above g_A result was used as input. The constraints arising from this g_A result lead to the most stringent limits [2] compared to those due to W^- and Higgs boson production and pion decays.

CHAPTER 4

Short Range Contributions to $0\nu\beta\beta$

In this chapter, leading order contributions from short range interaction processes relevant to $0\nu\beta\beta$ are obtained, for the first time, with LQCD. These can serve as input for the determination of $0\nu\beta\beta$ decay rates induced by the short range interactions.

Most of the recent research on $0\nu\beta\beta$ has been focused on the light majorana exchange mechanism in a long-range interaction process. On the other hand, short-range interactions have been considered to be relatively small compared to the above because of suppression by the heavy mass neutrino. Nevertheless, as pointed out in [116] a helicity flip, proportional to the light neutrinos mass, is required for the light majorana neutrino exchange. Thus, if neutrino masses are generated by the seesaw mechanism, the light neutrino mass would be suppressed as well by a heavy scale corresponding to the new physics.

At the present time, the mechanisms and nature of the neutrino masses are still unknown, and short-range contributions should not be discarded as they may contribute equally in certain BSM models. Therefore, the long and short-range physics relative importance must be assessed (for a given particle physics model) and calculating short-range contributions becomes necessary.

For $0\nu\beta\beta$ via the above mentioned short-range mechanism, the interaction would happen at distance scales several orders of magnitude smaller than the size of the neutron. Despite this short distance nature, the leading contribution comes from a $\pi^- \rightarrow \pi^+ e^- e^-$ transition, and so can act at distance scales of order the size of the nucleus. The resulting $0\nu\beta\beta$ decay would not be observed in isolation, but only in the presence of a large nucleus such as Ge-76 and Xe-136 so the interaction would be further renormalized by the many-body nuclear interactions, also dictated by QCD. It is thus very important to understand the effects of the underlying QCD interactions involved in $0\nu\beta\beta$, however, as the energies relevant to nuclear physics lie in the low-energy regime, a non-perturbative solution is required. Fortunately, because the clear separation of scales, an appropriate framework to study the QCD contributions is given by EFTs. Using EFT, 9 local four-quark operators which can contribute to $0\nu\beta\beta$ at leading order have been found [117, 69], among those, three important process arise when matching to a nuclear EFT, these are illustrated in figure 4.1.

From the contributions shown in figure 4.1, the focus will be on the relevant processes for $0^+ \rightarrow 0^+$ nuclear transitions, which to LO corresponds to diagrams (a) and (d). At the present time, there is only a theoretical estimation of these contributions [118] to $0\nu\beta\beta$ and in this work the first LO calculations from the pion exchange interaction $\pi^- \rightarrow \pi^+$ is performed using LQCD. In addition, this work proposes a strategy to tackle the calculation of four nucleon contact operators which are significantly more complicated.

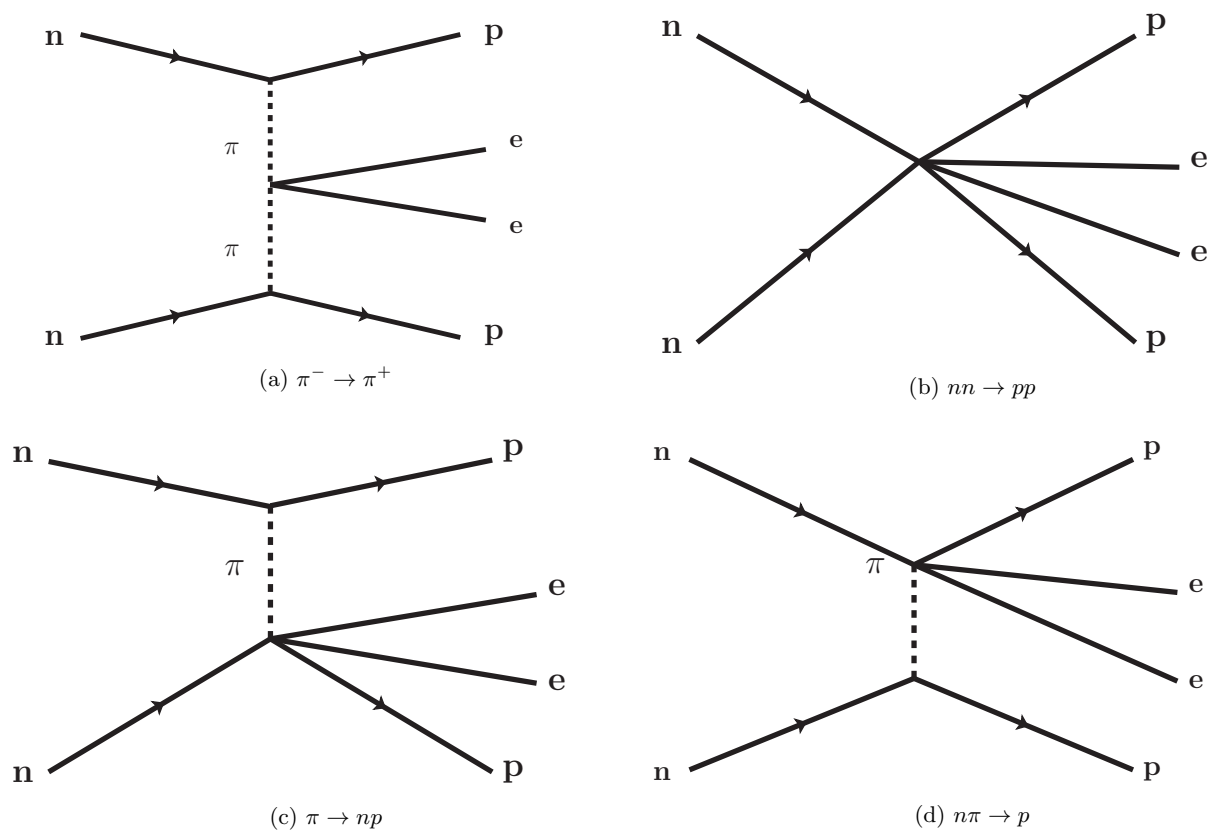


FIG. 4.1: Diagrams for processes contributing to $0\nu\beta\beta$ through short range interactions.

4.1 $\pi^- \rightarrow \pi^+$ Contribution

4.1.1 Four-quark Operators

To determine the matrix elements arising from diagram (a) in 4.1, the most convenient framework is EFT as mentioned above, in which case rather than computing the full $n\bar{n} \rightarrow p\bar{p}e\bar{e}$ transitions one can instead calculate the on-shell transition $\pi^- \rightarrow \pi^+$ amplitude. The advantages of this approach for LQCD are avoiding the signal-to-noise problem [119] and the scattering states in a finite volume [120, 121]. From the operators relevant to this process and found in [117], here only the parity even operators have non-zero contributions, whereas the vector operators are suppressed by a power of the electron mass and thus are not considered here. The set of operators to study are:

$$\begin{aligned}
\mathcal{O}_{1+}^{++} &= (\bar{q}_L \tau^+ \gamma^\mu q_L) [\bar{q}_R \tau^+ \gamma_\mu q_R] \\
\mathcal{O}_{2+}^{++} &= (\bar{q}_R \tau^+ q_L) [\bar{q}_R \tau^+ q_L] + (\bar{q}_L \tau^+ q_R) [\bar{q}_L \tau^+ q_R] \\
\mathcal{O}_{3+}^{++} &= (\bar{q}_L \tau^+ \gamma^\mu q_L) [\bar{q}_L \tau^+ \gamma_\mu q_L] + (\bar{q}_R \tau^+ \gamma^\mu q_R) [\bar{q}_R \tau^+ \gamma_\mu q_R] \\
\mathcal{O}'_{1+}{}^{++} &= (\bar{q}_L \tau^+ \gamma^\mu q_L) [\bar{q}_R \tau^+ \gamma_\mu q_R] \\
\mathcal{O}'_{2+}{}^{++} &= (\bar{q}_R \tau^+ q_L) [\bar{q}_R \tau^+ q_L] + (\bar{q}_L \tau^+ q_R) [\bar{q}_L \tau^+ q_R]
\end{aligned} \tag{4.1}$$

The color contractions are indicated by using $()$ and $[\]$ to enclose the quarks following the Takahashi notation [122]. For example $(\bar{q}q)[\bar{q}q] = \bar{q}^a q^a \bar{q}^b q^b$ while $(\bar{q}q)[\bar{q}q] = \bar{q}^a q^b \bar{q}^b q^a$. Also the operators, $\mathcal{O}'_{i+}{}^{++}$ are included because of the mixing of operators with the same chirality due to renormalization from the weak to the QCD scale [69].

4.1.2 Numerical Method

It has been shown in [76] for general cases, that some matrix elements can be extracted from correlation function ratios. For the matrix element to compute here, this works as

well given that the following ratio is used:

$$\mathcal{R}_i(\mathbf{t}) \equiv C_i^{3\text{pt}}(\mathbf{t}, \mathbb{T} - \mathbf{t}) / (C_\pi(\mathbf{t})C_\pi(\mathbb{T} - \mathbf{t})) = \frac{\alpha^4 \langle \pi | \mathcal{O}_{i^+}^{++} | \pi \rangle}{(\alpha^2 Z_0^\pi)^2} + \mathcal{R}_{e.s.}(\mathbf{t}) \quad (4.2)$$

In the last equation, $C_i^{3\text{pt}}$ corresponds to a three-point function with an operator inserted and C_π is the pion correlation function and $Z_n^\pi = \sum_{\mathbf{x}} \langle \Omega | \Pi^+ | \mathbf{n} \rangle$. $|\pi\rangle$ represents the pion ground states while excited states contributions are given by $\mathcal{R}_{e.s.}(\mathbf{t}) \propto e^{-(E_n^\pi - E_0^\pi)t}$.

In this ratio, the exponential time dependence in the numerator is canceled by the denominator, and a fit to a constant should be sufficient to extract the matrix element provided excited state contamination is suppressed. The three-point function to employ in order to construct \mathcal{R} is the following:

$$C_i^{3\text{pt}}(\mathbf{t}_i, \mathbf{t}_f) = \sum_{\alpha} \sum_{\mathbf{x}, \mathbf{y}} e^{-E_\alpha \mathbb{T}} \langle \alpha | \Pi^+(\mathbf{t}_f, \mathbf{x}) \mathcal{O}_i(\mathbf{0}, \mathbf{0}) \Pi^+(\mathbf{t}_i, \mathbf{y}) | \alpha \rangle \quad (4.3)$$

where $\Pi^+(\mathbf{t}_f, \mathbf{x}) = \bar{\mathbf{d}}\gamma^5\mathbf{u}$ is the annihilation operator for a π^+ particle at a time \mathbf{t}_f and $\Pi^+(\mathbf{t}_i, \mathbf{y}) = \Pi^{-\dagger}(\mathbf{t}_i)$ is the creation operator for a π^- particle at time \mathbf{t}_i . The four-quark operator \mathcal{O}_i corresponds to the i operator in the basis 4.1. The two point correlation function is given by:

$$C_\pi(\mathbf{t}) = \sum_{\mathbf{x}, \alpha} \langle \alpha | \Pi^+(\mathbf{t}, \mathbf{x}) \Pi^+(\mathbf{0}, \mathbf{0}) | \alpha \rangle \quad (4.4)$$

$$= \sum_{\mathbf{n}} \frac{|Z_{\mathbf{n}}^\pi|^2}{2E_{\mathbf{n}}^\pi} \left(e^{-E_{\mathbf{n}}^\pi t} + e^{-E_{\mathbf{n}}^\pi(\mathbb{T}-t)} \right) + \dots \quad (4.5)$$

To compute $C_i^{3\text{pt}}(\mathbf{t}, \mathbb{T} - \mathbf{t})$ on the lattice, all the Wick contractions must be performed.

One of them, for example is:

$$\begin{aligned}
C^{3\text{pt}}(t_f, t_i) &= \left\langle \underbrace{\bar{d}(z)\gamma^5 \overbrace{u(z) \bar{u}(0)\Gamma^1 d(0)}^{\text{meson}} \overbrace{u(0)\Gamma^2 \bar{d}(0)}^{\text{meson}} d(x)\gamma^5 u(x)} \right\rangle \quad (4.6) \\
&= -\gamma_{\alpha\beta}^5 \gamma_{\kappa\epsilon}^5 \Gamma_{\delta\sigma}^1 \Gamma_{\gamma\rho}^2 D(0, \mathbf{x})_{\rho\kappa ce} D(0, \mathbf{z})_{\sigma\alpha ba} U(\mathbf{z}, 0)_{\beta\gamma ac} U(\mathbf{x}, 0)_{\epsilon\delta eb}
\end{aligned}$$

in the last equation D and U represent the d and u quark propagators and the prime is used to indicate that only one Wick contraction is included. The calculation of 4.6 is implemented in two different ways and compared to an independent calculation.

In the first method, the following quantity is considered:

$$\Pi(0, \mathbf{x})_{\rho\delta cb} = \gamma_{\rho\rho'}^5 D(0, \mathbf{x})_{\rho'\kappa'ce}^\dagger \gamma_{\kappa'\kappa}^5 \gamma_{\kappa\epsilon}^5 U(\mathbf{x}, 0)_{\epsilon\delta eb}$$

this corresponds to two quarks propagators contracted to form a pion at one end, and at the other end the quarks indices are kept uncontracted, often referred to as a meson block. $\Pi(0, \mathbf{x})$ can be obtained with a single propagator inversion as the $D(0, \mathbf{x})^\dagger$ can be obtained through γ^5 -hermiticity. The open indices will later be used to contract with the Dirac-color structure of the operator. Replacing $\Pi(0, \mathbf{x})$ in the expression for $C^{3\text{pt}}(t_f, t_i)$ the result is:

$$C^{3\text{pt}}(t_i, t_f) = \sum_{\mathbf{z}, \mathbf{x}} \Gamma_{\delta\sigma}^1 \Gamma_{\gamma\rho}^2 \Pi(\mathbf{z}, t_f; 0)_{\sigma\gamma cb} \Pi(0; \mathbf{x}, t_i)_{\rho\delta cb} \quad (4.7)$$

4.7 shows that it is valid to perform a momentum projection at the sink of each $\Pi(\mathbf{y}, \mathbf{x})$ structure before contracting with Γ^1 and Γ^2 . This results in a computational efficient method for this case and it is thus employed for data production. In figure 4.2 the diagram representing the calculation $C^{3\text{pt}}(t_i, t_f)$ with this implementation is illustrated.

The second method serves as a cross-check of results obtained with the previous one.

In this case the following quantity is used:

$$S(z, \mathbf{x})_{\beta\kappa\alpha e} = U(z, 0)_{\beta\gamma\alpha c} \Gamma_{\gamma\rho}^2 D(0, \mathbf{x})_{\rho\kappa c e} \quad (4.8)$$

Here S corresponds to a sequential propagator with a current inserted at a single space-time point. Using S , the three-point function can be written as:

$$\begin{aligned} C^{3\text{pt}}(t_f, t_i) &= - \sum_{\mathbf{x}, \mathbf{y}} S(t_f, \mathbf{z}; t_i, \mathbf{x})_{\beta\kappa\alpha e} S(t_i, \mathbf{x}; t_f, \mathbf{z})_{\beta\kappa\alpha e}^\dagger \\ &= \begin{cases} -S(t_f, \mathbf{z}; t_i, \mathbf{x})_{\beta\kappa\alpha e} S(t_f, \mathbf{z}; t_i, \mathbf{x})_{\kappa\beta e\alpha} & \text{for } [\gamma^5, \Gamma] = 0 \\ S(t_f, \mathbf{z}; t_i, \mathbf{x})_{\beta\kappa\alpha e} S(t_f, \mathbf{z}; t_i, \mathbf{x})_{\kappa\beta e\alpha} & \text{for } \{\gamma^5, \Gamma\} = 0 \end{cases} \end{aligned} \quad (4.9)$$

Then, only a contraction of two sequential propagators is required to obtain $C^{3\text{pt}}(z, \mathbf{x})$.

For the implementation of both of these methods, the Lalibe software ¹ suit was

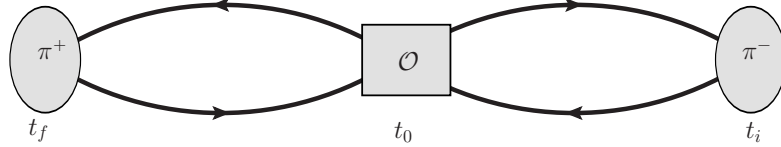


FIG. 4.2: Three-point function diagram for four-quark operators contributing to $\pi^- \rightarrow \pi^+$.

employed to generate the quark and sequential propagators and saved into hdf5, a format for storing and managing data. Then, contractions for both methods were implemented in python. The resulting error of calculating a given three-point correlation function was found to be within rounding error. Additionally, as mentioned before, this results were confirmed by an independent cross-check. The results obtained are shown in 4.3.

¹This software will be available soon at <https://github.com/callat-qcd/lalibe>

4.1.3 Chiral, continuum and infinite volume extrapolations

In order to determine observables from lattice calculations, chiral, continuum and infinite volume extrapolations are required. The first considered here is the chiral extrapolation. It was mentioned above that operators \mathcal{O}'_i have the same chiral structure as the corresponding unmixed \mathcal{O}_i , therefore it is only necessary to derive the χ PT formulas for the unprimed set as they differ from the primed set only in the LECs.

The chiral transformations for the operators under $SU(2)$ are given by:

$$\begin{aligned}
\mathcal{O}_{1+}^{++} &\sim \tau_L^+ \otimes \tau_R^+ \\
\mathcal{O}_{2+}^{++} &\sim \tau_{RL}^+ \otimes \tau_{RL}^+ + \tau_{LR}^+ \otimes \tau_{LR}^+ \\
\mathcal{O}_{3+}^{++} &\sim \tau_L^+ \otimes \tau_L^+ + \tau_R^+ \otimes \tau_R^+
\end{aligned} \tag{4.10}$$

with the spurions operators $\tau_L^+, \tau_R^+, \tau_{RL}^+$ transforming as:

$$\begin{aligned}
\tau_L^+ &\rightarrow L\tau_L^+L^\dagger & \tau_R^+ &\rightarrow R\tau_R^+R^\dagger \\
\tau_{LR}^+ &\rightarrow L\tau_{LR}^+R^\dagger & \tau_{RL}^+ &\rightarrow R\tau_{RL}^+L^\dagger
\end{aligned} \tag{4.11}$$

In order to compute the $\pi^- \rightarrow \pi^+$ transition amplitudes, the spurious operators are set to the raising operator

$$\tau^+ = \begin{pmatrix} 0 & 1 \\ 0 & 0 \end{pmatrix} \tag{4.12}$$

The low-energy operators arising in χ PT for the $\pi^- \rightarrow \pi^+ e^- e^-$ operators can be obtained by considering the power-counting arguments outlined in [117], and lead to the

following chiral Lagrangian:

$$\mathcal{L}^X = \bar{e}e^c \frac{G_F^2}{\Lambda_{\beta\beta}} \frac{\Lambda_{\chi_0}^4}{(4\pi)^2} \frac{F^2}{4} \left[c_1^W \beta_1 \mathcal{O}_{1+}^X - c_2^W \frac{\beta_2}{2} \mathcal{O}_{2+}^X - c_3^W \beta_3 \mathcal{O}_{3+}^X \right] \quad (4.13)$$

The constant G_F is Fermi's weak decay constant, $\Lambda_{\beta\beta}$ corresponds to the ultraviolet scale at which the new physics, lepton number violating, may arise. The chiral symmetry breaking scale is $\Lambda_{\chi_0} = 4\pi F$ where F is the pion decay constant in the chiral limit with normalization $F_\pi^{\text{phys}} \simeq 92.2$ MeV. The Wilson coefficients, c_i^W , incorporate the effects of the heavy BSM physics integrated out to match to the local Lagrangian in terms of SM fields. Finally, the dimensionless LECs are β_i and must be determined to predict the strength of the various $\pi^- \rightarrow \pi^+$ transition operators.

The standard parameterization of the pions is done using the following ξ^2 , Σ fields:

$$\xi^2 = \Sigma = e^{\sqrt{2}i\phi/F} \quad (4.14)$$

where the ϕ matrix containing the pion fields is given by:

$$\phi = \begin{pmatrix} \frac{\pi^0}{\sqrt{2}} & \pi^+ \\ \pi^- & -\frac{\pi^0}{\sqrt{2}} \end{pmatrix} \quad (4.15)$$

and

$$\begin{aligned} \Sigma_L^\mu &= \Sigma \partial^\mu \Sigma^\dagger \\ \Sigma_R^\mu &= \Sigma^\dagger \partial^\mu \Sigma \end{aligned} \quad (4.16)$$

At the hadronic level, the operators are dimensionless and given by:

$$\mathcal{O}_{1+}^{\chi} = \text{Tr} (\Sigma^{\dagger} \tau_L^+ \Sigma \tau_R^+) , \quad (4.17)$$

$$\mathcal{O}_{2+}^{\chi} = \text{Tr} (\Sigma^{\dagger} \tau_{LR}^+ \Sigma^{\dagger} \tau_{LR}^+ + \Sigma \tau_{RL}^+ \Sigma \tau_{RL}^+) , \quad (4.18)$$

$$\mathcal{O}_{3+}^{\chi} = \frac{1}{\Lambda_{\chi_0}^2} \text{Tr} (\Sigma_{L\mu} \tau_L^+ \Sigma_L^{\mu} \tau_L^+ + \Sigma_{R\mu} \tau_R^+ \Sigma_R^{\mu} \tau_R^+) , \quad (4.19)$$

Then, in order to renormalize loop integrals appearing at NLO order in the chiral expansion, counter terms must be constructed from higher dimensional operators. Therefore, NLO operators will be required:

$$\mathcal{O}_{1+}^{\text{nlo}} = \frac{\text{Tr} (\partial_{\mu} \Sigma^{\dagger} \tau_L^+ \partial^{\mu} \Sigma \tau_R^+)}{\Lambda_{\chi_0}^2} \quad (4.20)$$

$$\mathcal{O}_{2+}^{\text{nlo}} = \frac{\text{Tr} (\partial_{\mu} \Sigma^{\dagger} \tau_{LR}^+ \partial^{\mu} \Sigma^{\dagger} \tau_{LR}^+ + \partial_{\mu} \Sigma \tau_{RL}^+ \partial^{\mu} \Sigma \tau_{RL}^+)}{2\Lambda_{\chi_0}^2} \quad (4.21)$$

$$\mathcal{O}_{3+}^{\text{nlo}} = \frac{\text{Tr} (\Sigma \chi_+^{\dagger} \tau_L^+ \Sigma \chi_+^{\dagger} \tau_L^+ + \Sigma^{\dagger} \chi_+ \tau_R^+ \Sigma^{\dagger} \chi_+ \tau_R^+)}{\Lambda_{\chi_0}^4} \quad (4.22)$$

Then, at NLO, these operators in the chiral expansion take the following form²:

$$\begin{aligned} \mathcal{O}_1 &= \frac{\beta_1 \Lambda_{\chi_0}^4}{(4\pi)^2} [1 - \epsilon_{\pi}^2 (3 \ln(\epsilon_{\pi}^2) + 1 + c_1)] \\ \mathcal{O}_2 &= \frac{\beta_2 \Lambda_{\chi_0}^4}{(4\pi)^2} [1 - \epsilon_{\pi}^2 (3 \ln(\epsilon_{\pi}^2) + 1 + c_2)] \\ \frac{\mathcal{O}_3}{\epsilon_{\pi}^2} &= \frac{\beta_3 \Lambda_{\chi_0}^4}{(4\pi)^2} [1 - \epsilon_{\pi}^2 (5 \ln(\epsilon_{\pi}^2) + 1 - c_3)] \end{aligned} \quad (4.23)$$

The parameters in the last equation are given by:

$$\Lambda_{\chi} = 4\pi F_{\pi} , \quad \epsilon_{\pi} = \frac{m_{\pi}}{\Lambda_{\chi}} , \quad (4.24)$$

²These correspond to the corrected expressions for the expansions in [92], where a contribution from a pion loop was mistakenly excluded.

$F_\pi = F_\pi(\mathbf{m}_\pi)$ is the pion decay constant at a given pion mass, normalized such that $F_\pi(\pi^{\text{phys}}) = 92.2$ MeV, Λ_χ is the chiral symmetry breaking scale and ϵ_π^2 is the small expansion parameter for χPT .

The above equations serve to describe the pion mass dependence of the operators in the continuum theory. Nevertheless, LQCD quantities are computed at finite lattice spacing and finite volume, and these finite effects must be incorporated in addition to 4.23. Then, the LQCD results can be extrapolated to the physical point. This must be incorporated according to the action employed, here a Mixed Action. Thus following Mixed Action EFT [123, 124, 125, 126, 127, 128, 129, 130, 131], the finite lattice spacing effects can be incorporated.

The finite-volume effects can be incorporated into the chiral expansion by employing a finite volume version of the tadpole integral:

$$\mathcal{I}(\mathbf{m}, \mathbf{mL}) = \int \frac{d^4\mathbf{k}}{(4\pi)^4} \frac{i}{k^2 - m^2 + i\epsilon} + \frac{4m^2}{(4\pi)^2} \sum_{|\mathbf{n}| \neq \mathbf{0}} \frac{K_1(mL|\mathbf{n}|)}{mL|\mathbf{n}|}. \quad (4.25)$$

the tadpole integral in the continuum can be computed using dimensional regularization with a modified minimal subtraction and yields:

$$\mathcal{I}(\mathbf{m}) = \frac{m^2}{(4\pi)^2} \ln \left(\frac{m^2}{\mu^2} \right). \quad (4.26)$$

Additionally, there is partially-quenched hairpin contribution to account for and which is given by the following integral [128]

$$\mathcal{I}^{\text{PQ}}(\mathbf{m}) = \int \frac{d^4\mathbf{k}}{(4\pi)^4} \frac{i\Delta_{\text{PQ}}^2}{(k^2 - m^2 + i\epsilon)^2} = \Delta_{\text{PQ}}^2 \frac{\partial}{\partial m^2} \mathcal{I}(\mathbf{m}) \quad (4.27)$$

where $\Delta_{\text{PQ}}^2 \equiv m_{\pi, \text{sea}}^2 - m_{\pi, \text{val}}^2$. Lastly, the enhanced finite volume correction from the

hairpin contribution can be obtained using 4.27:

$$\mathcal{I}(\mathbf{m}, \mathbf{mL}) = \frac{1 + \ln(\mathbf{m}^2/\mu^2)}{(4\pi)^2} - 2 \sum_{|\mathbf{n}| \neq \mathbf{0}} \frac{K_0(\mathbf{mL}|\mathbf{n}|)}{(4\pi)^2}. \quad (4.28)$$

The final expressions for the operators extrapolation formulae are:

$$\begin{aligned} \mathcal{O}_1 = \frac{\beta_1 \Lambda_\chi^4}{(4\pi)^2} & \left[1 + 2\epsilon_{\text{vs}}^2 \left(\ln(\epsilon_{\text{vs}}^2) + f_1(\mathbf{m}_{\text{vs}}\mathbf{L}) \right) - \epsilon_\pi^2 \left(\ln(\epsilon_\pi^2) + 1 + f_0(\mathbf{m}_\pi\mathbf{L}) - c'_1 \right) \right. \\ & \left. + \alpha_1 \epsilon_a^2 + \alpha_1^{(4)} \epsilon_a^4 + c_1^{(4)} \epsilon_\pi^4 + m_1 \epsilon_a^2 \epsilon_\pi^2 \right], \end{aligned} \quad (4.29)$$

$$\begin{aligned} \mathcal{O}_2 = \frac{\beta_2 \Lambda_\chi^4}{(4\pi)^2} & \left[1 + 2\epsilon_{\text{vs}}^2 \left(\ln(\epsilon_{\text{vs}}^2) + f_1(\mathbf{m}_{\text{vs}}\mathbf{L}) \right) - \epsilon_\pi^2 \left(\ln(\epsilon_\pi^2) + 1 + f_0(\mathbf{m}_\pi\mathbf{L}) - c'_2 \right) \right. \\ & \left. - 2\epsilon_{\text{PQ}}^2 \left(\ln(\epsilon_\pi^2) + 1 + f_0(\mathbf{m}_\pi\mathbf{L}) \right) + \alpha_2 \epsilon_a^2 + \alpha_2^{(4)} \epsilon_a^4 + c_2^{(4)} \epsilon_\pi^4 + m_2 \epsilon_a^2 \epsilon_\pi^2 \right], \end{aligned} \quad (4.30)$$

$$\frac{\mathcal{O}_3}{\epsilon_\pi^2} = \frac{\beta_3 \Lambda_\chi^4}{(4\pi)^2} \left[1 - \epsilon_\pi^2 \left(3 \ln(\epsilon_\pi^2) + 1 - c'_3 + 2f_1(\mathbf{m}_\pi\mathbf{L}) + f_0(\mathbf{m}_\pi\mathbf{L}) \right) + \alpha_3 \epsilon_a^2 + \alpha_3^{(4)} \epsilon_a^4 + c_3^{(4)} \epsilon_\pi^4 + m_3 \epsilon_a^2 \epsilon_\pi^2 \right], \quad (4.31)$$

where we have defined

$$f_0(\mathbf{mL}) = \sum_{|\mathbf{n}| \neq \mathbf{0}} K_0(\mathbf{mL}|\mathbf{n}|) \quad f_1(\mathbf{mL}) = \sum_{|\mathbf{n}| \neq \mathbf{0}} \frac{K_1(\mathbf{mL}|\mathbf{n}|)}{\mathbf{mL}|\mathbf{n}|} \quad (4.32)$$

The small expansion parameters are given as defined in [105] for the mixed action

$$\begin{aligned} \epsilon_\pi &\equiv \frac{m_\pi}{4\pi F_\pi} & \epsilon_{\text{vs}} &\equiv \frac{m_{\text{vs}}}{4\pi F_\pi} \\ \epsilon_{\text{PQ}}^2 &\equiv \frac{a^2 \Delta_1}{(4\pi F_\pi)^2} & \epsilon_a^2 &\equiv \frac{1}{4\pi} \frac{a^2}{w_0^2} \end{aligned} \quad (4.33)$$

where $w_0 \sim 0.17$ fm is a gradient-flow scale [106] and m_{vs} is the mass of a pion made out a valence and sea quark. The valence quark masses are tuned as in [105], and in the limit

$a \rightarrow 0, m_{\nu s} \rightarrow m_{\pi}$

4.1.4 Extrapolation and Results

In a preliminary proceedings [132], the ratios \mathcal{R} were presented and good signals were observed for almost all the different ensembles, and with suppressed excited states contributions. Here, the final results are presented. The leading contamination comes from the first excited state and it is canceled in the ratio for the pion correlation functions, and thus this might explain the reduced contamination. Moreover, little variation is noticed for point and smeared sources. In this way, a fit to a constant is enough to determine \mathcal{R} in the different ensembles. A sample plot of the results obtained for these ratios is shown in figure 4.3.

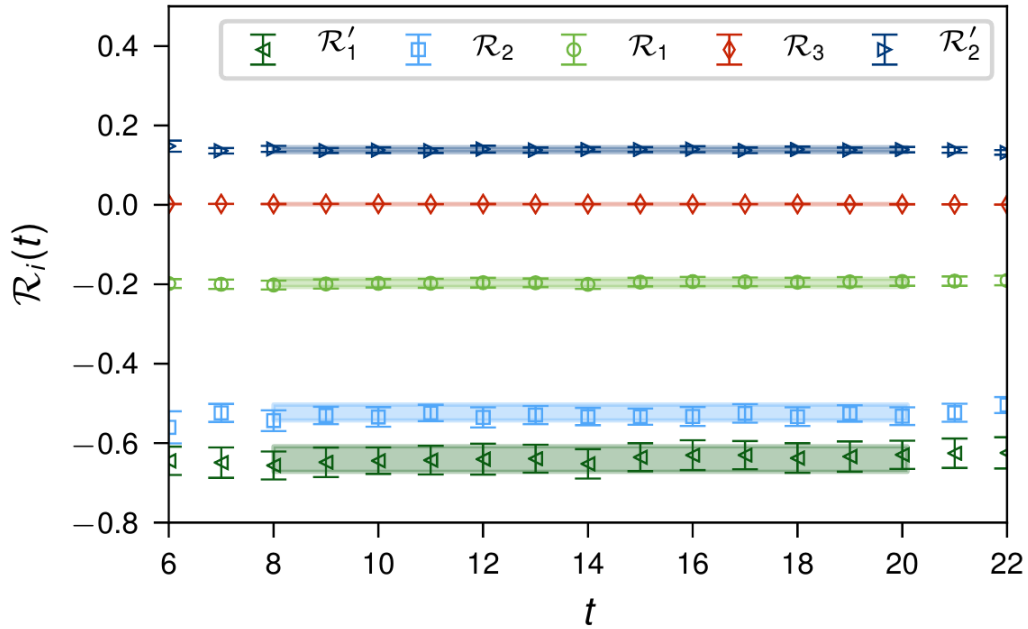


FIG. 4.3: Fits to the ratios \mathcal{R}_i for the different operators.

Using the results from the fitted ratios and the necessary extrapolation formulas from last section, the extrapolations are performed by fitting the renormalized operators to the

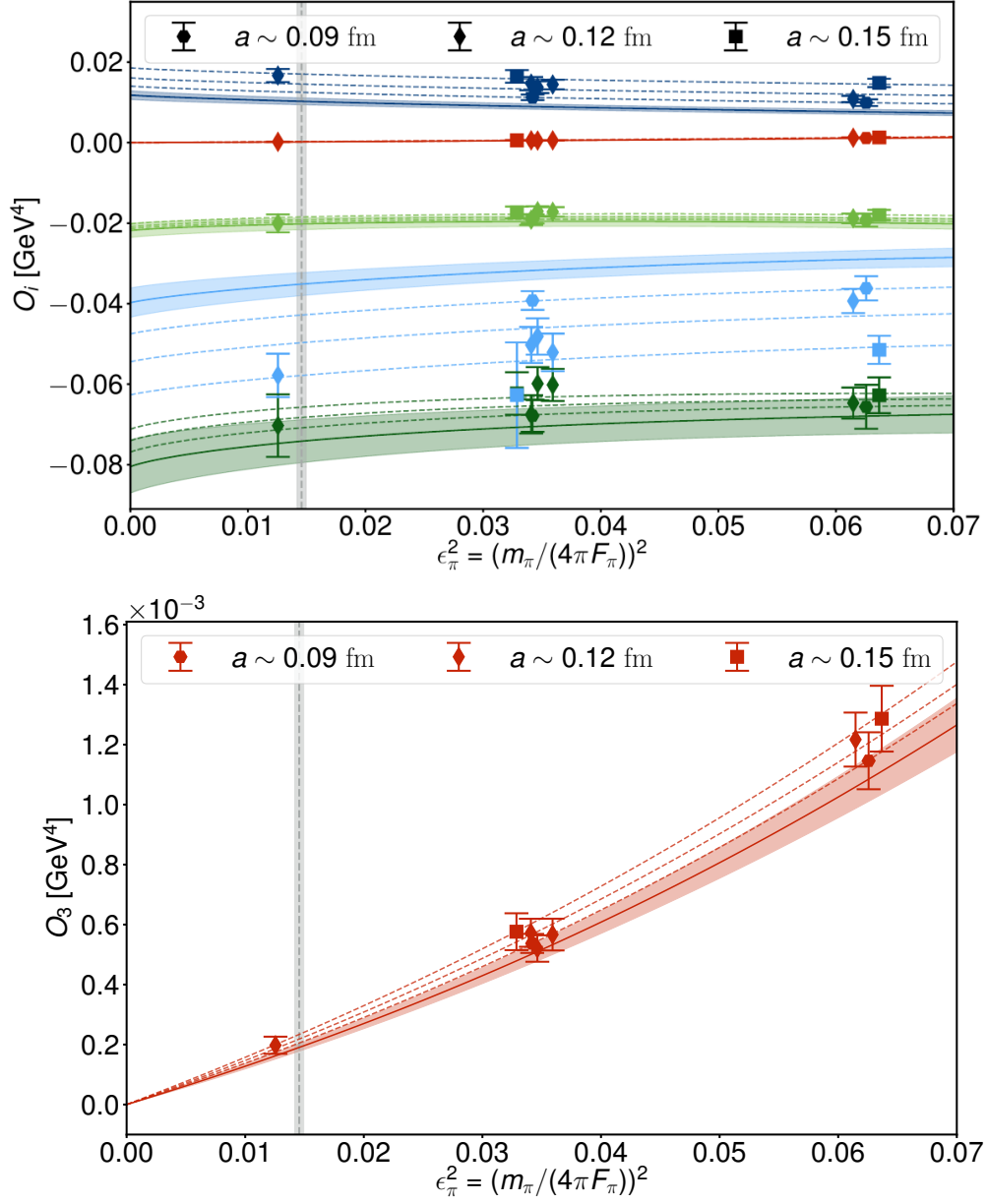


FIG. 4.4: Fits to the chiral extrapolation formulae for the different operators. The physical point is indicated by the vertical gray band. On the top all the operators are displayed. In the bottom a zoom plot for the operator \mathcal{O}_3 is shown.

TABLE 4.1: LEC values determined from fits

β_1	c_1	β'_1	c'_1	β_2
-1.88(12)	4.0(1.3)	-6.99(45)	3.8(1.3)	-3.56(26)
c_2	β'_2	c'_2	β_3	c_3
2.4(1.3)	1.063(80)	1.2(1.2)	1.093(63)	9.0(2.0)

formulas 4.29, 4.30, 4.31. When on-shell renormalized quantities are used the behavior of the perturbative χ PT extrapolation tends to improve [129, 133, 134].

The fits are performed using a linear least squares fit, and in order to study the MA and finite volume effects, the corresponding terms were turned off. The results of these extrapolations were consistent suggesting MA and finite volume effects are mild.

The fit results are shown in figures 4.4. In the top plot, the data for all the different operators is shown and the color bands are used to display their continuum limit. Moreover, as Λ_χ introduces an m_π dependence through F_π in the chiral expansion 4.20, the operators are normalized by Λ_χ for plotting. In this way, the effects of NLO contributions are easier to observe, and are seen to be small as there is little variation as the pion mass varies. Also, as predicted by the chiral expansion, the matrix element for \mathcal{O}_3 is suppressed with respect to the others, however a zoom plot for this operator shows a non-zero value.

The results for the determined matrix element values are listed in table 4.2. Also the corresponding LEC values resulting from the fits are listed in table 4.1. These results can be compared to values obtained using flavor $\text{SU}(3)$ in [118] and are found to agree around the two-sigma level with $\mathcal{O}(20 - 40\%)$ uncertainties given [118]. In the next section, a brief look at how $0\nu\beta\beta$ decay rates are computed from the above results is presented and their impact on BSM physics constraints from $0\nu\beta\beta$ decay.

This is the first time a LQCD determination of these matrix elements has appeared in the literature. It is exciting that we were able to provide control over all sources of uncertainty in this first publication.

TABLE 4.2: Resulting matrix elements extrapolated to the physical point, renormalized in RI/SMOM and $\overline{\text{MS}}$, both at $\mu = 3 \text{ GeV}$.

$O_i[\text{GeV}]^4$	RI/SMOM $\mu = 3 \text{ GeV}$	$\overline{\text{MS}}$ $\mu = 3 \text{ GeV}$
O_1	$-1.95(15) \times 10^{-2}$	$-1.93(14) \times 10^{-2}$
O'_1	$-7.25(55) \times 10^{-2}$	$-7.85(59) \times 10^{-2}$
O_2	$-3.48(30) \times 10^{-2}$	$-3.56(30) \times 10^{-2}$
O'_2	$1.02(09) \times 10^{-2}$	$1.09(10) \times 10^{-2}$
O_3	$1.78(08) \times 10^{-4}$	$1.79(08) \times 10^{-4}$

4.1.5 Nuclear Potentials and $nn \rightarrow ppe^-e^-$ Decay Amplitude

There are several approaches for estimating the contributions to $0\nu\beta\beta$ decay rates from short range interactions, therefore we will look briefly at available literature.

In [135] matrix elements are estimated by means of factorization, and the contributions from $\pi\pi$ and πN processes are ignored. These contributions have been previously discussed in [69, 136] where their relevance was indicated. Therefore, when the matching is performed to the nucleon level this method yields underestimated results [48].

On the other hand, other approaches use χPT [117, 69] to match from quark to hadronic operators. In these $\pi\pi$ and πN contributions are considered. However, in particular [117] omits operators that mix flavors under renormalization when going from the electroweak to the QCD scale.

This work computes the different $\pi\pi$ contributions are computed and all operators (including operators that mix) that have not been considered in previous work, and thus allow us the estimation of their contributions to $0\nu\beta\beta$ decay rates within an EFT framework as it is shown next.

With the results of the previous section, their contributions to the nuclear decay rate due to $\pi^- \rightarrow \pi^+$ matrix elements can be computed by constructing the $nn \rightarrow pp$ potentials induced by the above processes. The contribution for the strong interacting part for matrix

element \mathcal{O}_i is given by:

$$\begin{aligned} V_i^{nn \rightarrow pp}(|\mathbf{q}|) &= -\mathcal{O}_i P_{1+} P_{2+} \frac{\partial}{\partial m_\pi^2} V_{1,2}^\pi(|\mathbf{q}|) \\ &= -\mathcal{O}_i \frac{g_A^2}{4F_\pi^2} \tau_1^+ \tau_2^+ \frac{\boldsymbol{\sigma}_1 \cdot \mathbf{q} \boldsymbol{\sigma}_2 \cdot \mathbf{q}}{(|\mathbf{q}|^2 + m_\pi^2)^2}, \end{aligned} \quad (4.34)$$

In the last equation, the long-range pion-exchange potential is denoted by $V_{1,2}^\pi(|\mathbf{q}|) = -\boldsymbol{\tau}_1 \cdot \boldsymbol{\tau}_2 \boldsymbol{\sigma}_1 \cdot \mathbf{q} \boldsymbol{\sigma}_2 \cdot \mathbf{q} / (|\mathbf{q}|^2 + m_\pi^2)$ and $P_{1,2}^+$ project onto the isospin raising operator for each nucleon. The electrons $\bar{e}e$ and the prefactor $\frac{G_F^2}{\Lambda_{\beta\beta}}$ are not included in this potential.

Furthermore, calculations for nuclear matrix elements arising from a given nucleon potential already exist, in which the sum of the all the two nucleon potentials appears in the form $\langle 0^+ | \sum_{mn} V^{nm}(\mathbf{q}) | 0^+ \rangle$. Therefore from 4.34 it is easy to see that computing the contributions to $0\nu\beta\beta$ decay rates, corresponding to a given operator \mathcal{O}_i , only requires multiplying the \mathcal{O}_i matrix element and the existing nuclear matrix elements. As a consequence, existing nuclear matrix element calculations [116, 137, 138] can be employed to study the phenomenological impact of the results obtained here.

It is then convenient to employ a master formula for the calculation of the $0\nu\beta\beta$ decay rate which is found in [48]. Basically, the formula is written as a sum of terms corresponding to different contributions, such that each contribution can be turned on and off according to the model to study. In the master formula, short and long range contributions appear in the same form as they were shown in chapter 1:

$$\frac{1}{T_{1/2}^{0\nu}} = G^\nu(Q, Z) |M^\nu|^2 \begin{cases} |\epsilon_\nu|^2 & \text{Short range} \\ \langle m_{\beta\beta} \rangle^2 & \text{Long range} \end{cases} \quad (4.35)$$

The last equation shows that existing limits on the decay rates can be used to impose limits on the effective neutrino masses $\langle m_{\beta\beta} \rangle^2$ from long range contributions. On the other hand,

in the context of EFT, the short range interactions arising from higher order operators are suppressed by powers of Λ_{LNV} , i.e. $\epsilon_\nu \propto \Lambda_{\text{LNV}}^{-n}$, hence limits on $0\nu\beta\beta$ decay rates can be used to constraint the LNV scales. Using matrix elements reported on [116], the following LNV constraints (from ${}^{76}\text{Ge}$ half-life limits), arising from the short range contributions computed here for $\pi^- \rightarrow \pi^+$ processes, were found:

$$\begin{aligned} \Lambda^1 &> 3.3 & \Lambda^2 &> 5.2 & & (4.36) \\ \Lambda^3 &> 6.9 & \Lambda^4 &> 5.2 & \Lambda^5 &> 4.1 \end{aligned}$$

4.2 Four-quark Feynman-Hellman Method

The next step to determine the short-range contributions to $0\nu\beta\beta$ is the calculation of the four nucleon contact operators. This presents several complications which do not arise in the $\pi^- \rightarrow \pi^+$ case. In the first place, computing a three point function to extract the matrix element, as shown in section 4.1.2, is far more complicated for nucleons. For example, in a four-quark operator insertion in between two nucleon states there are quarks that do not couple to the operator, so there is not a meson block-like structure to facilitate the calculation. Moreover, a momentum projection can only be done after the coupled and uncoupled quarks are contracted, which is contrary to the $\pi^- \rightarrow \pi^+$ case and would result in a significantly more computational costly calculation.

A more convenient approach is to use the Feynman-Hellmann method, however complications arise again in the implementation as a sum over operator insertions at all space-time is required. In the case of a bilinear current, using a sequential propagator this sum is made automatically. For a four-quark operator insertion, the operator couples to two quarks and there is no analog that would automatically do the sum. Then, each current insertion must be performed individually leading to a cost increased by order volume

calculations. Typical volumes range from 16^3 to 64^3 .

This cost increase would significantly limit the size of the statistics than can be used, and thus become a problem for the four contact nucleon operator due to the signal-to-noise ratio problem. In order to overcome the computational cost, a new approach is proposed which allows us to make use of the Feynman-Hellman method and sequential propagators to reduce the cost. In order to extract the matrix element of interest employing the Feynman-Hellman theorem, the quantity that must be computed is the following:

$$\partial_\lambda C_\lambda(t) \Big|_{\lambda=0} = \int d^4x \langle \Omega | \mathcal{O}(t) \mathcal{J}(x) \mathcal{O}^\dagger(0) | \Omega \rangle \quad (4.37)$$

In the case of baryons with a bilinear current insertion, this quantity can be efficiently computed using a sequential propagator to automatically sum over all the current insertion locations. However, in the case of four-quark operators, if the current were to be inserted in the same way, two sums, one for each quark line, would be introduced when the two propagators are contracted to obtain 4.37. To overcome this problem, a Hubbard-Stratonovich transformation can be used to relate the matrix elements for bilinear and four-quark operators.

What is proposed is to perform the calculation in a theory where an additional field mediating the quark interactions is introduced, then the Hubbard-Stratonovich transformation [139, 140] can be used to integrate out the mediating field and recover the original theory. This is similar to the Gross-Neveu model [141] but with a generic bilinear instead of $\bar{\psi}\psi$ and 4 dimensions instead of 2. In the original theory, the action is defined as $S = S_0 + S_{\lambda_{ij}}$ where:

$$S_{\lambda_{ij}} = i\lambda_{ij} \int d^4x \bar{\psi} \Gamma^i \psi \bar{\psi} \Gamma^j \psi \quad (4.38)$$

The theory to be used for the numerical calculation, which will be called the σ theory, is specified by the action $S = S_0 + \int d^4x \frac{\sigma}{4} + S'_\lambda$:

$$S_{\lambda'_i} = \lambda'_i \int d^4x \bar{\psi} \Gamma^i \psi \quad (4.39)$$

The field σ is a real scalar and gauge independent field, which is static. If the field σ is local and ranges from $-\infty$ to ∞ , then the Hubbard-Stratonovich transformation can be used to integrate out the σ field. This, for example, is analogous to four fermion interactions mediated by a W/Z boson, in which case the heavy W/Z bosons are integrated out leaving an effective interaction described by a four fermion contact term. For the σ theory, this can be illustrated using the correlation function:

$$C_{\lambda'_i}(t) = \frac{1}{Z_{\lambda'_i}} \int D\Phi e^{-S_0} \int_{-\infty}^{\infty} d\sigma' e^{\int d^4x (\frac{\sigma'}{2})^2 + \lambda'_i \sigma' (\bar{\psi} \Gamma^i \psi)} \mathcal{O}(t) \mathcal{O}^\dagger(0) \quad (4.40)$$

Now, let $\sigma = \sigma' - i\lambda \bar{\psi} \Gamma^i \psi$, then:

$$\int_{-\infty}^{\infty} d\sigma e^{-\int d^4x \{ \frac{\sigma^2}{4} + \lambda'_i i \sigma (\bar{\psi} \Gamma^i \psi) \}} = \int_{-\infty}^{\infty} d\sigma' e^{-\int d^4x \sigma'^2} e^{-\lambda_i'^2 \int d^4x (\bar{\psi} \Gamma^i \psi)^2} = \alpha e^{-\lambda_i'^2 \int d^4x (\bar{\psi} \Gamma^i \psi)^2} \quad (4.41)$$

where α is a constant. Substituting 4.41 into 4.40:

$$C_{\lambda'_i}(t) = \frac{1}{Z_{\lambda'_i}} \int D\Phi e^{-S_0 - \lambda'^2 \int d^4x \bar{\psi} \Gamma^i \psi \bar{\psi} \Gamma^i \psi} \quad (4.42)$$

For $\lambda_{ii} = \lambda'^2$, after integration the original correlation function is recovered. To find an expression for 4.37 in the σ theory partial derivatives with respect to λ'_i must be taken. Before proceeding, it is important to notice that the integrand in the 4.40 is even with respect to the σ integral. It is this property which will serve to take care of the

additional sum appearing when contracting two sequential propagators. Also notice that if just one partial derivative is taken the integrand becomes odd and thus the integral vanishes. Therefore, the following second partial derivative is considered:

$$\partial_{\lambda^i}^2 C'_{\lambda^i}(t) = -\frac{(\partial_{\lambda^i}^2 \mathcal{Z}'_{\lambda^i}) C'_{\lambda^i}(t)}{\mathcal{Z}'_{\lambda^i}} - \frac{(\partial_{\lambda^i} \mathcal{Z}'_{\lambda^i})}{\mathcal{Z}'_{\lambda^i}} \partial_{\lambda^i} C'_{\lambda^i}(t) + \frac{(\partial_{\lambda^i} \mathcal{Z}'_{\lambda^i})^2}{\mathcal{Z}'_{\lambda^i}{}^2} C'_{\lambda^i}(t) \quad (4.43)$$

$$+ \frac{i(\partial_{\lambda^i} \mathcal{Z}'_{\lambda^i})}{\mathcal{Z}'_{\lambda^i}{}^2} \int \mathcal{D}\Phi \int_{-\infty}^{\infty} d\sigma \int d^4x e^{-S'-S'_{\lambda^i}} \mathcal{T}\{\mathcal{O}(t) \sigma \bar{\psi} \Gamma^i \psi \mathcal{O}^\dagger(0)\} \quad (4.44)$$

$$- \frac{1}{\mathcal{Z}'_{\lambda^i}} \int \mathcal{D}\Phi \int_{-\infty}^{\infty} d\sigma \int d^4x \int d^4y e^{-S'-S'_{\lambda^i}} \mathcal{T}\{\mathcal{O}(t) \sigma_x \bar{\psi}_x \Gamma^i \psi_x \sigma_y \bar{\psi}_y \Gamma^i \psi_y \mathcal{O}^\dagger(0)\} \quad (4.45)$$

As calculations in the σ theory will require an integration over σ , it is sufficient to consider the terms which are non-zero after this integration, thus the most relevant quantity to compute in the σ theory is:

$$\mathbf{N}(t) = -\frac{1}{\mathcal{Z}'_{\lambda^i}} \int \mathcal{D}\Phi \int_{-\infty}^{\infty} d\sigma \int d^4x \int d^4y e^{-S'-S'_{\lambda^i}} \mathcal{T}\{\mathcal{O}(t) \sigma_x \bar{\psi}_x \Gamma^i \psi_x \sigma_y \bar{\psi}_y \Gamma^i \psi_y \mathcal{O}^\dagger(0)\} \quad (4.46)$$

Recalling that σ is a field defined at each space-time point, then in order to obtain an even integrand in the last equation we must have $x = y$, hence the integral over σ becomes $\delta^4(x - y)$, simplifying one of the sums:

$$\mathbf{N}(t) = -\alpha' \frac{1}{\mathcal{Z}_{\lambda^i}} \int \mathcal{D}\Phi \int d^4x e^{-S'-S'_{\lambda^i}} \mathcal{T}\{\mathcal{O}(t) \bar{\psi}_x \Gamma^i \psi_x \bar{\psi}_y \Gamma^i \psi_y \mathcal{O}^\dagger(0)\} \quad (4.47)$$

In the lattice, one would implement the calculation appearing in 4.46. The strategy in this case is to compute two sequential propagators with the σ field times the current inserted. In this way, the sum over the insertion positions is performed automatically. An illustration of the diagram corresponding to the $\pi^- \rightarrow \pi^+$ three-point correlation function

is shown in 4.5. The first thing to notice is that with this implementation, the order

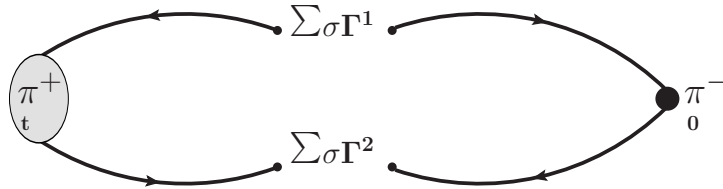


FIG. 4.5: Diagram for the three-point function in the σ theory.

volume operator insertions are exchanged by a integral over σ which should significantly reduce the computational cost and allow us to sample higher statistics. Second, four-quark insertions are exchanged by bilinear insertions in sequential propagators, as a consequence the sequential propagators can be reused for computing additional four-quark operators.

Both of the implementation advantages mentioned above would be significant for the determination of the four nucleon contact operator matrix elements as they would allow to increase the statistics necessary to overcome the signal-to-noise ratio problem. In addition to, the advantages of the Feynman-Hellman method, such as access to variable time separations would be available too.

In order for the method to be worthwhile, we must demonstrate that the extra noise introduced by the σ field can be suppressed down to the gauge noise with much less than the volume statistics needed in the method with individually inserted currents (brute force).

A first step toward this test has been already taken and the brute force method has been implemented. In fact, the implemented code has been used to cross-check code for the method employed here to compute the $\pi^- \rightarrow \pi^+$ matrix elements. However, as the brute force method is very costly, a calculation on a large enough size lattice has not been

performed yet.

The second step for the testing of the method is the implementation of the calculation in σ theory. In order to do this, a modification to the code for computing quark propagators will be done such the σ are correctly incorporated into the calculation. Using quarks propagators obtained with the modified code these can be contracted to compute the required three-points entering in the Feynman-Hellman relation.

Finally, matrix elements for $\pi^- \rightarrow \pi^+$ transitions will be computed with both the brute force method and the method proposed here. Nevertheless, the extraction of the matrix element from the data is a little bit different than was has been presented in the first subsection of this chapter. The difference lies in the observable used to obtain the matrix element, basically normalization factors and excited states contamination are different, and thus they must be carefully determined for a precise comparison of the resulting errors.

Summary

In this chapter the first LQCD calculation of the $\pi^- \rightarrow \pi^+$ matrix elements contributing to $0\nu\beta\beta$ was performed. As the nature and mechanism giving the neutrino its mass are still unknown, this calculation is relevant to understand the contributions from the short range interactions. As it was showed, this calculation alone is not sufficient to predict the decay rate, however it provides a mean to constraint the corresponding scales at which these mechanism may contribute to $0\nu\beta\beta$ and thus help in the interpretation of results in case a positive signal is observed in the $0\nu\beta\beta$ experiments.

Additionally, a new method is proposed for the calculation of the short range contributions from the four nucleon contact interactions. These calculations are far more complicated than the $\pi^- \rightarrow \pi^+$ contributions for several reasons, among them high computational cost and the large statistics required. The new method is expected to contribute to overcoming these problems as it allows for a computationally cheaper implementation of

the calculation.

CHAPTER 5

Conclusions And Future Work

This work addressed the short-range interaction contributions to $0\nu\beta\beta$. The LO contribution due to the process $\pi^- \rightarrow \pi^+$ was presented. This contribution is the simplest to compute using LQCD both because the ease to implement the calculation and to extract the matrix elements.

To report physically meaningful quantities, the non-perturbative renormalization of the operators was performed and renormalization constants are expressed both in the RI-SMOM scheme as well as $\overline{\text{MS}}$, both at 3GeV. In this way, it is possible to use the results here to match into the underlying nuclear theory once the wilson coefficients has been obtained.

A precise calculation of the nucleon axial charge g_A is briefly presented here as well. Non-pertubative renormalization of g_A was performed as necessary step to produce a percentage level precise determination. The method employed is based on the Feynman-Hellman method, and was originally developed for baryons and here the method was extended to meson quantities in order to explore alternatives to tackle the four-nucleon contact interaction contributions determination. Finally a method is proposed to compute

the four nucleon contact operator which also contributes to $0\nu\beta\beta$. This method proposes the combined use of the Feynman-Hellman theorem and a Hubbard-Stratonovich transformation in order to reduce the computational cost of implementing the calculation. This would allow to use higher statistics in the calculation which can hopefully alleviate the signal-to-noise ratio problem suffered by baryonic quantities. The very next step after this work is the implementation of the proposed method. Afterwards, the $\pi^- \rightarrow \pi^+$ can be reexamined to assess the performance of the method before proceeding to test it with the four-nucleon contact contributions.

APPENDIX A

Gamma Matrices

An explicit representation of the Euclidean γ matrices is given by:

$$\begin{aligned} \gamma_1 &= \begin{pmatrix} 0 & 0 & 0 & -i \\ 0 & 0 & -i & 0 \\ 0 & i & 0 & 0 \\ i & 0 & 0 & 0 \end{pmatrix} & \gamma_2 &= \begin{pmatrix} 0 & 0 & 0 & -1 \\ 0 & 0 & 1 & 0 \\ 0 & 1 & 0 & 0 \\ -1 & 0 & 0 & 0 \end{pmatrix} & \gamma_3 &= \begin{pmatrix} 0 & 0 & -i & 0 \\ 0 & 0 & 0 & i \\ i & 0 & 0 & 0 \\ 0 & -i & 0 & 0 \end{pmatrix} \\ \gamma_4 &= \begin{pmatrix} 0 & 0 & 1 & 0 \\ 0 & 0 & 0 & 1 \\ 1 & 0 & 0 & 0 \\ 0 & 1 & 0 & 0 \end{pmatrix} & \gamma_5 &= \begin{pmatrix} 1 & 0 & 0 & 0 \\ 0 & 1 & 0 & 0 \\ 0 & 0 & -1 & 0 \\ 0 & 0 & 0 & -1 \end{pmatrix} \end{aligned} \tag{A.1}$$

APPENDIX B

Fierz Transformations

Here the Fierz Transformations are used to convert from the mixed basis, used for the calculation of $\pi^- \rightarrow \pi^+$ matrix elements, to the unmixed basis used for the renormalization of the four quark operators in chapter 2. The mixed basis is given by the following set of operators:

$$\begin{aligned}
 \mathcal{O}_{1+}^{++} &= (\bar{q}_L \tau^+ \gamma^\mu q_L) [\bar{q}_R \tau^+ \gamma_\mu q_R] \\
 \mathcal{O}_{2+}^{++} &= (\bar{q}_R \tau^+ q_L) [\bar{q}_R \tau^+ q_L] + (\bar{q}_L \tau^+ q_R) [\bar{q}_L \tau^+ q_R] \\
 \mathcal{O}_{3+}^{++} &= (\bar{q}_L \tau^+ \gamma^\mu q_L) [\bar{q}_L \tau^+ \gamma_\mu q_L] + (\bar{q}_R \tau^+ \gamma^\mu q_R) [\bar{q}_R \tau^+ \gamma_\mu q_R] \\
 \mathcal{O}'_{1+}{}^{++} &= (\bar{q}_L \tau^+ \gamma^\mu q_L) [\bar{q}_R \tau^+ \gamma_\mu q_R] \\
 \mathcal{O}'_{2+}{}^{++} &= (\bar{q}_L \tau^+ q_L) [\bar{q}_L \tau^+ q_L] + (\bar{q}_R \tau^+ q_R) [\bar{q}_R \tau^+ q_R]
 \end{aligned} \tag{B.1}$$

where $\tau^+ = \begin{pmatrix} 0 & 1 \\ 0 & 0 \end{pmatrix}$.

For the matrix elements of interested, only the parity even components of these operators contribute. Moreover, unmixed and mixed operators can be related by Fierz Identities, and in this case it is convenient to use the following basis $\{\Gamma_A\} = \{P_R, P_L, P_R \gamma_\mu, P_L \gamma_\mu, \sigma_{\mu\nu}\}$

and the Chiral Fierz Identities [91]. The orthogonality of the basis $\text{Tr}[\Gamma_A \Gamma^B] = 2\delta_A^B$ yields the completeness relation:

$$\text{Tr}[\Gamma_A \Gamma^A] = \text{Tr}[\mathbf{P}_R \mathbf{P}_R] + \text{Tr}[\mathbf{P}_L \mathbf{P}_L] + \text{Tr}[\mathbf{P}_R \gamma_m \mathbf{u} \mathbf{P}_R \gamma^m \mathbf{u}] + \text{Tr}[\mathbf{P}_L \gamma_m \mathbf{u} \mathbf{P}_L \gamma^m \mathbf{u}] + \frac{1}{4} \text{Tr}[\sigma^{\mu\nu} \sigma_{\mu\nu}] \quad (\text{B.2})$$

and the Fierz Identity:

$$(\Gamma^A)_{ii} (\Gamma^B)_{jj} = \frac{1}{4} \text{Tr}[\Gamma^A \Gamma^C \Gamma^B \Gamma_D] (\Gamma^D)_{ij} (\Gamma^C)_{ji} \quad (\text{B.3})$$

Then, the basis in B.1 can be first written in terms of the u and d quarks (with explicitly Dirac and color indices shown) as:

$$\mathcal{O}_{1+}^{++} = (\bar{\mathbf{u}}_a^\alpha (\gamma^\mu \mathbf{P}_L)_{\alpha\beta} \delta^{ab} \mathbf{d}_b^\beta) (\bar{\mathbf{u}}_c^\rho (\gamma^\mu \mathbf{P}_R)_{\rho\epsilon} \delta^{cd} \mathbf{d}_b^\epsilon) \quad (\text{B.4})$$

$$\mathcal{O}_{2+}^{++} = (\bar{\mathbf{u}}_a^\alpha (\mathbf{P}_L)_{\alpha\beta} \delta^{ab} \mathbf{d}_b^\beta) (\bar{\mathbf{u}}_c^\rho (\mathbf{P}_L)_{\rho\epsilon} \delta^{cd} \mathbf{d}_b^\epsilon) + (\bar{\mathbf{u}}_a^\alpha (\mathbf{P}_R)_{\alpha\beta} \delta^{ab} \mathbf{d}_b^\beta) (\bar{\mathbf{u}}_c^\rho (\mathbf{P}_R)_{\rho\epsilon} \delta^{cd} \mathbf{d}_b^\epsilon)$$

$$\mathcal{O}_{3+}^{++} = (\bar{\mathbf{u}}_a^\alpha (\gamma^\mu \mathbf{P}_L)_{\alpha\beta} \delta^{ab} \mathbf{d}_b^\beta) (\bar{\mathbf{u}}_c^\rho (\gamma^\mu \mathbf{P}_L)_{\rho\epsilon} \delta^{cd} \mathbf{d}_d^\epsilon) + (\bar{\mathbf{u}}_a^\alpha (\gamma^\mu \mathbf{P}_R)_{\alpha\beta} \delta^{ab} \mathbf{d}_b^\beta) (\bar{\mathbf{u}}_c^\rho (\gamma^\mu \mathbf{P}_R)_{\rho\epsilon} \delta^{cd} \mathbf{d}_b^\epsilon)$$

$$\mathcal{O}'_{1+}{}^{++} = (\bar{\mathbf{u}}_a^\alpha (\gamma^\mu \mathbf{P}_L)_{\alpha\beta} \delta^{bc} \mathbf{d}_b^\beta) (\bar{\mathbf{u}}_c^\rho (\gamma^\mu \mathbf{P}_R)_{\rho\epsilon} \delta^{ad} \mathbf{d}_b^\epsilon) \quad (\text{B.5})$$

$$\mathcal{O}'_{2+}{}^{++} = (\bar{\mathbf{u}}_a^\alpha (\mathbf{P}_L)_{\alpha\beta} \delta^{bc} \mathbf{d}_b^\beta) (\bar{\mathbf{u}}_c^\rho (\mathbf{P}_L)_{\rho\epsilon} \delta^{ad} \mathbf{d}_b^\epsilon) + (\bar{\mathbf{u}}_a^\alpha (\mathbf{P}_R)_{\alpha\beta} \delta^{bc} \mathbf{d}_b^\beta) (\bar{\mathbf{u}}_c^\rho (\mathbf{P}_R)_{\rho\epsilon} \delta^{ad} \mathbf{d}_b^\epsilon)$$

For the operators that do not mix different quark flavors, it is just sufficient to take the parity even part. For the remaining operators, use of B.2 is required and the result is:

$$\mathcal{O}_{1+}^{++} = \frac{1}{4} (\bar{\mathbf{u}}_a (\gamma^\mu (1 - \gamma_5)) \mathbf{d}_a) (\bar{\mathbf{u}}_b (\gamma^\mu (1 + \gamma_5)) \mathbf{d}_b) = \frac{Q_2}{4} \quad (\text{B.6})$$

$$\mathcal{O}_{2+}^{++} = \frac{1}{4} (\bar{\mathbf{u}}_a (1 - \gamma_5) \mathbf{d}_a) (\bar{\mathbf{u}}_b (1 - \gamma_5) \mathbf{d}_b) + \frac{1}{4} (\bar{\mathbf{u}}_a (1 + \gamma_5) \mathbf{d}_a) (\bar{\mathbf{u}}_b (1 + \gamma_5) \mathbf{d}_b) = \frac{Q_4}{2}$$

$$\mathcal{O}_{3+}^{++} = \frac{1}{4} (\bar{\mathbf{u}}_a (\gamma^\mu (1 - \gamma_5)) \mathbf{d}_a) (\bar{\mathbf{u}}_b (\gamma^\mu (1 - \gamma_5)) \mathbf{d}_b) + (\bar{\mathbf{u}}_a (\gamma^\mu (1 + \gamma_5)) \mathbf{d}) (\bar{\mathbf{u}}_b (\gamma^\mu (1 + \gamma_5)) \mathbf{d}_b) = \frac{Q_3}{2} \quad (\text{B.7})$$

For the mixed components of the basis, the using the Fierz Identity written above one finds:

$$\begin{aligned}\mathcal{O}'_{1+}{}^{++} &= (\bar{\mathbf{u}}_a^\alpha (\gamma^\mu \mathbf{P}_L)_{\alpha\beta} \delta^{bc} \mathbf{d}_b^\beta) (\bar{\mathbf{u}}_c^\rho (\gamma^\mu \mathbf{P}_R)_{\rho\epsilon} \delta^{ad} \mathbf{d}_b^\epsilon) = -\frac{Q_3}{2} \tag{B.8} \\ \mathcal{O}'_{2+}{}^{++} &= (\bar{\mathbf{u}}_a^\alpha (\mathbf{P}_L)_{\alpha\beta} \delta^{bc} \mathbf{d}_b^\beta) (\bar{\mathbf{u}}_c^\rho (\mathbf{P}_L)_{\rho\epsilon} \delta^{ad} \mathbf{d}_b^\epsilon) + (\bar{\mathbf{u}}_a^\alpha (\mathbf{P}_R)_{\alpha\beta} \delta^{bc} \mathbf{d}_b^\beta) (\bar{\mathbf{u}}_c^\rho (\mathbf{P}_R)_{\rho\epsilon} \delta^{ad} \mathbf{d}_b^\epsilon) = -(Q_4 - Q_5)\end{aligned}$$

BIBLIOGRAPHY

- [1] A. Aprahamian et al., *Reaching for the horizon: The 2015 long range plan for nuclear science* (2015), URL https://science.energy.gov/~media/np/nsac/pdf/2015LRP/2015_LRPNS_091815.pdf.
- [2] C. C. Chang et al., *Nature* **558**, 91 (2018), 1805.12130.
- [3] P. Vogel, *Proc. Int. Sch. Phys. Fermi* **170**, 49 (2009), 0807.2457.
- [4] K. Abe et al. (T2K), *Phys. Rev. Lett.* **112**, 061802 (2014), 1311.4750.
- [5] P. Adamson et al. (MINOS), *Phys. Rev. Lett.* **110**, 171801 (2013), 1301.4581.
- [6] P. Adamson et al. (MINOS), *Phys. Rev. Lett.* **110**, 251801 (2013), 1304.6335.
- [7] M. H. Ahn et al. (K2K), *Phys. Rev.* **D74**, 072003 (2006), hep-ex/0606032.
- [8] J. K. Ahn et al. (RENO), *Phys. Rev. Lett.* **108**, 191802 (2012), 1204.0626.
- [9] Y. Abe et al. (Double Chooz), *Phys. Lett.* **B723**, 66 (2013), 1301.2948.
- [10] F. P. An et al. (Daya Bay), *Phys. Rev. Lett.* **112**, 061801 (2014), 1310.6732.
- [11] A. Gando et al. (KamLAND), *Phys. Rev.* **D88**, 033001 (2013), 1303.4667.
- [12] A. Gando et al. (KamLAND), *Phys. Rev.* **C92**, 055808 (2015), 1405.6190.
- [13] G. Bellini et al. (BOREXINO), *Nature* **512**, 383 (2014).

- [14] B. Aharmim et al. (SNO), Phys. Rev. **C88**, 025501 (2013), 1109.0763.
- [15] A. Renshaw et al. (Super-Kamiokande), Phys. Rev. Lett. **112**, 091805 (2014), 1312.5176.
- [16] J. N. Abdurashitov et al. (SAGE), J. Exp. Theor. Phys. **95**, 181 (2002), [Zh. Eksp. Teor. Fiz.122,211(2002)], astro-ph/0204245.
- [17] M. Altmann et al. (GNO), Phys. Lett. **B616**, 174 (2005), hep-ex/0504037.
- [18] B. T. Cleveland, T. Daily, R. Davis, Jr., J. R. Distel, K. Lande, C. K. Lee, P. S. Wildenhain, and J. Ullman, Astrophys. J. **496**, 505 (1998).
- [19] M. G. Aartsen et al. (IceCube), Phys. Rev. Lett. **111**, 081801 (2013), 1305.3909.
- [20] S. Adrian-Martinez et al. (ANTARES), Phys. Lett. **B714**, 224 (2012), 1206.0645.
- [21] P. Adamson et al. (MINOS), Phys. Rev. **D86**, 052007 (2012), 1208.2915.
- [22] M. Ambrosio et al. (MACRO), Phys. Lett. **B566**, 35 (2003), hep-ex/0304037.
- [23] M. C. Sanchez et al. (Soudan 2), Phys. Rev. **D68**, 113004 (2003), hep-ex/0307069.
- [24] Y. Fukuda et al. (Super-Kamiokande), Phys. Rev. Lett. **81**, 1562 (1998), hep-ex/9807003.
- [25] R. Becker-Szendy et al., Phys. Rev. **D46**, 3720 (1992).
- [26] Y. Fukuda et al. (Kamiokande), Phys. Lett. **B335**, 237 (1994).
- [27] Q. R. Ahmad et al. (SNO), Phys. Rev. Lett. **89**, 011301 (2002), nucl-ex/0204008.
- [28] Q. R. Ahmad et al. (SNO), Phys. Rev. Lett. **87**, 071301 (2001), nucl-ex/0106015.

- [29] P. Langacker, *The standard model and beyond* (2010), ISBN 9781420079067.
- [30] A. Gando et al. (KamLAND-Zen), Phys. Rev. Lett. **110**, 062502 (2013), 1211.3863.
- [31] M. Agostini et al. (GERDA), Phys. Rev. Lett. **111**, 122503 (2013), 1307.4720.
- [32] J. B. Albert et al. (EXO-200), Nature **510**, 229 (2014), 1402.6956.
- [33] S. Andringa et al. (SNO+), Adv. High Energy Phys. **2016**, 6194250 (2016), 1508.05759.
- [34] A. Gando et al. (KamLAND-Zen), Phys. Rev. Lett. **117**, 082503 (2016), [Addendum: Phys. Rev. Lett.117,no.10,109903(2016)], 1605.02889.
- [35] S. R. Elliott et al., J. Phys. Conf. Ser. **888**, 012035 (2017), 1610.01210.
- [36] M. Agostini et al. (2017), [Nature544,47(2017)], 1703.00570.
- [37] J. B. Albert et al. (EXO), Phys. Rev. Lett. **120**, 072701 (2018), 1707.08707.
- [38] C. Alduino et al. (CUORE), Phys. Rev. Lett. **120**, 132501 (2018), 1710.07988.
- [39] O. Azzolini et al. (CUPID-0), Phys. Rev. Lett. **120**, 232502 (2018), 1802.07791.
- [40] V. Dabhi, S. Pincha, and V. Singh, DAE Symp. Nucl. Phys. **62**, 976 (2017).
- [41] L. Cassina et al., Springer Proc. Phys. **213**, 202 (2018).
- [42] M. Walter and G. Collaboration, in *Proceedings, 9th Patras Workshop on Axions, WIMPs and WISPs (AXION-WIMP 2013): Mainz, Germany, June 24-28, 2013* (2013), pp. 281–286.
- [43] Y. S. Yoon (AMoRE), PoS **ICRC2017**, 1056 (2018).

- [44] J. Shirai (KamLAND-Zen), PoS **NEUTEL2017**, 027 (2018).
- [45] B. Mong (nEXO), PoS **HQL2016**, 074 (2017).
- [46] N. Lopez March (NEXT), JINST **13**, C01048 (2018).
- [47] J. D. Vergados, H. Ejiri, and F. Simkovic, Rept. Prog. Phys. **75**, 106301 (2012), 1205.0649.
- [48] V. Cirigliano, W. Dekens, J. de Vries, M. L. Graesser, and E. Mereghetti (2018), 1806.02780.
- [49] F. Simkovic, G. Pantis, J. D. Vergados, and A. Faessler, Phys. Rev. **C60**, 055502 (1999), hep-ph/9905509.
- [50] G. Pantis, F. Simkovic, J. D. Vergados, and A. Faessler, Phys. Rev. **C53**, 695 (1996), nucl-th/9612036.
- [51] J. Kotila and F. Iachello, Phys. Rev. **C85**, 034316 (2012), 1209.5722.
- [52] O. Cremonesi and M. Pavan, Adv. High Energy Phys. **2014**, 951432 (2014), 1310.4692.
- [53] L. Graf, F. F. Deppisch, and F. Iachello (2018), 1806.06058.
- [54] W. C. Haxton and G. J. Stephenson, Prog. Part. Nucl. Phys. **12**, 409 (1984).
- [55] S. Dell’Oro, S. Marcocci, M. Viel, and F. Vissani, Adv. High Energy Phys. **2016**, 2162659 (2016), 1601.07512.
- [56] J. Schechter and J. W. F. Valle, Phys. Rev. **D25**, 2951 (1982), [,289(1981)].
- [57] M. Fukugita and T. Yanagida, Phys. Lett. **B174**, 45 (1986).

- [58] A. Strumia, in *Particle physics beyond the standard model. Proceedings, Summer School on Theoretical Physics, 84th Session, Les Houches, France, August 1-26, 2005* (2006), pp. 655–680, [hep-ph/0608347](#).
- [59] S. Weinberg, *Physica* **A96**, 327 (1979).
- [60] S. Weinberg, *Phys. Lett.* **B251**, 288 (1990).
- [61] D. B. Kaplan, in *The structure of baryons. Proceedings, 8th International Conference, Baryons'98, Bonn, Germany, September 22-26, 1998* (1998), pp. 160–174, [nucl-th/9901003](#).
- [62] J.-W. Chen, G. Rupak, and M. J. Savage, *Nucl. Phys.* **A653**, 386 (1999), [nucl-th/9902056](#).
- [63] E. Epelbaum, *PoS ConfinementX*, 014 (2012), [1302.3241](#).
- [64] U. van Kolck, *Nucl. Phys.* **A787**, 405 (2007).
- [65] A. Kobach, *Phys. Lett.* **B758**, 455 (2016), [1604.05726](#).
- [66] S. Weinberg, *Phys. Rev. Lett.* **43**, 1566 (1979).
- [67] L. Lehman, *Phys. Rev.* **D90**, 125023 (2014), [1410.4193](#).
- [68] V. Cirigliano, W. Dekens, J. de Vries, M. L. Graesser, and E. Mereghetti, *JHEP* **12**, 082 (2017), [1708.09390](#).
- [69] M. L. Graesser, *JHEP* **08**, 099 (2017), [1606.04549](#).
- [70] M. E. Peskin and D. V. Schroeder, *An Introduction to quantum field theory* (Addison-Wesley, Reading, USA, 1995), ISBN 9780201503975, 0201503972, URL <http://www.slac.stanford.edu/~mpeskin/QFT.html>.

- [71] D. J. Gross and F. Wilczek, Phys. Rev. Lett. **30**, 1343 (1973), [,271(1973)].
- [72] H. D. Politzer, Phys. Rev. Lett. **30**, 1346 (1973), [,274(1973)].
- [73] D. J. Gross and F. Wilczek, Phys. Rev. **D8**, 3633 (1973).
- [74] D. J. Gross and F. Wilczek, Phys. Rev. **D9**, 980 (1974).
- [75] K. G. Wilson, Phys. Rev. **D10**, 2445 (1974), [,319(1974)].
- [76] C. Gattringer and C. B. Lang, Lect. Notes Phys. **788**, 1 (2010).
- [77] D. A. Brantley, B. Joo, E. V. Mastropas, E. Mereghetti, H. Monge-Camacho, B. C. Tiburzi, and A. Walker-Loud (2016), 1612.07733.
- [78] M. Luscher, R. Narayanan, P. Weisz, and U. Wolff, Nucl. Phys. **B384**, 168 (1992), hep-lat/9207009.
- [79] G. Martinelli, C. Pittori, C. T. Sachrajda, M. Testa, and A. Vladikas, Nucl. Phys. **B445**, 81 (1995), hep-lat/9411010.
- [80] P. Korcyl (2017), 1705.06119.
- [81] Y. Bi, H. Cai, Y. Chen, M. Gong, K.-F. Liu, Z. Liu, and Y.-B. Yang, Phys. Rev. **D97**, 094501 (2018), 1710.08678.
- [82] J. Green, N. Hasan, S. Meinel, M. Engelhardt, S. Krieg, J. Laeuchli, J. Negele, K. Orginos, A. Pochinsky, and S. Syritsyn, Phys. Rev. **D95**, 114502 (2017), 1703.06703.
- [83] P. A. Boyle, N. Garron, R. J. Hudspith, C. Lehner, and A. T. Lytle (RBC, UKQCD), JHEP **10**, 054 (2017), 1708.03552.

- [84] C. Sturm, Y. Aoki, N. H. Christ, T. Izubuchi, C. T. C. Sachrajda, and A. Soni, Phys. Rev. **D80**, 014501 (2009), 0901.2599.
- [85] M. Gockeler, R. Horsley, H. Oelrich, H. Perlt, D. Petters, P. E. L. Rakow, A. Schafer, G. Schierholz, and A. Schiller, Nucl. Phys. **B544**, 699 (1999), hep-lat/9807044.
- [86] R. Arthur and P. A. Boyle (RBC, UKQCD), Phys. Rev. **D83**, 114511 (2011), 1006.0422.
- [87] R. Arthur, P. A. Boyle, S. Hashimoto, and R. Hudspith, Phys. Rev. **D88**, 114506 (2013), 1306.0835.
- [88] Y. Aoki, PoS **LAT2009**, 012 (2009), 1005.2339.
- [89] M. Papinutto, C. Pena, and D. Preti, Eur. Phys. J. **C77**, 376 (2017), [Erratum: Eur. Phys. J.C78,no.1,21(2018)], 1612.06461.
- [90] A. Donini, V. Gimenez, G. Martinelli, M. Talevi, and A. Vladikas, Eur. Phys. J. **C10**, 121 (1999), hep-lat/9902030.
- [91] C. C. Nishi, Am. J. Phys. **73**, 1160 (2005), hep-ph/0412245.
- [92] A. Nicholson et al. (2018), 1805.02634.
- [93] T. Bhattacharya, V. Cirigliano, S. Cohen, R. Gupta, H.-W. Lin, and B. Yoon, Phys. Rev. **D94**, 054508 (2016), 1606.07049.
- [94] R. G. Edwards, G. T. Fleming, P. Hagler, J. W. Negele, K. Orginos, A. V. Pochinsky, D. B. Renner, D. G. Richards, and W. Schroers (LHPC), Phys. Rev. Lett. **96**, 052001 (2006), hep-lat/0510062.

- [95] S. Capitani, M. Della Morte, G. von Hippel, B. Jager, A. Juttner, B. Knippschild, H. B. Meyer, and H. Wittig, Phys. Rev. **D86**, 074502 (2012), 1205.0180.
- [96] R. Horsley, Y. Nakamura, A. Nobile, P. E. L. Rakow, G. Schierholz, and J. M. Zanotti, Phys. Lett. **B732**, 41 (2014), 1302.2233.
- [97] G. S. Bali, S. Collins, B. Glssle, M. Gckeler, J. Najjar, R. H. Rdl, A. Schfer, R. W. Schiel, W. Sldner, and A. Sternbeck, Phys. Rev. **D91**, 054501 (2015), 1412.7336.
- [98] A. Abdel-Rehim et al., Phys. Rev. **D92**, 114513 (2015), [Erratum: Phys. Rev.D93,no.3,039904(2016)], 1507.04936.
- [99] C. Alexandrou, M. Constantinou, K. Hadjiyiannakou, K. Jansen, C. Kallidonis, G. Koutsou, and A. Vaquero Aviles-Casco, Phys. Rev. **D96**, 054507 (2017), 1705.03399.
- [100] S. Capitani, M. Della Morte, D. Djukanovic, G. M. von Hippel, J. Hua, B. Jger, P. M. Junnarkar, H. B. Meyer, T. D. Rae, and H. Wittig (2017), 1705.06186.
- [101] M. Constantinou, PoS **LATTICE2014**, 001 (2015), 1411.0078.
- [102] C. Bouchard, C. C. Chang, T. Kurth, K. Orginos, and A. Walker-Loud, Phys. Rev. **D96**, 014504 (2017), 1612.06963.
- [103] A. Bazavov et al. (MILC), Phys. Rev. **D87**, 054505 (2013), 1212.4768.
- [104] C. Allton et al. (RBC-UKQCD), Phys. Rev. **D78**, 114509 (2008), 0804.0473.
- [105] E. Berkowitz et al., Phys. Rev. **D96**, 054513 (2017), 1701.07559.
- [106] S. Borsanyi et al., JHEP **09**, 010 (2012), 1203.4469.

- [107] V. Bernard, N. Kaiser, J. Kambor, and U. G. Meissner, Nucl. Phys. **B388**, 315 (1992).
- [108] E. E. Jenkins and A. V. Manohar, Phys. Lett. **B259**, 353 (1991).
- [109] J. Kambor and M. Mojzis, JHEP **04**, 031 (1999), hep-ph/9901235.
- [110] S. R. Beane and M. J. Savage, Phys. Rev. **D70**, 074029 (2004), hep-ph/0404131.
- [111] J. Gasser and H. Leutwyler, Nucl. Phys. **B307**, 763 (1988).
- [112] K. Symanzik, Nucl. Phys. **B226**, 187 (1983).
- [113] K. Symanzik, Nucl. Phys. **B226**, 187 and 205 (1983).
- [114] C. Patrignani et al. (Particle Data Group), Chin. Phys. **C40**, 100001 (2016).
- [115] S. Alioli, V. Cirigliano, W. Dekens, J. de Vries, and E. Mereghetti, JHEP **05**, 086 (2017), 1703.04751.
- [116] J. Menéndez, J. Phys. **G45**, 014003 (2018), 1804.02105.
- [117] G. Prezeau, M. Ramsey-Musolf, and P. Vogel, Phys. Rev. **D68**, 034016 (2003), hep-ph/0303205.
- [118] V. Cirigliano, W. Dekens, M. Graesser, and E. Mereghetti, Phys. Lett. **B769**, 460 (2017), 1701.01443.
- [119] G. P. Lepage, in *Boulder ASI 1989:97-120* (1989), pp. 97–120.
- [120] R. A. Briceo and M. T. Hansen, Phys. Rev. **D94**, 013008 (2016), 1509.08507.
- [121] L. Lellouch and M. Luscher, Commun. Math. Phys. **219**, 31 (2001), hep-lat/0003023.

- [122] Y. Takahashi (1987).
- [123] O. Bar, G. Rupak, and N. Shoresh, Phys. Rev. **D67**, 114505 (2003), [hep-lat/0210050](#).
- [124] O. Bar, G. Rupak, and N. Shoresh, Phys. Rev. **D70**, 034508 (2004), [hep-lat/0306021](#).
- [125] B. C. Tiburzi, Nucl. Phys. **A761**, 232 (2005), [hep-lat/0501020](#).
- [126] O. Bar, C. Bernard, G. Rupak, and N. Shoresh, Phys. Rev. **D72**, 054502 (2005), [hep-lat/0503009](#).
- [127] B. C. Tiburzi, Phys. Rev. **D72**, 094501 (2005), [Erratum: Phys. Rev. **D79**, 039904(2009)], [hep-lat/0508019](#).
- [128] J.-W. Chen, D. O'Connell, R. S. Van de Water, and A. Walker-Loud, Phys. Rev. **D73**, 074510 (2006), [hep-lat/0510024](#).
- [129] J.-W. Chen, D. O'Connell, and A. Walker-Loud, Phys. Rev. **D75**, 054501 (2007), [hep-lat/0611003](#).
- [130] J.-W. Chen, D. O'Connell, and A. Walker-Loud, JHEP **04**, 090 (2009), [0706.0035](#).
- [131] J.-W. Chen, M. Golterman, D. O'Connell, and A. Walker-Loud, Phys. Rev. **D79**, 117502 (2009), [0905.2566](#).
- [132] A. Nicholson, E. Berkowitz, C. C. Chang, M. A. Clark, B. Joo, T. Kurth, E. Rinaldi, B. Tiburzi, P. Vranas, and A. Loud, PoS **LATTICE2016**, 017 (2016), [1608.04793](#).

- [133] J. Noaki et al. (TWQCD, JLQCD), Phys. Rev. Lett. **101**, 202004 (2008), 0806.0894.
- [134] S. Aoki et al., Eur. Phys. J. **C77**, 112 (2017), 1607.00299.
- [135] H. Pas, M. Hirsch, H. V. Klapdor-Kleingrothaus, and S. G. Kovalenko, Phys. Lett. **B498**, 35 (2001), hep-ph/0008182.
- [136] A. Faessler, S. Kovalenko, F. Simkovic, and J. Schwieger, Phys. Rev. Lett. **78**, 183 (1997), hep-ph/9612357.
- [137] J. Barea, J. Kotila, and F. Iachello, Phys. Rev. **C91**, 034304 (2015), 1506.08530.
- [138] J. Hyvriinen and J. Suhonen, Phys. Rev. **C91**, 024613 (2015).
- [139] R. L. Stratonovich, Doklady Akad. Nauk S.S.S.R. **115**, 1097 (1957).
- [140] J. Hubbard, Phys. Rev. Lett. **3**, 77 (1959).
- [141] D. J. Gross and A. Neveu, Phys. Rev. **D10**, 3235 (1974).

VITA

Henry Monge-Camacho

Henry Monge-Camacho was born on December 22, 1983 in Cartago, Costa Rica and raised in a traditional family of coffee farmers in the lands of Tarrazú. He began his formal education in 1991 at Escuela de Guadalupe de Tarrazú, San José, Costa Rica and in 1997, he entered Colegio Técnico Profesional José Daniel Flores Zavaleta high school in Dota, San José, Costa Rica. In 2003, he joined the University of Costa Rica where he finished his Physics major in 2007. He entered The College of William and Mary in Williamsburg, Virginia in Fall 2014. In 2015, he initially joined the Nuclear Theory group and started working with Dr. André Walker-Loud. Then in 2016, he followed Dr. André Walker-Loud to Lawrence Berkeley National Laboratory where he performed his thesis research until he finished it in 2018.